Nano Materials Science 8 (2026) 117–174

Contents lists available at ScienceDirect

Nano Materials Science

journal homepage: www.keaipublishing.com/cn/journals/nano-materials-science/

Novel advancements in synthesis, modulation, and potential applications of conjugated microporous polymer-based materials

Hamid Ali [a], Obaid Iqbal [b], Muhammad Sadiq [c], Yumeng Cheng [a], Xiao Yan [a], Basem Al Alwan [d], Atef El Jery [d], Hameed ur Rahman [e], Yongteng Qian [f], Asif Hayat [g], Dewu Yue [a,*], Zeeshan Ajmal [h]

[a] Information Technology Research Institute, Shenzhen Institute of Information Technology, Shenzhen 518172, China
[b] School of Materials Science and Engineering, Anhui University, Hefei 230601, China
[c] School of Computer Science, Shenzhen Institute of Information Technology, Shenzhen 518172, China
[d] Department of Chemical Engineering, College of Engineering, King Khalid University, Abha 61411, Saudi Arabia
[e] Department of Soil and Environment Sciences, Agricultural University Peshawar, Pakistan
[f] College of Pharmacy, Jinhua Polytechnic, Jinhua 321007, China
[g] Department of Chemistry, Lishui University, Lishui 323000, China
[h] College of Geography and Environmental Sciences, Zhejiang Normal University, Jinhua 321004, China

ARTICLE INFO

Keywords:
Conjugated microporous polymers
Synthesis reactions
Functionalization
Morphologies
Potential applications

ABSTRACT

Conjugated microporous polymers (CMPs) are a unique class of organic porous materials characterized by π-conjugated structures and permanent micropores, distinguishing them from non-porous polymers and conventional π-conjugated polymers. CMPs offer extensive versatility in synthetic approaches, enabling the synthesis of cross-linked and mesoporous structures. Advances in chemical processes, structural design, and synthesis methodologies have been developed, resulting in a diverse range of CMPs with unique configurations and properties, contributing to the fast expansion of the field. CMPs are particularly notable for their ability to enable the competitive utilization of π-conjugated structures within mesoporous configurations, making them valuable for investigations across various domains. They have shown considerable promise in addressing fuel and environmental challenges, demonstrated by their exceptional performance in applications such as vapor adsorption, heterogeneous catalysis, light emission, light harvesting, and energy generation. This review examines the chemical engineering principles underlying CMPs, including synthesis approaches, systemic research advancements, multifunctional investigations boundaries, potential applications, and progress in synthesis, dimensionality, and morphology studies. Specifically, it offers a comparative analysis of CMPs and linear polymeric materials, aiding in the development of functional polymers. Furthermore, this review explores the primary fundamental limitations of CMPs in fuel-related domains and discusses alternative strategies, including novel synthesis methods incorporating interactions and morphologies, to address these challenges. Ultimately, this assessment aims to provide a valuable and inspiring resource for professionals in the field of fuel management, guiding future research and development efforts.

1. Introduction

Porous materials are essential in various research and development domains and have garnered significant interest as structures for multifunctional material innovation. Historically, the skeletal structures of porous polymers have evolved from the inorganic configurations of zeolites and mesoporous silicates [1], to metals organic frameworks (MOFs) or porous coordination polymers (PCPs) and more recently, organic porous polymers [2–6]. There are non-covalent and covalent methods for synthesizing organic porous polymers. Organic caged crystallization is a typical group of organic porous non-covalent composites [7]. In contrast, porous organic polymers (POPs) [8], hyper crosslinked polymers (HCPs) [9,10], polymeric systems of integral mesoporous (PIMs) [11], covalent organic frameworks (COFs) [12], porous aromatic frameworks (PAFs) [13], and conjugated microporous polymers (CMPs) [14,15] exhibit the conventional categories of covalently bonded organic

* Corresponding author.
E-mail addresses: hamid422@sziit.edu.cn (H. Ali), yuedewu@sziit.edu.cn (D. Yue).

https://doi.org/10.1016/j.nanoms.2024.08.008

Available online 4 March 2025

composite materials, characterized by high porosity, lightweight properties, and strong covalent bonds. Among all these chemically connected organic porous materials, CMPs are a unique family of polymers characterized by joining constituent units in a π-conjugated manner, forming three-dimensional (3D) systems. These molecular properties are exclusive to CMPs and are not observed in other porous polymers, which are typically not π-conjugated, or in regular conjugated polymers, which are non-porous. Since Cooper et al. [16] discovered the first CMP by using the Sonogashira-Hagihara cross-coupling reaction, many researchers have entered this field, leading to the fast expansion of the CMP group. This approach synthesized a CMP system with prolonged π-conjugation across its porous structure, making it distinct from other porous polymer materials. Since then, the number of publications on CMPs has significantly expanded. CMPs have tremendous promise in various chemical, electrical, and optical applications due to their rich carbon-carbon bond-forming chemistry and variable ligand composition [17]. However, PAFs are not π-conjugated across their structures, while imine-based COFs are π-conjugated but exhibit significant crystallinity; thus, neither of these materials would be classified as CMPs. From a chemical configuration standpoint, the most distinguishing feature of CMPs is their extensive series of π-conjugated systems. CMPs have been synthesized using basic building units ranging from conventional phenyl subunits to extended arenes, heterocyclic subunits, and large macrocycles [18,19]. CMPs may consistently change their π-conjugated porous frameworks, allowing for modifying the structure and properties since there are reduced limitations on dimension, shape, and functionality associations. In addition, CMPs have appeared as a significant tool for addressing the environmental and sustainable issues. For instance, CMPs have found extensive application as adsorbents [20], heterogeneous catalysts [21], illumination-harvestat composites [22], luminescent composites [23], photovoltaic composites [24], and photocatalysis [25] due to their numerous advantageous properties, which include the following: (i) The photovoltaic materials [26] benefit from the π-conjugated structure that extends along the skeleton of the polymer, an abundant porous structure, and a large specific surface area (SSA). (ii) The strongly crosslinked polymeric composition and substantial give more pore vacancy to accept charge carriers and wide SSA to reduce ion diffusion gap, resulting in strong electrochemical action and fast kinetics [27]. (iii) The strongly crosslinked polymer configuration efficiently inhibits the dissolution of the activae sites in the organic electrolyte, increasing cycle performance [28]. Chemical interactions for synthesizing linearly functionalized polymeric materials, including the Suzuki cross-coupling reactions [29], Yamamoto reactions [30], Sonogashira-Hagihara reactions [31], oxidative bonding [32], Schiff-base interaction [33], cyclo-trimerization [34], phenazine ring fusion response [35], and Friedel-Crafts arylation [36], are impactful for the synthesis of CMP. CMPs are an ideal framework for designing novel organic porous materials due to various essential component elements and the extensive accessibility of diverse reaction types [37,38]. Current advances in combining conjugated frameworks and nanopores show significant possibilities for investigating novel multifunctional polymers to tackle demanding fuel and ecological concerns [39–41]. The remarkable efficiency of CMPs in gaseous absorption, heterogeneous catalysis, light emission, light harvested, and electrical power retention illustrates such promise. Furthermore, the unique combination of high SSA, tunable properties, biocompatibility, and versatility makes CMPs promising candidates for various medical usages such as drug delivery, imaging, tissue engineering, and biosensing. We present an overview of CMPs throughout our study, including fundamental designing ideas and building blocks, recent advances in synthesis processes, post-synthetic functionalization, morphologies, dimensionality aspects, utilization of CMPs in wide range of applications, functioning exploring boundaries, and possible implications of such a distinctive group of organic porous materials. The main fundamental features addressed in this review are presented in Fig. 1.

2. Development and synthesis strategies

2.1. Geometrical specifications

The synthesis of CMPs requires building blocks with at least two reactive subgroups. Cross-coupling these structural blocks with diverse configurations forms the 3D polymeric structures necessary for porosity, while co-condensation processes facilitate the homocoupling of structural units [42,43]. For convenience, the designs of structural units are categorized as C_2, C_3, C_4, and C_6 (Fig. 2). The co-condensation process, including $C_2 + C_2 + C_2$ [44], $C_3 + C_3$ [45], or $C_4 + C_4$ [46], results in the formation of 3D systems. In comparison, crossing-coupling interactions often include variations such as $C_2 + C_3$ [16], $C_2 + C_4$ [47], $C_2 + C_6$ [48], $C_3 + C_4$, $C_3 + C_6$, or $C_4 + C_6$ [49]. Both situations include embedding nanopores in 3D systems via covalent linkages, resulting in the formation of CMPs with persistent porosity.

2.1.1. Different building units

Various p subunits, including arenas, integrating functional groups, phenylethynylene analogues, heteroaromatic groups, and macrocyclic complexes, have been synthesized as the basic building blocks for the synthesis of CMPs (Fig. 2) [50]. The active units used in the synthesis of CMPs include bromoarenes, iodoarenes, conjugated boronic acids, cyano-functionalized arenes, aliphatic-aldehydes, ethynyl-modified arenes, and amino-functionalized arenes. The CMPs exhibit unique structural frameworks and diverse properties due to the different structural units and the wide range of active groups.

2.2. Synthesis reactions

The synthesis of CMP materials has been enhanced by the catalytic impact of noble metals, leading to higher cross-linking efficiency and increased flexibility [51]. CMPs can be tailored by regulating the molar ratio and reaction conditions of the co-monomers. This approach offers several advantages: (i) a favorable reaction environment, a wide range of available substrates, high selectivity, facile post-synthesis processes, and the incorporation of functional groups, and (ii) efficient synthesis process, simple reaction route, high yield of synthesized products, and outstanding surface area. Recently, noble metallic-catalyzed cross-linked reactions have been used to synthesize many novel CMPs that are suitable and versatile. These CMPs are specifically designed for use in green energy systems [52]. This section examines the latest scientific advancements, including cross-linking achieved through Sonogashira-Hagihara and Suzuki reactions and Yamamoto and Buchwald-Hartwig couplings.

2.2.1. Sonogashira-Hagihara reaction

The highly porous nature of CMPs implies the relationship of synthesis units with different geometries. The monomers are initially bonded together by π-conjugated interactions, resulting in covalently porous materials using Pd-functionalized synthesis [53]. Jiang et al. [54] linked the C_3 coherent core to the constant C_2 linker via the Sonogashira-Hagihara reaction, resulting in several polymer structures, such as CMP/1, CMP/2, CMP/3, and CMP/4. The bonding distance can be changed to change the pore diameter, the surface area, and the gas absorption of such polymers. CMP1 has two acetylenes and one benzene group [53], and its Brunauer-Emmett-Teller (BET) surface area is higher than that of the remaining three CMPs, implying that the surface area of polymer edges decreases with increasing length [55]. Sonogashira-Hagihara reaction synthesized the triazine-based polymer structures TCMP/0, TMP/2, TMP/3, and TMP/5 in 2012. They discovered that the structure of these networks such as CMP/3 [54], CMP/0 [56], CMP/5 [53], and NCMP/2 are similar to those previously described [57]. The benzene nodes within these chains formed by triazines undergo

the exchange of TCMPs with 1,3,5-triazine groups, thereby proving the possibility of minor variation and shifting of CMP nodes. They compare the porosity of such polymers to the CMP systems with 1,3,5-linked benzene; however, TCMPs demonstrated improved CO_2 absorbing ability. The TNCMP/2 has the highest surface area of 995 m^2g^{-1}, and the capacity to absorb CO_2 of 1.45 $mmolg^{-1}$ and 1 bar at 298 K. The choice of monomers with comparable porosity may enhance the polymer structure's physicochemical strength and absorption properties. Li et al. [58] utilized the Sonogashira-Hagihara process to synthesize the CMPs via thiophene parts. The individual component of electron-thiophene has much more porosity and structure than the interlinked structure, resulting in enhanced absorption capabilities. Li et al. [59] used 2, 6-dibromomethyl pyridine and arylethynylenes as raw materials, and by the Sonogashira-Hagihara reaction, they obtained unique and efficient CMPs containing pyridine units, known as PCMPs. They determined that their selection of vinyl monomer initially influenced the ultimate BET surface area of CMPs. Similarly, the molar ratio of the monomer significantly effects the surface area, which influences the gas absorption capacity of CMPs [60]. Thomas et al. [61] revealed that it is feasible to synthesize a complete catalyzed Sonogashira-Hagihara reaction phase, which allows for the artificial synthesis of CMP composites. It significantly enhances the ability to study new chemical linkages and facilitate the research of prospective CMP materials. One example of such interaction is the widely used artificial pathways for CMP composites. The cross-coupling mechanism persists in conforming to an oxidative inclusion and reducing exclusion pathway. The addition of vinyl halogens to Pd(0) metal complexes involves oxidative inclusion and is enhanced by trans-metalation using copper(I)-acetylide. Their study showed that these products were reduced and excluded, leading to the need for catalyst renewal. Fig. 3a displays all aspects of catalytic performance. The Sonogashira-Hagihara process is highly expensive due to the significant cost of the required Pd catalyst, posing a major limitation in developing potential CMP composites. However, the efficiency of hydrophilic systems can be leveraged to enhance the photocatalytic performance of other conventional photocatalysts. As a result, hydrophilic CMP-based photocatalysts achieve optimal efficiency. Roy et al. [62] synthesized electrochemically active CMPs, namely TPA-BP-1 and TPATPE-2, using Sonogashira-Hagihara couplings of tris(4-bromophenyl)amine with 1,1, 2,2,−4,4'-diethynylbiphenyl and tetrakis(4-ethynylphenyl)ethane. The structure of the designed CMPs include a localized nitrogen site that readily forms bonds with oxygen atoms. The CMPs frameworks consists of with a densely arranged nitrogen sites, which allows for easy interaction to oxygen atoms. It includes tris(4-bromophneyl) amine as hole-transported groups, and 1,1,2,2, tetrakis(4-ethynylphenyl)ethane and 4,4'-diethynylbiphenyl as appropriate acceptors. The whole structure may be used to transfer electrons and transmit electrocatalytic reduction, and it demonstrates a favorable ability to initiate the ORR and great stability in terms of energy (Fig. 3b).

2.2.2. Suzuki cross-coupling reaction

Suzuki reaction signifies the interaction of aryl or boric acid esters or alkenyl boric acids with aryl iodine, bromide, chloride, or olefins facilitated through complexes based on the metal Pd [63]. This approach has several advantages, including the cost-effective accessibility of boric acid, various structural units, and ideas with minimized variability [64]. It has a significant metric. Nevertheless, the Suzuki reaction is susceptible to oxygen, creating homocoupling and deprotonation as unwanted byproducts. Thus, this reaction approach should lead to a complete gas reduction. Pyrene, benzothiadiazole, and benzene (or biphenyl) were used as donor, receptor, and inter-linkers agents, resulting in the formation of several groups of donor-π-receptor (D-π-A) with distinct polymer elements and topologies by Suzuki reaction in CMPs [65]. By modifying the co-monomer structure and adjusting the pyrene-to-benzothiazole ratio in the synthesis process, the molecular structure of CMPs can be tailored. This enables the formation of efficient photocatalytic systems, highlighting the importance of chemical composition in developing high-efficiency organic photocatalysts. The ability to create a diverse range of CMPs for renewable energy applications allows for the exploration of various electron acceptor and donor groups, as well as the broad application of the Suzuki reaction in these systems. Similarly, Liu et al. [66] demonstrated that CMPs can be synthesized using a non-metallic amino-catalyzed organocatalytic Suzuki-Miyaura coupling method, providing the first evidence of this feasibility. This approach yields CMPs with diverse components and achieves a surface area of up to 1269 m^2/g, significantly higher than that obtained with traditional metallic catalysts. This method also enables the synthesis of acetylene-related CMPs under non-metallic conditions. The synthesized CMPs exhibit outstanding gas absorption and luminescence properties (Fig. 3c). Wang et al. [67] synthesized a large-scale, electron-enrich Pd-N-heterocyclic carbene (NHC)-based CMP (PdPEPPSI-CMP) using a post-synthetic method. This composite employed a PdPEPPSI-IPr molecular catalyst, which endowed it with exceptional catalytic activity in Suzuki cross-coupling reactions involving (hetero)aryl chlorides and (hetero)arylboronic acids. In comparison to other Pd-based materials, this technique demonstrated remarkable environmental sustainability with minimal Pd deposition. It remained compatible with a diverse array of functional categories and exhibited enhanced catalytic performance on a gram scale. Importantly, this composite was utilized in the synthesis of bioactive materials and the direct functionalization of pharmaceuticals (Fig. 3d).

2.2.3. Heck reaction

The Heck reaction, also known as the Mizoroki-Heck process, was extensively investigated by Heck and Mizoroki in the 1960s, has since become a widely adopted method for C–C bond formation [68]. The interaction of 1,3,5-tri(4-ethenylphenyl) benzene with aliphatic halogens resulted in the formation of a distinct class of luminous microporous organic polymers (LMOPs). These LMOPs exhibit significant surface area, narrow pore size distributions, and excellent luminescence properties (Fig. 4a) [69]. The one-pot synthesis approach has produced several POPs with luminescence properties, promising for organically photovoltaics and photocatalysis applications. Li et al. [70] proposed an innovative approach using thiophene-alkyne-predicated CMPs an efficient stabilizers for oxidizing Heck reactions. These units serve dual roles: as catalytic sites and as structural units in CMP synthesis (Fig. 4b). Zhou et al. [71] developed a precise method for selectively oxidizing simple olefins using CMP materials as ligands, achieving high linear selectivity in Heck reactions. These ligands incorporate various components, including C ≡ C and pyridine-N sites arranged in optimal coordination structures. CMP-1 exhibits a linear selectivity approximately 30 times higher than measured by monomeric ligands like bipyridine (Fig. 4c).

2.2.4. Yamamoto reaction

The Yamamoto reaction, utilizing nickel as a catalyst, facilitates the synthesis of halogenated aliphatic materials by C-C bond formation [72]. For example, coupling reactions of tetrakis(4-bromophenyl)-1,3,5,7 and tetrakis(4-iodophenyl)methane have successfully produced monomers leading to CMPs with a high surface area of 3160 and 3180 m^2/g [73]. Thomas et al. [74] synthesized a series of spirobifluorene-based CMPs, termed YSN-CMPs, achieving a high surface area of 1275 m^2/g (Fig. 4d). Their study highlights how the bond strength and arrangement of compositional units significantly influence the pore structure and BET surface area of CMPs. Modifications such as replacing 2,2,7,7-tetrabromo-9,9-spirobifluorene with p-dibromobenzene reduced the surface area to 887 m^2/g, and integrating m-dibromobenzene further decreased it to 361 m^2/g. Additionally, p-aryl co-monomers are commonly integrated to enhance porous structures [75]. Jiang et al. [76] utilized the Yamamoto coupling process to prepare a unique CMP, TPE/CMP, incorporating the p-aryl co-monomer tetrakis(4-bromophenyl)ethene (TPTBE). This approach effectively linked tetraphenylethene (TPE) building blocks, resulting in a rigid structure that restricts phenyl chain rotation and enhances luminescent activity. These CMPs are promising

Fig. 1. Graphical illustration of the fundamental features addressed in this review.

for photocatalytic hydrogen production via H_2O during visible light. However, a challenge of using the Yamamoto reaction lies in the fast oxidation and water absorption of the Ni metal catalyst, necessitating controlled conditions involving water and oxygen, which can increase the overall synthesis expenses of CMPs.

2.2.5. *Buchwald-Hartwig coupling reaction*

The Buchwald-Hartwig coupling reaction, also known as B-H coupling, utilizes a Pd catalyst to facilitate C-N interactions between aromatic amines and halogenated aromatic compounds [77,78]. Germain et al. [79] employed B-H coupling to polymerize the foundational structure of polyaniline, showing its direct utilization in hydrogen storage in 2008. Zhang et al. [80] introduced porous polytriphenylamine CMP electrodes for energy storage, which are efficient in accommodative Cl^- anions in a pseudocapacitive-dominant manner. Their distinct 3D, COFs-like conjugated structure enhances the accessibility and efficiency of nitrogen binding sites, ensuring strong physio-chemical stability over multiple charge/discharge cycles. This stability contributes to a zinc dual-ion battery system with significantly higher capacity and maximum efficiency than organic-predicated zinc batteries (Fig. 4e). Their research underscores the systematic development of advanced chemical cathodes based on CMPs for high-energy applications. To comprehensively understand various CMP synthesis methods, we have summarized their advantages and disadvantages in Table 1.

2.3. *Synthesis activated by non-noble metals*

Metal-catalyzed cross-coupling methods provide extremely significant MP polymers. The utilization of noble metal catalysts presents challenges such as elevated costs, susceptibility to oxygen, restricted recovery and reusability, and hazardous reaction conditions [90]. Consequently, there has been considerable effort in developing CMP materials using non-noble metal catalysts, offering benefits such as affordability, moderate reaction rates [91], higher yield, and the facile synthesis CMP process [92]. This section delves into the chemical processes enhanced by non-noble metals to produce microporous conjugated polymers (MCP), utilizing Schiff base reactions, oxidation coupling reactions, Friedel-Crafts reactions, phenazine ring fusion, cyclotrimerization, and formation of heterocyclic linkages. These methods provide an economical means to produce a long series of highly efficient CMP materials tailored for renewable energy applications.

2.3.1. *Oxidative coupling reaction*

Oxidative polymerization involves the removal of hydrogen from materials containing activated hydrogens with an oxidizing agent to produce polymers [93]. These polymerizations are classified into electrochemical and chemical oxidation polymerizations based on the method of oxidation. Chemical oxidation polymerization refers to the dehydrogenative polymerization of co-monomers using oxidizing agents

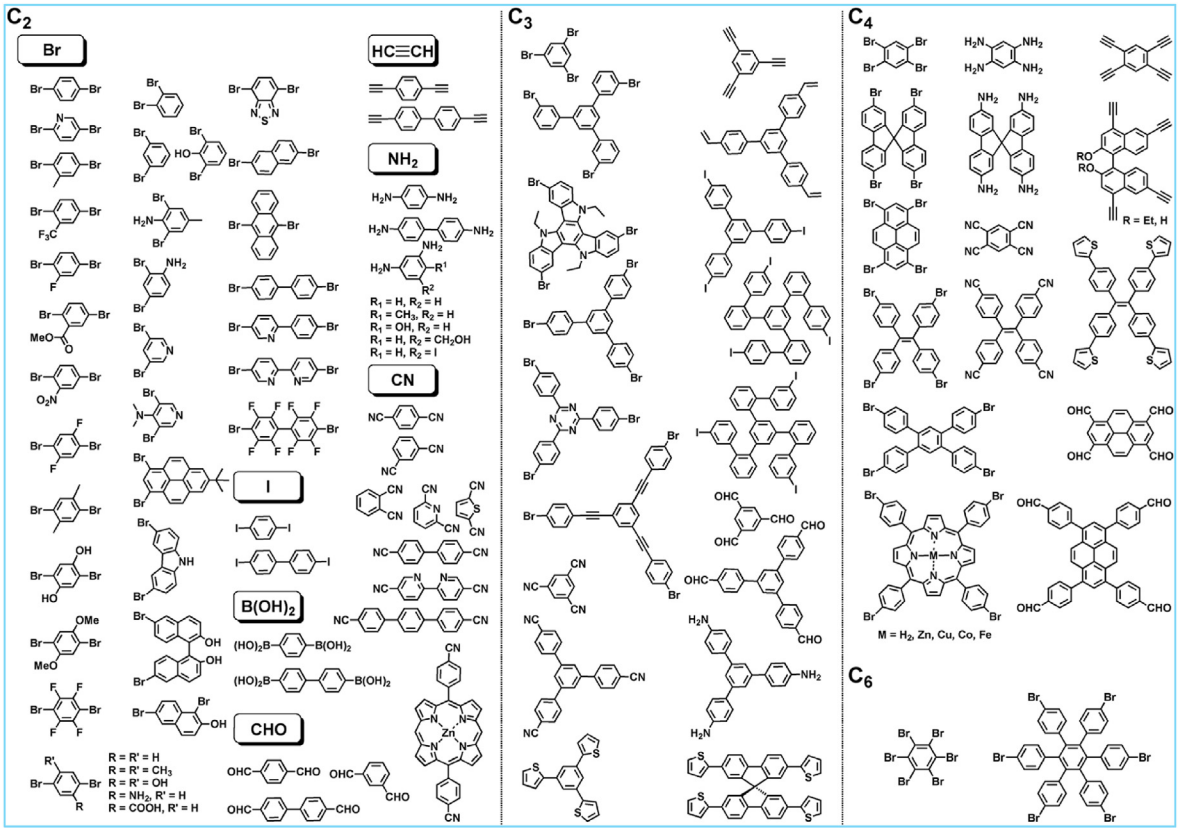

Fig. 2. Diagram depicting structural units of different structures, sizes, and active groups used in the synthesis of CMP [50] Copyright © 2013, Royal Society of chemistry.

like $FeCl_3$ [94]. Chen et al. [95] synthesized a series of microporous functionalized polycarbazoles (CPOP-2-7) with infinite porosity and unique functionalities through carbazole-dependent oxidative doping polymerization. The incorporation of carbazolyl chains into interconnected core structures facilitated the formation of polymeric structures with diverse functionalities (Fig. 5a). Fig. 5b illustrates the network synthesis of CPOPs by linking non-planar compacted structures with multifunctional carbazolyl cores as bonding units. Additional functional groups are necessary for doping polymerization, enhancing monomer-based features. The process is simple due to the presence of two active sites in each carbazole unit, resulting in constant and stable polymer pore structures with BET surface area ranging from 510 to 1430 m^2/g and pore widths from 0.59 to 0.66 nm. Carbazole-based CMPs synthesized via oxidative linked polymerization exhibit regular micropores, notable luminescence, and numerous nitrogen initiation sites, with substantial carbon dioxide (CO_2) adsorption capacity, making them promising in renewable energy applications [96]. In 2016, Chunyang et al. [97] used a $FeCl_3$-catalyzed oxidation coupling to synthesize four carbazole-based CMPs (PCzCn-Cz) with similar solid backbones and alkylene groups but varying pore sizes. These polymers revealed significant surface area (>750 m^2/g) and significant gas adsorption capabilities (CO_2, CO, H_2, CH_4), suitable for environmental engineering and renewable fuel applications. $FeCl_3$-catalyzed oxidizing doping between carbazole and electron-deficient groups offers an environmentally viable alternative for non-metal synthesis of solid CMP photocatalysts under visible light [98]. Recent studies also synthesized porphyrin-based CMPs (Porp-TPECMP and Porp-Py-CMP) via $FeCl_3$-catalyzed oxidation coupling using pyrrole and aromatic aldehyde as catalysts. These materials exhibit substantial gas adsorption capabilities with CO_2/N_2 and CO_2/CH_4 ratios of 55.28 and 4.11, and BET surface area of 547 and 31 m^2/g, highlighting their potential for greenhouse gas and hydrogen storage [99].

2.3.2. *Schiff-base reaction*

Schiff base reactions are essential in CMP synthesis, involving the acylation of Schiff bases with various substrates such as acid anhydrides, acid chlorides, and acyl cyanides, facilitating the addition of the C=N bond [100,101]. These processes are advantageous for synthesizing functional materials. Schiff bases play a vital role in polymer network activities by mediating interactions between primary amines and the carbonyl groups of aromatic molecules [102,103]. Chai et al. [104] introduced a novel keto-enamine functionalized CMP (KE/CMP-1) synthesized via Schiff-base reactions between m-phenylenediamine (m-PDA) and 1,3,5-triformylphloroglucinol (TFP) in 2016. This method employs a single reagent and benefits from non-metal catalysts without templates, achieving a BET surface area of up to 691 m^2/g. Additionally, introducing N-H groups within polymer pore walls enhances CO_2 adsorption efficiency by promoting N-H•••O and CO_2 coupling interactions. In 2018, Co/CMP and Zn/CMP were synthesized via Schiff-based condensation reactions involving metal-phthalocyanine tetra-amine and 4,4-(2,5-bis(pentyloxy)-1,4-phenylene)bis(ethyne-2, 1-diyl)dibenzaldehyde (OPE-5) [105]. Co/CMP demonstrated high electrocatalytic efficiency for OER due to Co^{2+} coordination within phthalocyanine (PC) N_4 sites, showing a low overpotential of 340 mV. Conversely, Zn/CMP was inactive towards OER, highlighting the critical role of metal inclusion and reactivity settings in preparing CMP electrocatalysts. Previously, a polymer system (FcTz/POP) synthesized via Schiff-base reactions incorporated iodine-affinity units, specifically ferrocene, into the polymer structure. This network exhibited superior stability and elevated excellent iodine vapor adsorption (396 wt% at 348 K and atmospheric pressure) compared to BpTz/POP (a polymer without ferrocene), which adsorbed only 216 wt% under the same conditions [105]. This demonstrates the profound impact of Schiff base interactions on CMP structures, enhancing their utility in renewable energy applications (Fig. 5c and d) [106].

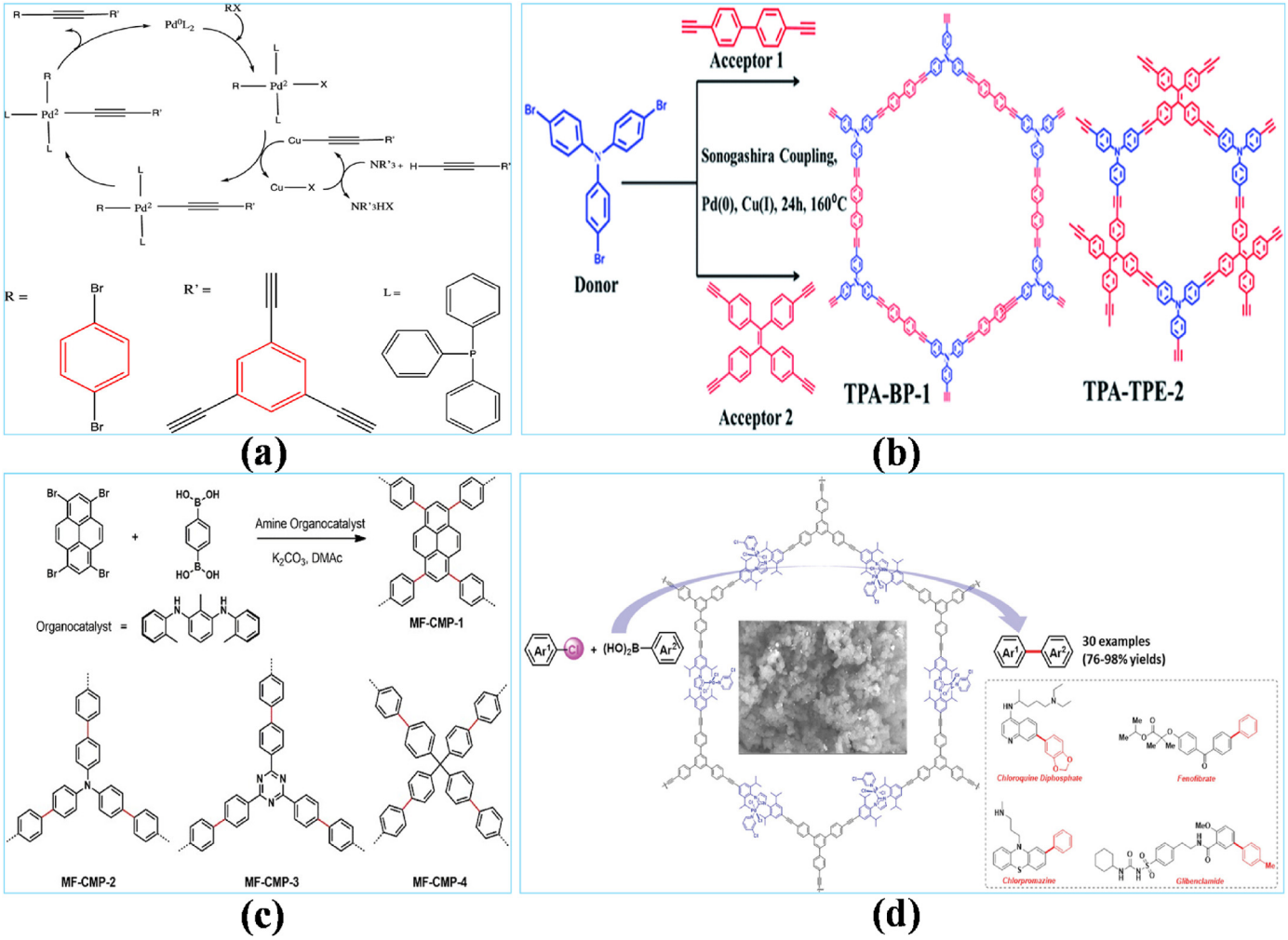

Fig. 3. (a) Cycling catalyzed for the Sonogashira-Hagihara carbons linkage process to yield CMP-1 [61], Copyright © 2020, American Chemical Society. (b) Synthetic scheme of two redox-active and semiconductor CMPs [62], Copyright © 2018, Royal Society of Chemistry. (c) Kinetics process for the synthesis of MF/CMP1 from pyrene-based monomers through non-metal mediated Suzuki couplings and illustrative structure of MF/CMP2, MF/CMP3, and MF/CMP4 [66], Copyright © 2021, Royal Society of Chemistry. (d) Schematic mechanism of the bulk Pd-PEPPSI-CMP [67], Copyright © 2022, Royal Society of Chemistry.

2.3.3. *Interaction across heterocyclic materials*

A macroporous benzimidazole network polymer has been prepared via a non-template condensation method using 2,3,6,7,10,11-hexaaminotriphenylene and tetrakis(4-formylphenyl)methane [19]. This polymer holds significant promise for applications in energy production and purification. Additionally, a solvent-free co-condensation method was employed to synthesize a microporous composite material by reacting aldehydes with dithiooxamide, forming thiazolothiazole linkages. This material exhibits notable CO_2 adsorption capabilities under moderate pressures and temperatures [107]. Feng et al. [108] revealed the process of innovative thiazolo[5,4-d]thiazole (TzTz) linkages and three innovative T_zT_z/POPs, namely T_zT_z/POP-3, T_zT_z/POP-4, and T_zT_z/POP-5, using triphenylbenzene, tetraphenylpyrene, and tetra(hydroxyphenyl) methane. Notably, T_zT_z-POP-3 displays selective removal of organic dye fluorescence (FL) from aqueous solutions containing Para fuchsine (FU), demonstrating its potential utility (Fig. 5e and f).

2.3.4. *Synthesis of aza-fused CMPs*

The modification of Aza-fused CMPs involves integrating Aza elements to form a porous structure [109]. This results in densely packed aza complexes and micropores, essential for creating barriers to charge dissipation and preserving structural integrity [110]. As a result, Aza-fused CMPs hold significant promise for advanced energy storage systems. Their conjugated structure, small aza units, and well-organized micropores enhance the synthesis of electrical charge barriers, leading to substantial inductance, high capacity, and efficient energy output. These properties make them particularly suitable for enhancing fuel efficiency and longevity in rechargeable batteries (Fig. 5g–i).

2.3.5. *Cyclo-trimerization reaction*

Cyclo-trimerization utilizes ionic energy to synthesize porous polymers by linking co-monomers with $ZnCl_2$, which serves as a solvent, catalyst, and structure inducer for pore creation [111]. CTFs refer to the CMPs that are prepared using this particular approach [112]. These polymers, known as Cyclo-Trimerized Structures (CTFs), were first fabricated by the Thomas research team in 2008 using 1,4-dicyanobenzene nitrile units annealed with $ZnCl_2$ at 400 °C [113]. The properties and pore structures of CTFs can be tailored by adjusting temperature conditions [114], co-monomer types [115], and process dynamic variables [114]. Liu et al. [115] demonstrated precise control over surface area and pore sizes by functionalizing alkynyl monomers through cyclotrimerization reactions of varying lengths in 2010. Kim et al. [116] utilized aldol reactions catalyzed by inexpensive reagents, often ignored in polymer synthesis, as a typical C-C bond-formation process that meets these conditions [117]. For example, under Lewis or Brønsted acid catalysis, methyl ketones initially form α,β-unsaturated ketones via water elimination, resulting in further cyclotrimerization under more stringent circumstances to produce 1,3,5-substituted arenes (Fig. 5j). In contrast,

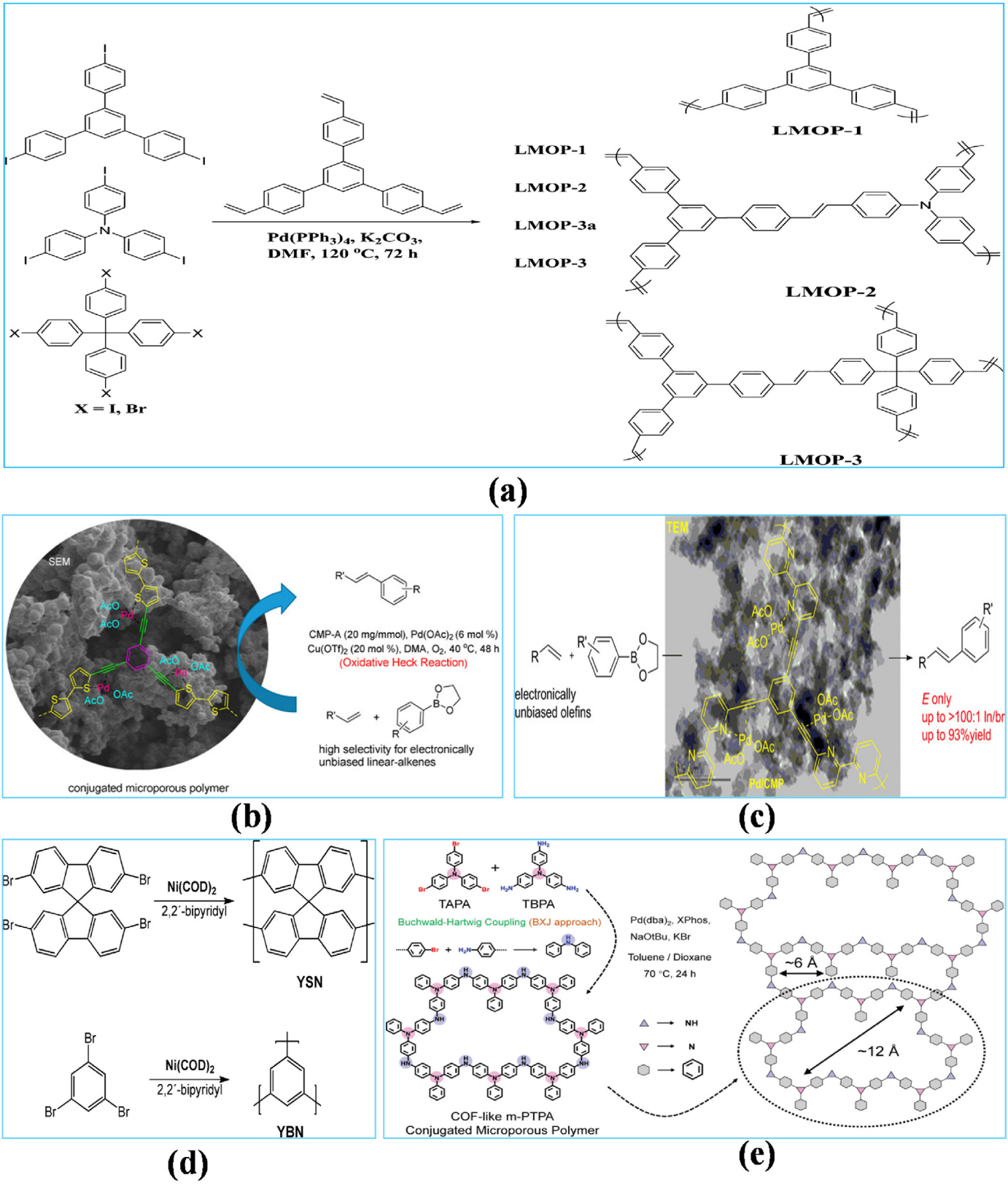

Fig. 4. (a) Preparation and the chemical configuration of LMOP through Heck reaction [69], Copyright © 2013, Royal Society of Chemistry. (b) Synthetic process of CMP via Heck reaction [70], Copyright © 2017, American Chemical Society. (c) Graphical illustration of CMP via Heck reaction [71], Copyright © 2017, American Chemical Society. (d) A group of spirobifluorene-CMPs based on YSN-CMPs using the Yamamoto-connected reaction [74], Copyright © 2009, American Chemical Society. (e) Graphical depiction of COF-shaped polytriphenylamine CMP syntesis and its structures [80], Copyright © 2021, John Wiley & Sons.

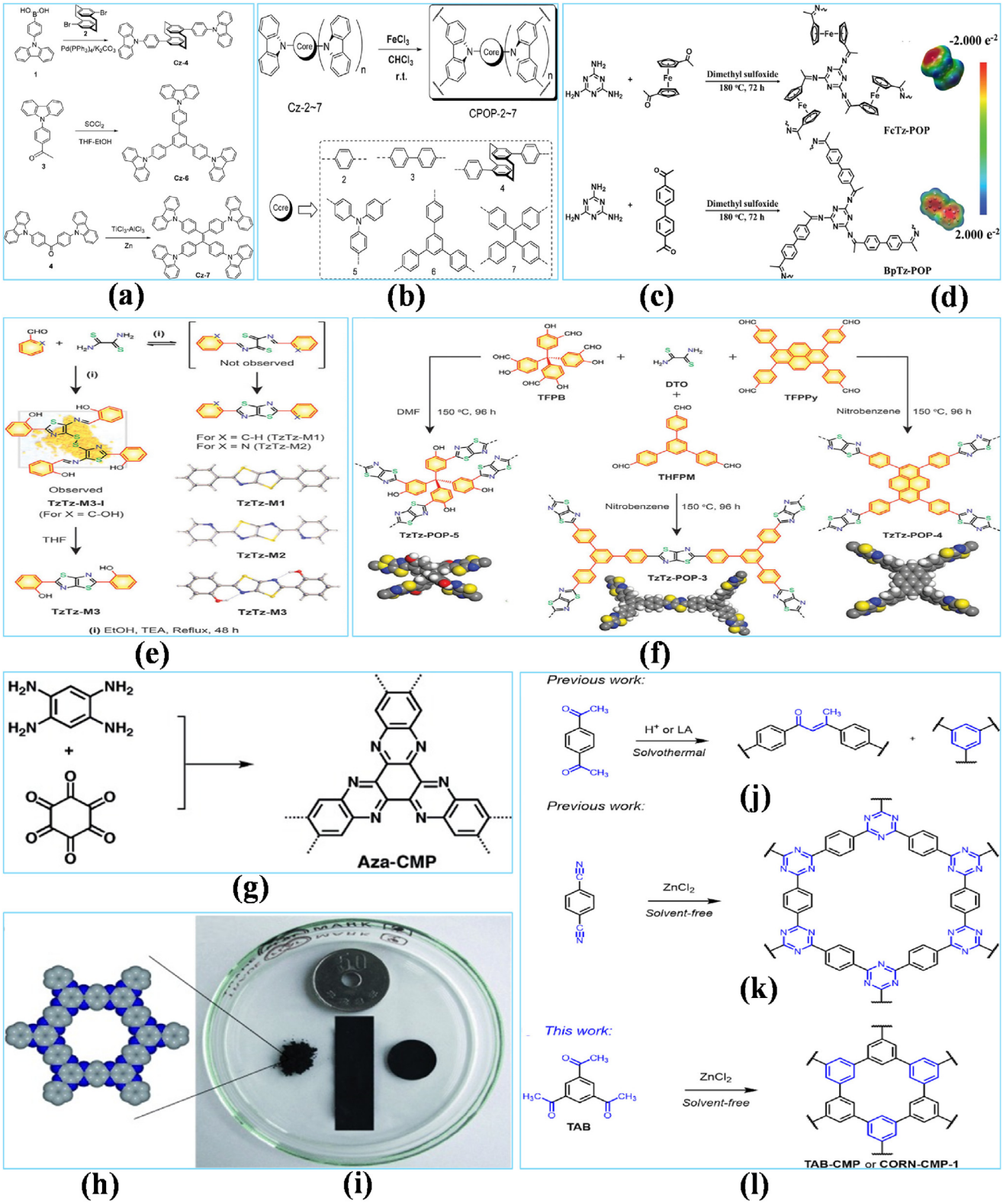

Fig. 5. (a) Synthesis strategies of Cz-4, Cz-6, and Cz-7 co-monomers; (b) Synthesis of CPOP-2~7 CMP [95], Copyright © 2013, John Wiley & Sons. (c) Synthetic process of POPs systems for the elimination of iodine; (d) Electrical possibility mapping of ferrocene and diphenyl derivatives [106], Copyright © 2020, Elsevier. (e) Single approach of synthesis of prototype complexes based on thiazolo[5,4-d]thiazoles (T_zT_z) links and precursors; (f) Synthetic of T_zT_z associated porous POPs via various asymmetric arylaldehydes and dithiooxamide (DTO, The localized configuration of T_zT_z-POPs is shown at the bottom by a space-filling modeling of optimal segments of T_zT_z-POP-3, -4, and -5 generated utilizing materials master versions 2017) [108], Copyright © 2018, John Wiley & Sons. (g) Synthesis of an aza-fused π-Aza/CMP); (h) The elemental porous structure of Aza/CMPs using the Gaussian 03 method at the B_3LYP/3-21G (d) phase (the C structure is grey and N is blue); (i) Image of powders and elastic thinner sheets with distinct Aza/CMPs forms [110], Copyright © 2011, John Wiley & Sons. (j) Synthesis of copolymers using cyclo-trimerization. (k) Dimerization/trimerizations of carbonyl groups catalyzed by solvothermal Brønsted acids (H^+) or Lewis's acids (LA); (l) The ionothermal trimerization of nitriles for the synthesis of CTFs [116], Copyright © 2021, American Chemical Society.

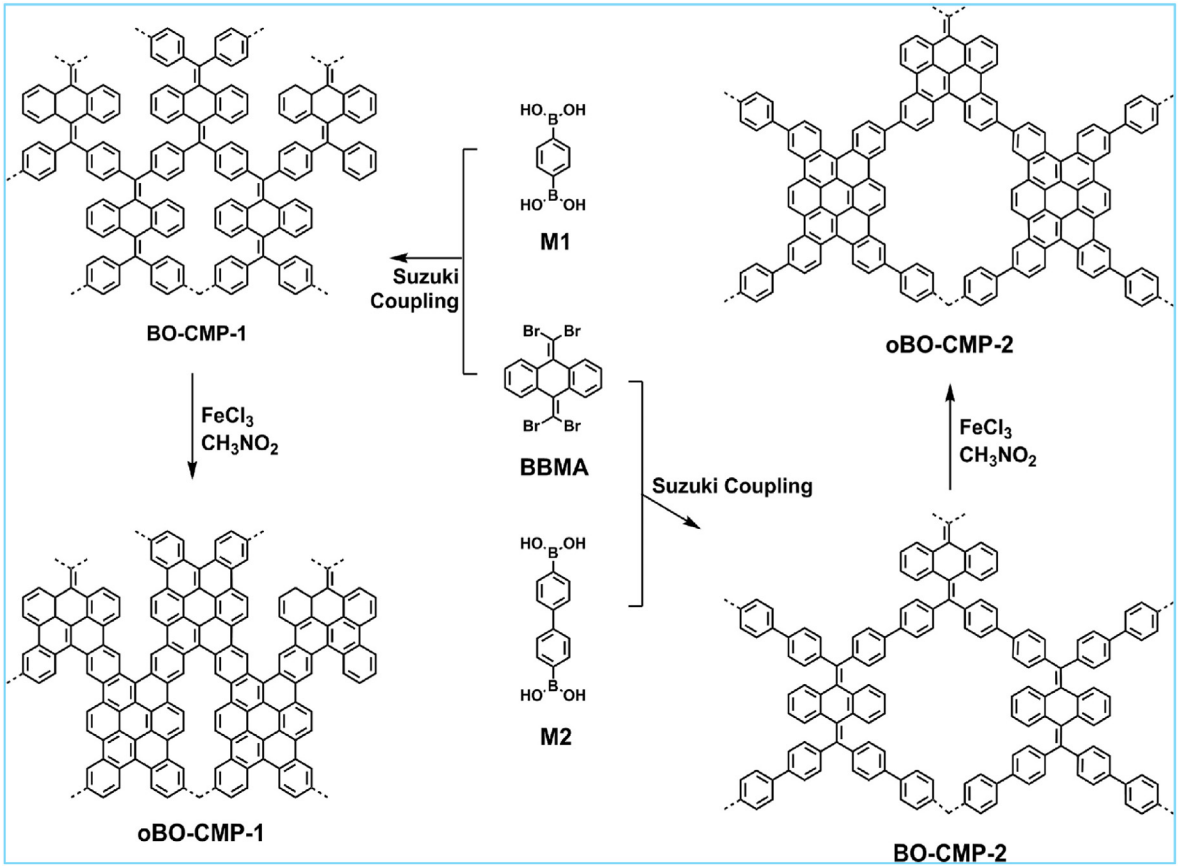

Fig. 6. Synthesis method of BO-CMP and oBO-CMP [132], Copyright © 2018, American Chemical Society.

cyclotrimerization has been extensively used to create intermediate arenes like truxenes, its adaptation for producing extended materials like CMPs remains challenging [118]. In contrast to carbonyl compounds, the cyclotrimerization of nitriles to synthesize CTFs has been widely reported (Fig. 5k) [119]. Initially proposed by Kuhn et al. [120], CTFs can be synthesized by accelerating cyclotrimerizations in molten Lewis acid salts such as $ZnCl_2$. Unlike conventional methods, this technique avoids the use of chemical solvents in the synthesis process. Researchers revealed that ionothermal cyclotrimerization of carbonyl groups using $ZnCl_2$ as the solvent can yielded highly homogenous CMPs, based on similar principles (Fig. 5l) [121]. Studies have shown that CMPs and related PAFs can be synthesized by cyclotrimerization of tri- and tetra-acetylated subunits under strong Lewis acid conditions, catalytically transforming ketones into 1,3,5-functionalized arenes. Specifically, 1,3,5-triacetylbenzene (TAB) synthesizes CMPs with significant surface area and Langmuir-type pore structures. The combination of large surface area and conjugation makes these CMPs highly suitable for supercapacitive energy preservation [122]. Overall, ionothermal cyclotrimerization of carbonyl groups offers a solvent-free route for synthesizing novel CMPs using conventional co-monomers.

2.4. *Post-synthesis functionalization of CMP*

Post-synthetic modification (PSM) is a valuable methodology for optimizing the design and properties of CMPs during their synthesis [123]. This approach involves adjusting the co-monomers chemical weight, ratios, and process parameters to synthesize the desired CMPs. To achieve homogeneous CMPs, polymer frameworks might incorporate various functional groups. An in-depth investigation has been carried out on the post-functionalization of organic compounds, focusing mainly on "click" chemistry techniques such as Huisgen reactions (copper-optimized 3 + 2 cycloadditions of azides), copper(I)-optimized alkyne-azide cycloadditions (CuAAC), thiol-yne cycloaddition, and thiol-ene cycloaddition in recent decades [124–126]. This research investigates the use of advanced synthesis processes to enhance the properties of CMP materials. By modifying the molecular structure of CMPs, advanced synthesis techniques can change their morphology and functional properties [127]. For instance, regulating the amount of thiol and the reaction of CMPs with thiol-yne radicals in aliphatic solvents can control their interaction, morphology, porosity, and adsorption properties [128]. A CMP modified with an amino group (CMP/1/NH_2) can effectively convert amines into amides with various alkyl clusters to regulate interface functional channels and microporosity. This process also moderately limits the surface area, pore volume, CO_2 adsorption properties, and isotropic thermal properties [129]. Through proportional alignment of azide chains, the process of "PSM" adjusts fluorine materials within the CMP systems to enhance the efficiency of gas mobility. For example, ZnP/XF/CMPs were synthesized by incorporating an azide sequence into the pores of ZnP/XN_3/CMPs, which are zinc-porphyrin CMPs with varying azide contents of 5 %, 25 %, and 50 % [130]. The as-synthesized materials of ZnP/XF/CMPs, where X represents the percentage of XF, namely 5 %, 25 %, and 50 %, exhibit CO_2 capacities of 34, 52, and 90 mg g^{-1}. These values are 1.31, 1.68, and 1.84 times higher than the CO_2 capability of ZnP/XN_3/CMPs, where X represents the percentage of XN_3, namely 5 %, 25 %, and 50 %. Furthermore, the structure of CMPs exhibits π-coupling and may be finely changed by post-oxidation reaction to yield a conjugated structure [131]. During the initial phase of the Suzuki process, two CMPs with similar structures and large SSAs, BO/CMP/1 and BO/CMP/2, were obtained. The biolefin benzoquinone units in the skeletal structure undergo oxidation interactions, resulting in the creation of tetrabenzocoronene moieties. This process results in the synthesis of oBO/CMP/1 and oBO/CMP/2, which have an enlarged π-configurations. The process utilizes monomers with elongated π-configurations to prevent polymerization challenges produced by fast

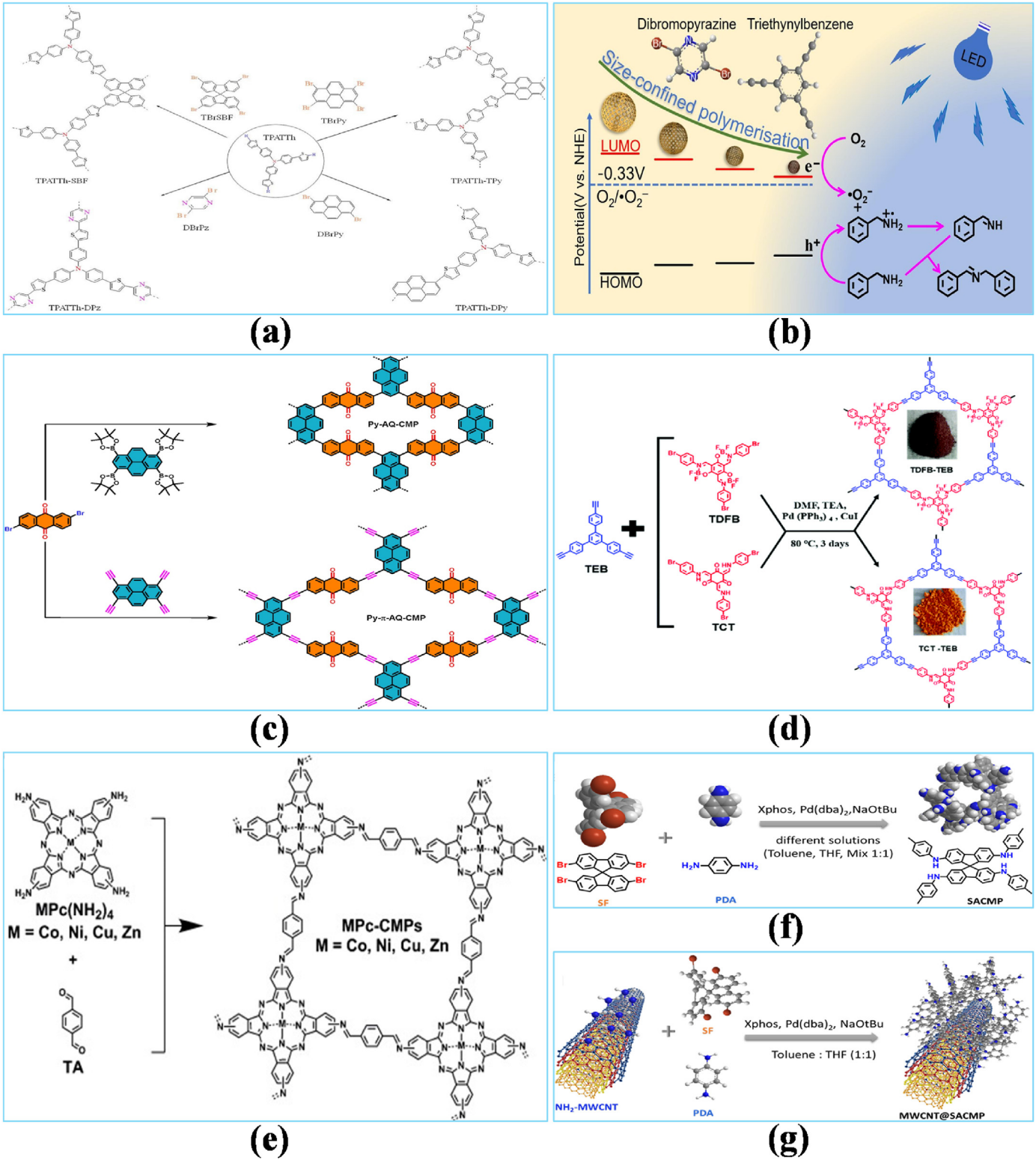

Fig. 7. (a) Synthesis of TPATTh-based CMPs via one-step direct arylation polymerizations [140], Copyright © 2023, Elsevier. (b) Synthetic process of amine-based CMPs [165], Copyright © 2024, Elsevier. (c) Schematic mechanism for synthesizing Py-AQ-CMP and Py-π-AQ-CMP [151], Copyright © 2023, Elsevier. (d) Chemical structure of boranil-based TDFB-TEB and TCT-TEB CMPs [157], Copyright © 2021, Royal Society of Chemistry. (e) Synthesis of MPc-CMPs [159], Copyright © 2015, John Wiley & Sons. Schematic mechanism of (f) SACMP; (g) MWCNT@SACMP by BH coupling [164], Copyright © 2021, American Chemical Society.

ordering during preparation. This method can modify the structure, pore size distribution, and gas absorption properties of the primary polymers, offering a simple and effective technique for the post-modulation of CMPs (Fig. 6) [132].

2.4.1. *Amine-based CMPs*

Post-polymerization is a specific method used to control the shape of materials by limiting their size or surface area during the synthesis process [133–135]. This technique is applied to polymer materials such as

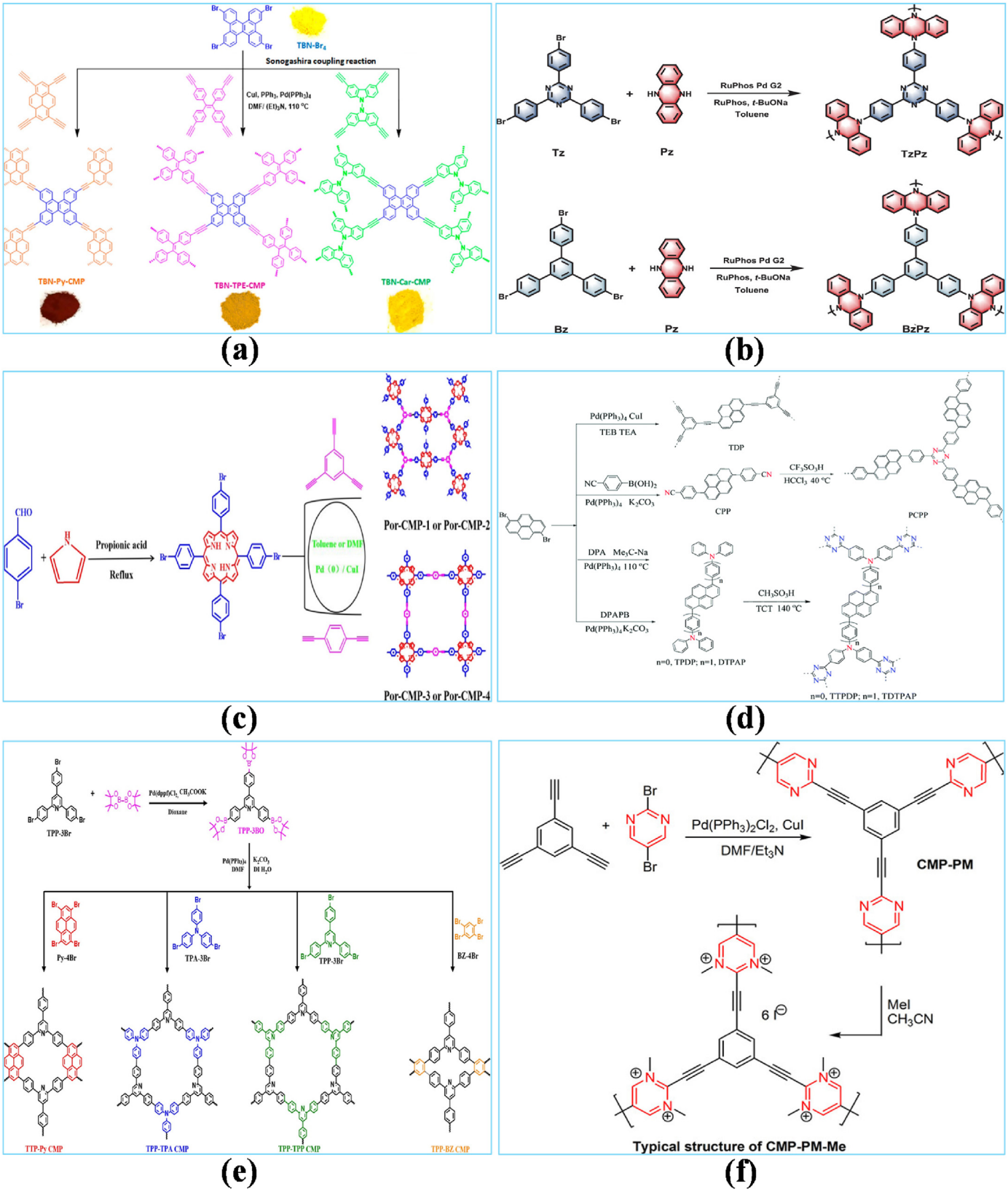

Fig. 8. (a) Schematic mechanism of naphthalene-based CMPs [171], Copyright © 2021, American Chemical Society. (b) The synthesis processes for TzPz and BzPz with hypothetical polymeric designs [178], Copyright © 2021, John Wiley & Sons. (c) Synthetic routes for Por-CMP-1-4 [183], Copyright © 2022, American Chemical Society. (d) Synthesis of TDP, PCPP, TTPDP, and TDTPAP [192], Copyright © 2020, Royal Society of Chemistry. (e) Schematic mechanism of pyridyl-based CMPs [199], Copyright © 2021, American Chemical Society. (f) Synthetic methodology for CMP-PM and CMP-PM-Me [205], Copyright © 2018, John Wiley & Sons.

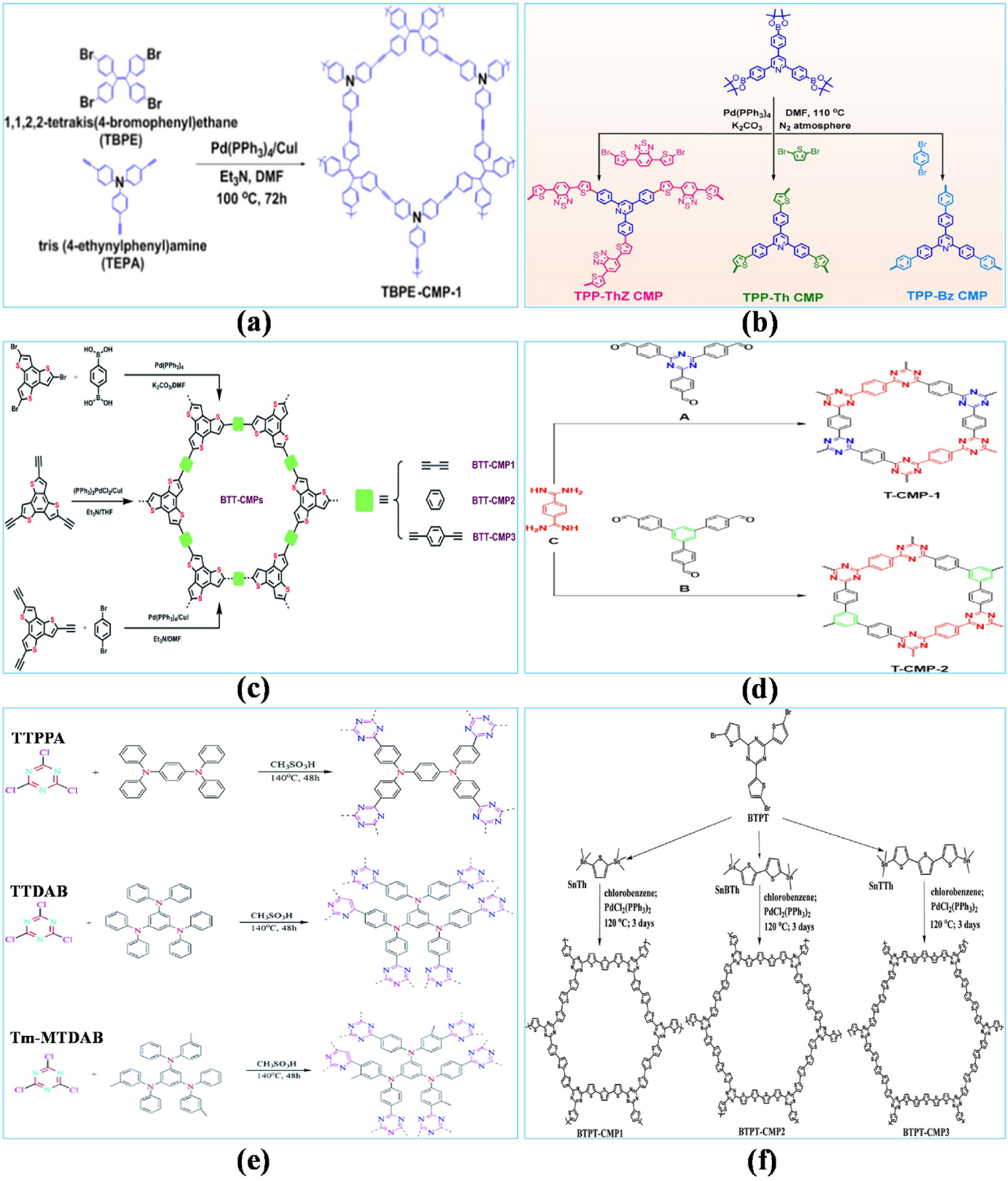

Fig. 9. (a) Schematic mechanism of tetraphenylenthene-based CMPs [217], Copyright © 2020, American Chemical Society. (b) Synthetic process of the TPP-based CMPs [221], Copyright © 2023, Royal Society of Chemistry. (c) Synthesis of BTT-CMPs [222], Copyright © 2021, Royal Society of Chemistry. (d) Synthetic process of T-CMP-1 and TCMP-2 [230], Copyright © 2021, American Chemical Society. (e) Synthesis of TTPPA, TTDAB, and Tm-MTDAB using the Friedel-Crafts process catalyzed by methane-sulfonic acid [231], Copyright © 2024, Royal Society of Chemistry. (f) Schematic mechanism of BTPT-CMP$_1$, BTPT-CMP$_2$ and BTPT-CMP$_3$ [232], Copyright © 2022, Royal Society of Chemistry.

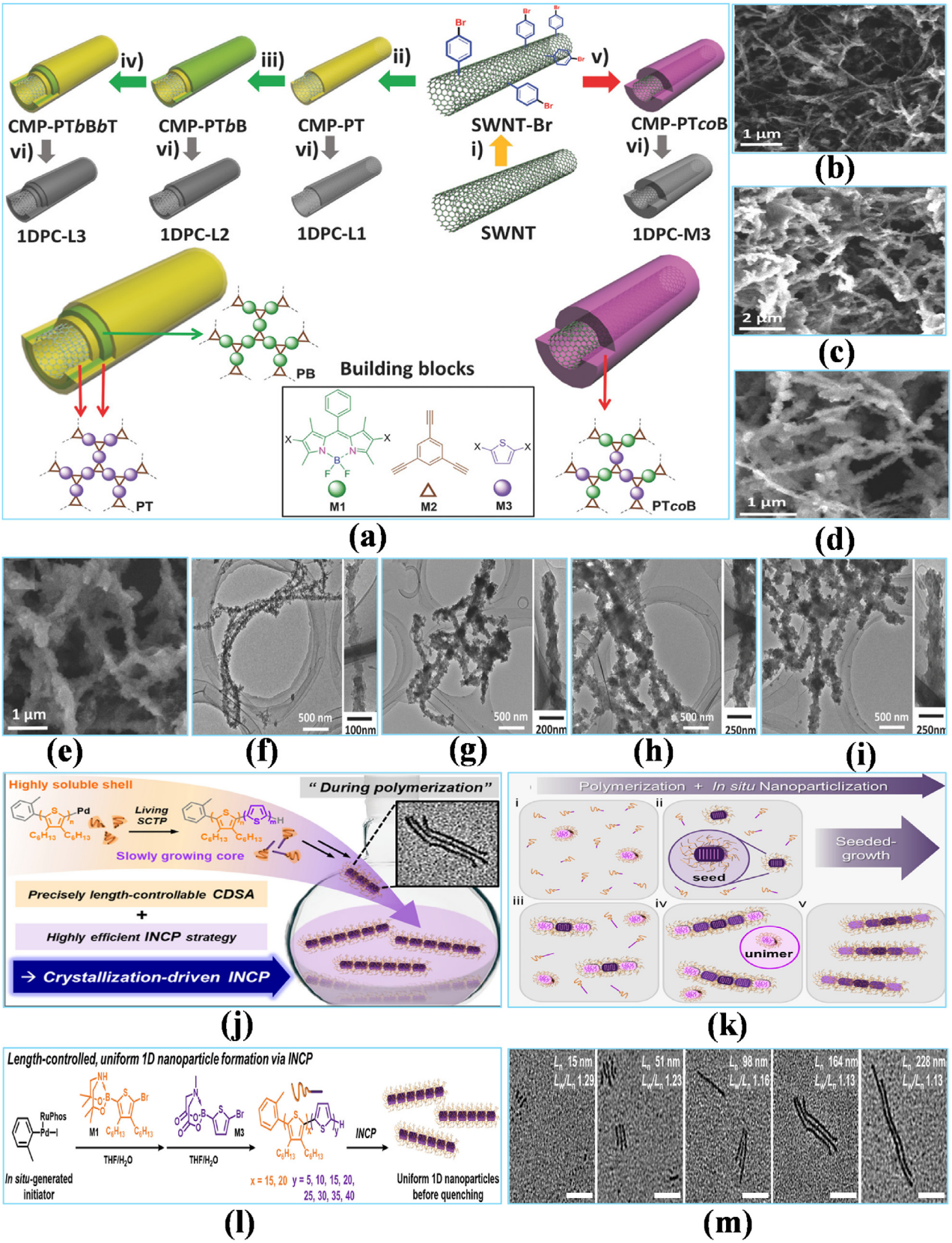

Fig. 10. (a) Randomized and layer-by-layer controlled synthesis of 1D CMPs. i) 4-Bromobenzenediazonium tetrafluoroborate, ambient calcination, 2 h; ii) nitrogen, M_2, M_3, $Pd(PPh_3)_4$, CuI, Et_3N, DMF, 80 °C, 72 h; iii) nitrogen, M_2, M_1, $Pd(PPh_3)_4$, CuI, Et_3N, DMF, 80 °C, 72 h; iv) nitrogen, M_2, M_3, $Pd(PPh_3)_4$, CuI, Et_3N, DMF, 80 °C, 72 h; v) nitrogen, M_1, M_2, M_3, $Pd(PPh_3)_4$, CuI, Et_3N, DMF, 80 °C, 72 h; and vi) nitrogen, pyrolyzed at 800 °C for 2 h. Structural analysis of the as-synthesized 1D CMPs: SEM and TEM analysis of (b, f) CMP-PT; (c, g) CMP-PT*b*B; (d, h) CMP-PT*b*B*b*T; (e, i) CMP-PT*co*B [243], Copyright © 2016, John Wiley & Sons. (j) Scheme depicting the synthesis of semiconductor 1D CP; (k) Proposed mechanism of CD-INCP; (l) Schematic illustration; (m) of narrow dispersed 1D Cp synthesized from P34DHT-*b*-PTs [244], Copyright © 2022, American Chemical Society.

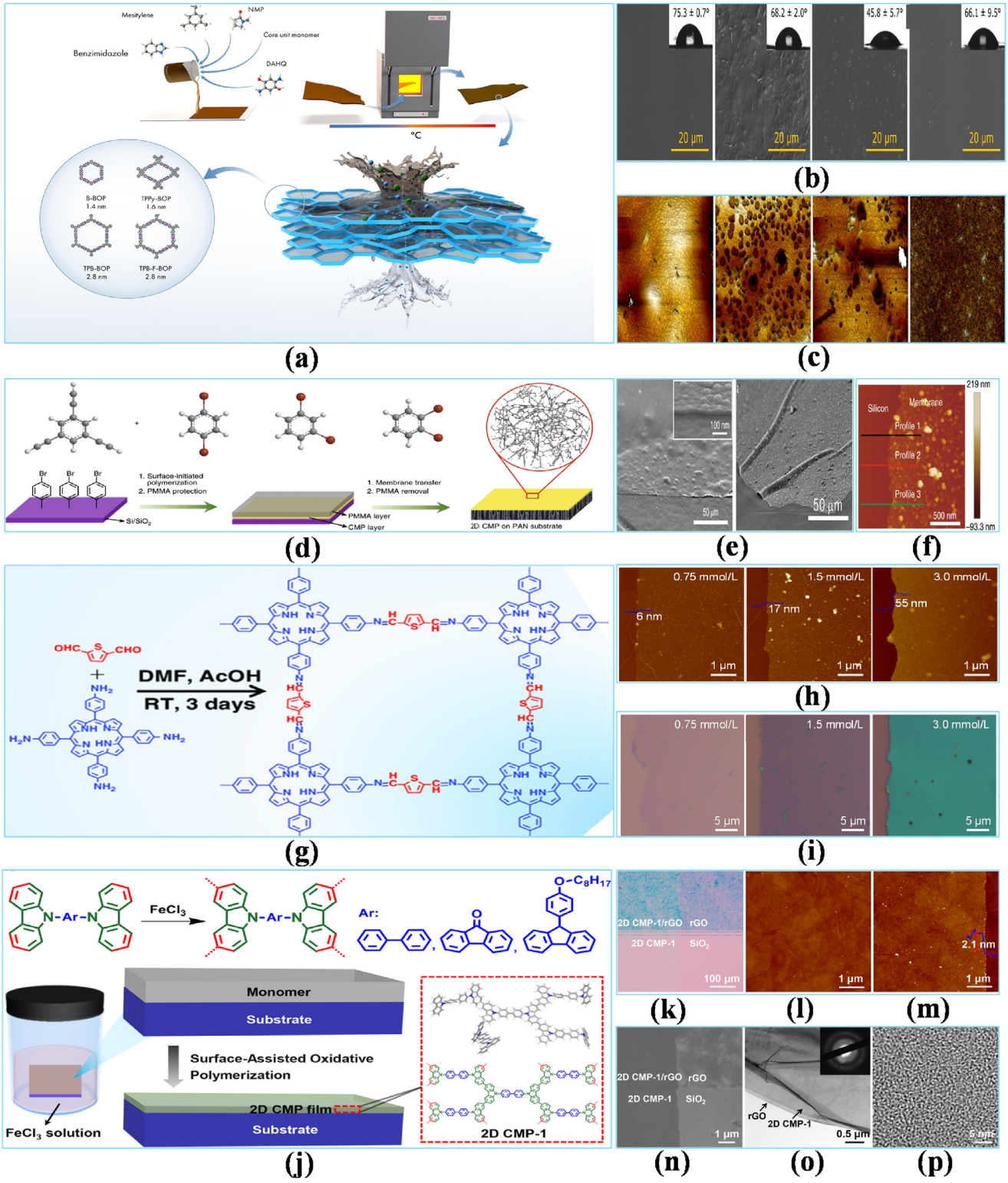

Fig. 11. (a) The mechanism for synthesizing benzobisoxazole-linked CMP freestanding membranes for organic solvent nanofiltration; Configurations of the 2D CMP membranes (b) SEM analysis; (c) AFM analysis [256], Copyright © 2023, Elsevier. (d) Illustrative schematics depicting the process of surface-initiated polymerization to yield 2D CMP films on the Si/SiO_2 substrate; corresponding (e) SEM analysis; (f) AFM analysis [257], Copyright © 2020, Springer Nature. (g) Graphical illustration of the synthesis of 2D CMP films by the condensation of Tapy units (blue) and ThCHO cells (red); (h) AFM images of CMP films on rGO surfaces and the corresponding thicknesses; (i) Optical micrographs of CMP films on SiO_2/Si substrates [258], Copyright © 2019, John Wiley & Sons. (j) A graphical illustration of the formation of cross-linkage 2D CMP films by $FeCl_3$-catalyzed surface-initiated oxidative polymerization; Characterization of 2D CMP-1 deposited on rGO film; (k) An optical microscopic image of 2D CMP-1 pasted on rGO film; Four distinct zones are shown: 2D CMP-1/rGO heterojunction, rGO sheet, 2D CMP-1, and pure SiO_2; (l) AFM image of the rGO film; (m) AFM image and altitude pattern of 2D CMP-1 formed on rGO film; The Z levels in (l) and (m) are 20 nm; (n) SEM images of the 2D CMP-1/rGO heterojunction, rGO film, 2D CMP-1, and bare SiO_2; (o) A TEM image of the 2D CMP-1/rGO heterojunction hung on a copper matrix. Inset: The appropriate SAED design; (p) HR-TEM image of the 2D CMP-1/rGO heterojunction [259], Copyright © 2018, American Chemical Society.

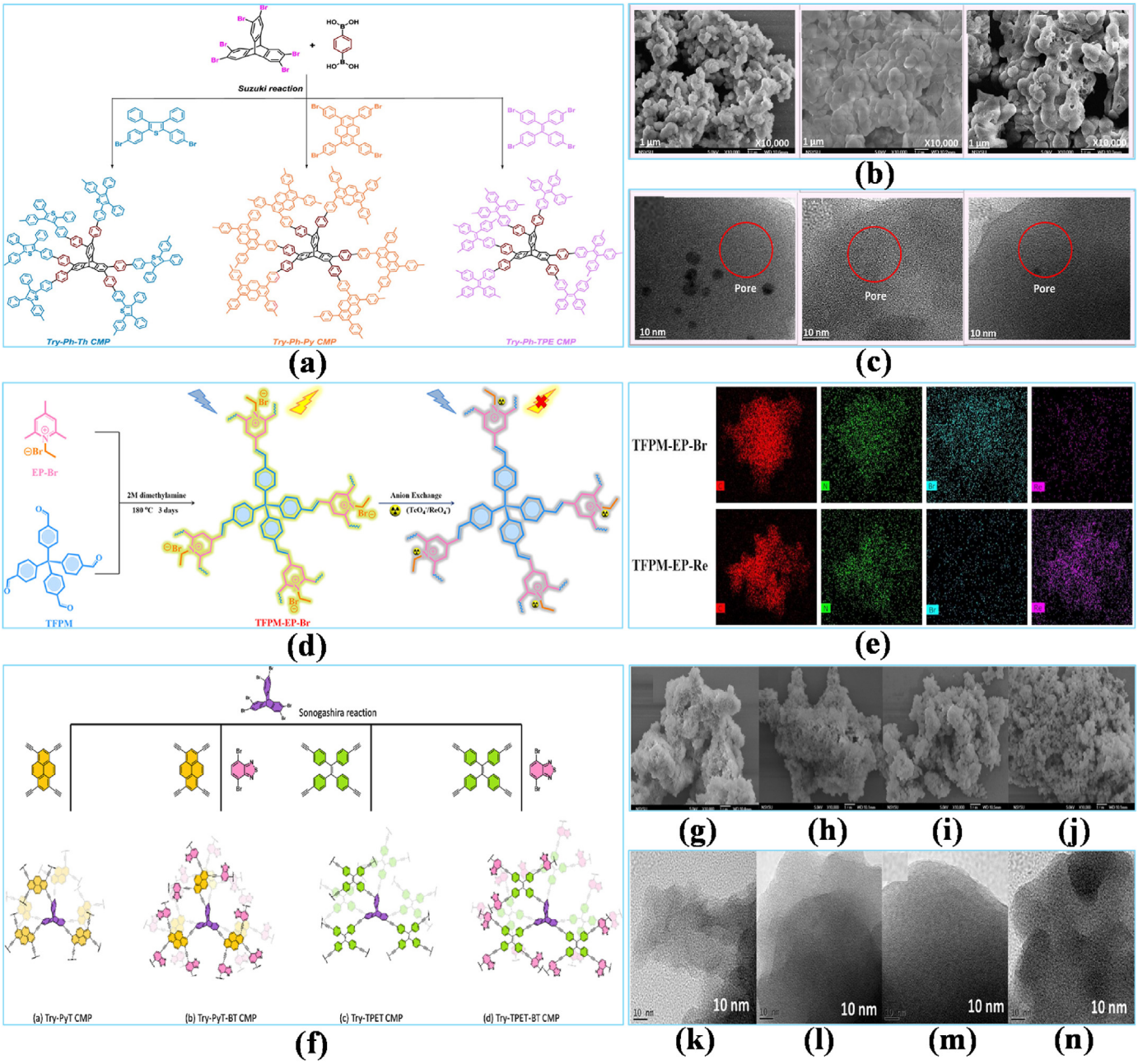

Fig. 12. (a) Schematic illustration of the steps involved in the synthesis of Try-Ph-Th, Try-Ph-Py, and Try-Ph-TPE 3D CMPs, and their analogues (b) SEM analysis; (c) AFM analysis [269], Copyright © 2022, American Chemical Society. (d) The synthesis process of TFPM-EP-Br for detecting and absorption of TcO_4^-/ReO_4^-; (e) TEM-EDS maps of TFPM-EP-Br and TFPM-EP-Re [270], Copyright © 2022, American Chemical Society. (f) The synthesis process of four triptycene (Try)-based 3D CMPs; (g, k) SEM and TEM of Try-PyT, (h, l) Try-PyT-BT, (i, m) Try-TPET, and (j, n) Try-TPET-BT CMPs [271], Copyright © 2023, American Chemical Society.

CMPs to produce polymers with unique structures [136]. Recent research has explored methods of post-functionalization for CMPs, including the production of size-confined particles via micro-emulsion and mesoporous substrates [137]. These materials demonstrate enhanced properties such as water solubility, electrical conductivity, fluorescence, and functionality. The photoelectrical properties of CMPs largely depend on their chemical orbital structure, with internal functional conjugated size being a major determinant. To optimize the spatial structure of organic semiconductors and improve their photoelectric efficiency, confined polymerization can improve conjugation elongation and polymer structure. This approach allows for the production of CMPs with superior photocatalytic performance [138,139]. Zhang et al. [140] prepared TPATTh-based CMPs through an easily synthesized method of C-H-directed arylation polymerization (DAP). This method includes thiophene-flanked amine, tris[4-(2-thienyl)phenyl]amine (TPATTh), and strategically accessible multi-brominated aryls, such as 2,2',7,7'-tetrabromo-9,9'-spirobifluorene (TBrSBF), 1,3,6,8-tetrabromopyrene (TBrPy), and 2,5-dibrom. The resultant TPATTh-based CMPs exhibit high thermal strength. The structure of the multi-brominated aryls enhances the porosity of the TPATTh-based CMPs. Both solid and solvent-dispersed TPATTh-based CMPs have strong fluorescence-emitting properties, displaying a range of colors under 365 nm light. They were utilized to detect fluorescence in I_2, PA, DNP, and o-NP with elevated Stern-Volmer quench factors (Ksv) (Fig. 7a) [140]. You et al. [119] synthesized amine-based CMPs as photocatalysts using a similar process. Results showed that electrical conductivity, optoelectronic properties, and band gap

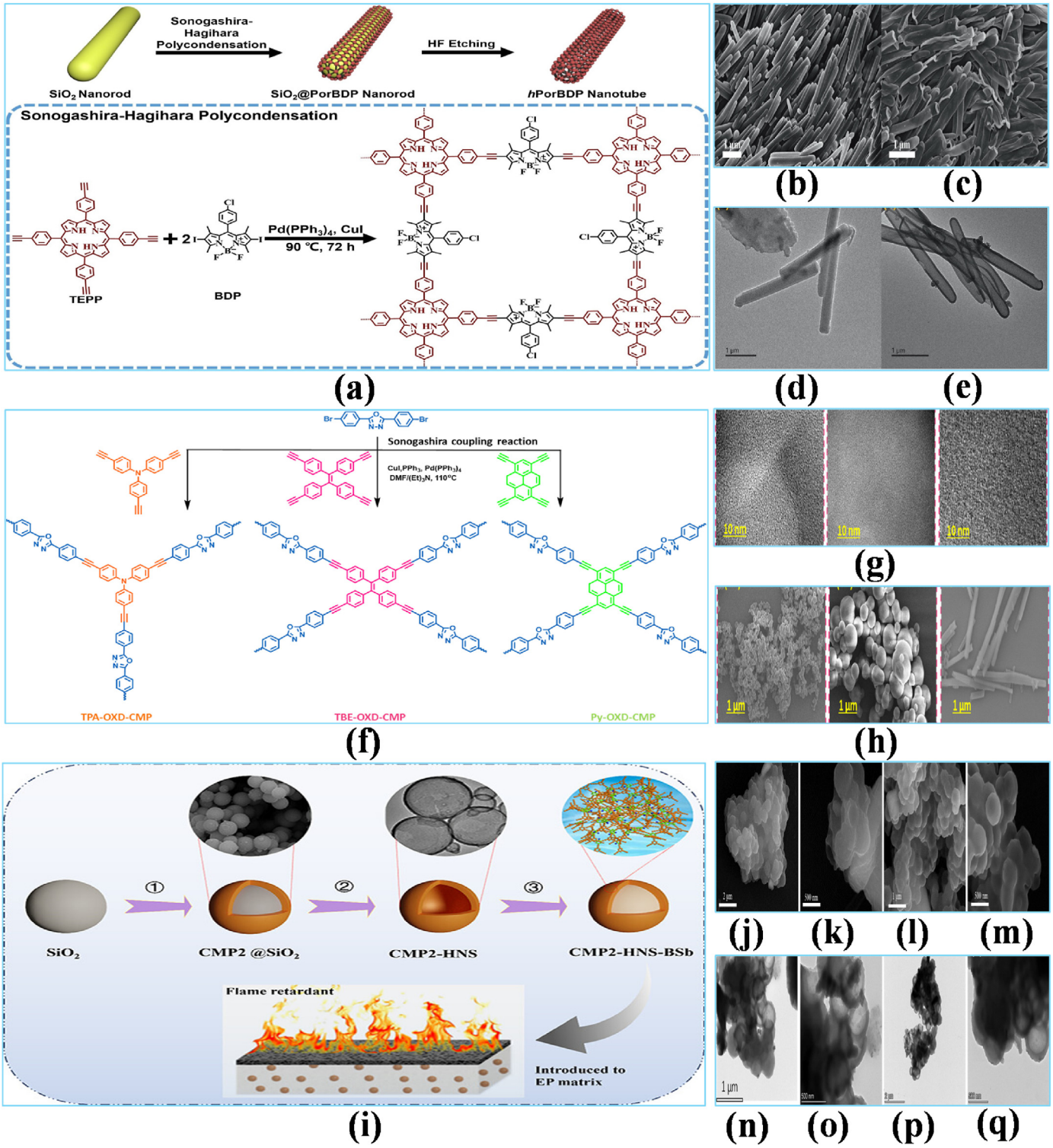

Fig. 13. (a) Synthetic routes for *h*PorBDP nanotube; FE-SEM and TEM of (b, d) SiO_2@PorBDP NRs; (c, e) *h*PorBDP NTs [285], Copyright © 2023, Elsevier. (f) Synthesis; (g) SEM; (h) TEM of TPA-OXD, TPE-OXD, and Py-OXD-CMPs [286], Copyright © 2022, American Chemical Society. (i) Synthesis route of CMPs-HNS; (j, k) SEM images of CMP_1-HNS-BSb; (l, m) SEM images of CMP_2-HNS-BSb; (n, o) TEM images of CMP_1-HNS-BSb; (p, q) TEM images of CMP_2-HNS-BSb [287], Copyright © 2024, American Chemical Society.

composition were all improved when the confined size of H-PyB CMPs was reduced, leading to more efficient crosslinking between polymeric monomers. Experiments with ultraviolet illumination demonstrated that these organic semiconductors could selectively oxidize amines. Moreover, the photocatalytic efficiency of these confined CMPs was influenced by changes in their size, with the photocatalytic oxidation of amines being enhanced by tiny hollow particles (Fig. 7b).

2.4.2. *Anthraquinone-based CMPs*

CMPs have been designed as promising photoactive polymers due to their broad π-conjugated structures and abundant porosities [141]. Their structural versatility opens up opportunities for efficiently controlling the

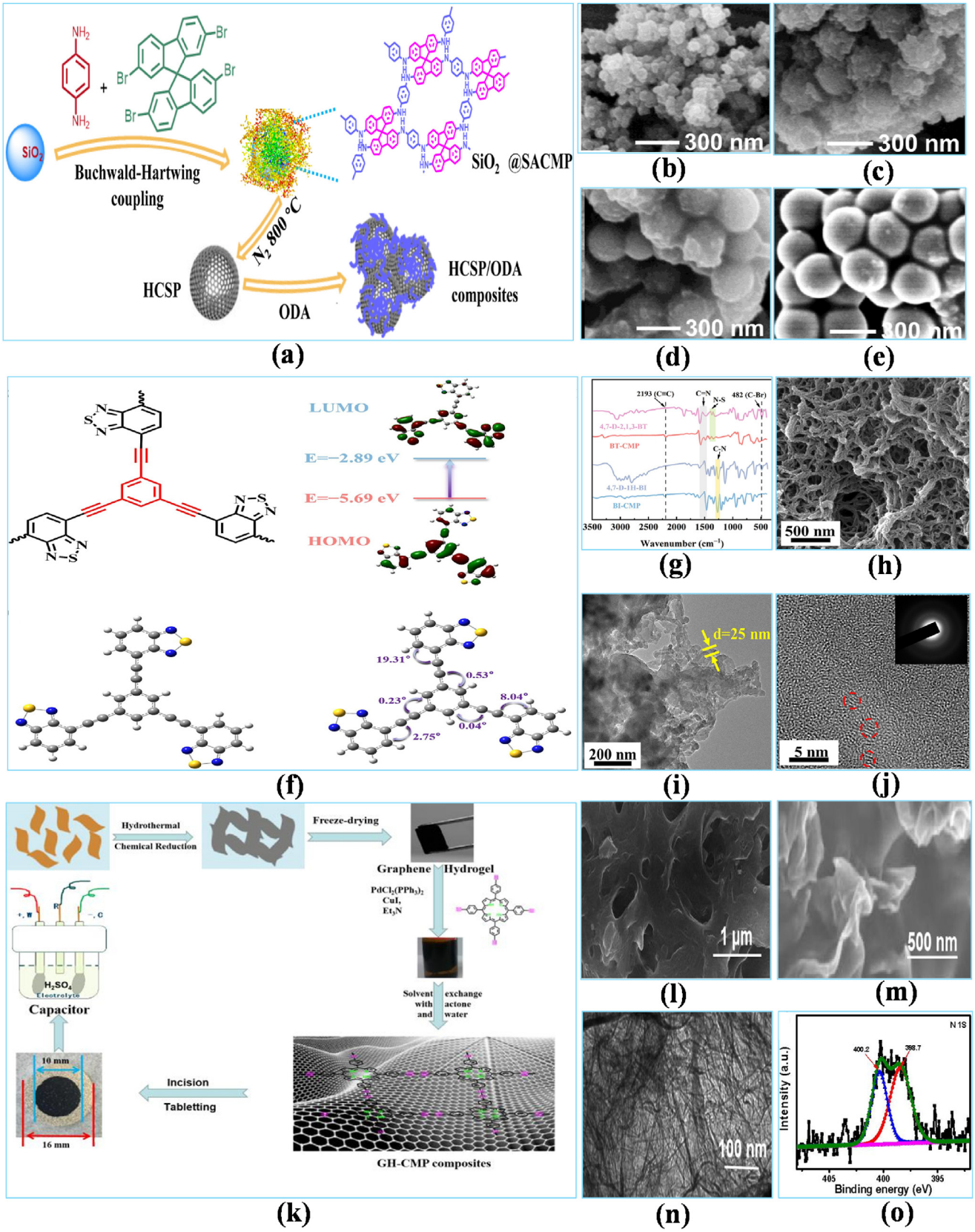

Fig. 14. (a) Graphical description of the formation of SiO_2@SACMPs, HCSPs, and HCSP/ODA composites; SEM of: (b–e) SEM of as-synthesized materials [161], Copyright © 2021, Elsevier. (f) The HUMO, LUMO distributions, and molecular space configuration of BT-CMP; (g) FT-IR spectra (h) SEM; (i) TEM; (j) HR-TEM of BT-CMP [290], Copyright © 2024, Elsevier. (k) Conceptual process for synthesizing GH-CMP composites and synthesizing GH-CMP electrode-based capacitors; (l, m) SEM; (n) TEM; (o) XPS of CP-CMP composite [291], Copyright © 2019, John Wiley & Sons.

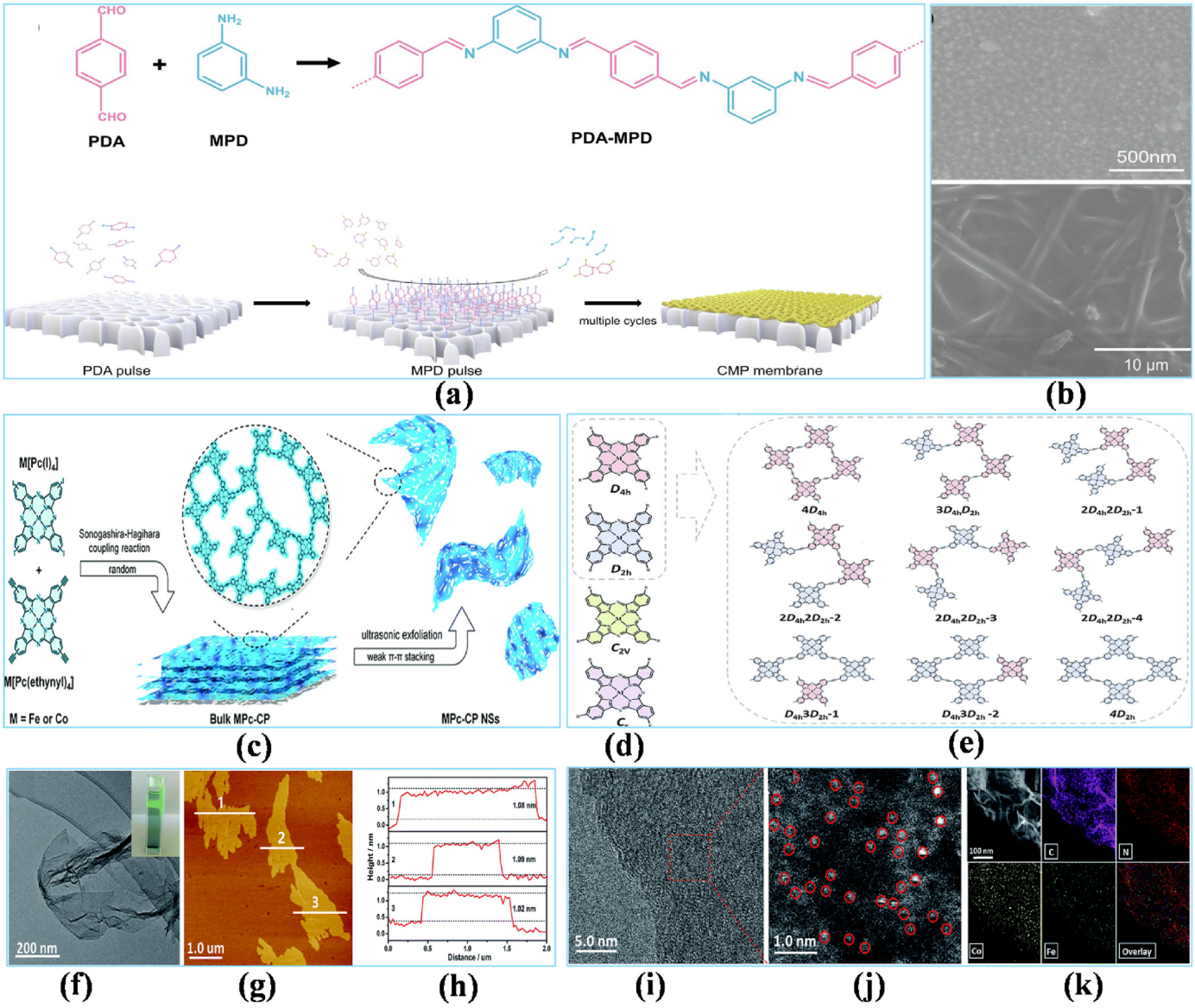

Fig. 15. (a) Formation of CMP by condensation polymerization of aldehyde monomer PDA and amine-based monomer MPD; SEM image of the large-area CMP membrane [297], Copyright © 2024, Elsevier. (c) The synthesis of the MPc/CP films; (d) Four types of isomers (with D_4h, D_2h, C_2v, and Cs identity) for tetra-β-replaced phthalocyanines are shown; (e) Four phthalocyanine atoms with D_4h or D_2h identities were used to synthesize nine quadruple patterns; (f) TEM of $Fe_{0.5}Co_{0.5}Pc/CP$ materials. Inset: illustration of the Tyndall impact of the $Fe_{0.5}Co_{0.5}Pc/CP$ materials; (g) AFM and (h) the equivalent elevation features of $Fe_{0.5}Co_{0.5}Pc/CP$ materials; (i) AC STEM and (j) larger depiction of $Fe_{0.5}Co_{0.5}Pc/CP$ materials; (k) HAADF-STEM and elemental depiction [301], Copyright © 2019, Royal Society of chemistry.

activity of CMPs by introducing specific units into their π-conjugated structures. These adaptable combinations enable CMPs to exhibit enhanced optoelectronic properties [142]. CMPs have been utilized in numerous fields due to their exceptional physicochemical stability and ease of processing [143]. Donor-acceptor (D-A) form CMPs were previously documented to exhibit enhanced photocatalytic performance [144]. This enhancement is attributed to their exceptional capacity for charge distribution and dissociation, facilitated by the improved electron push-pull effect. By modifying the steric hindrance experienced by fundamental elements and improving the uniformity and polarization of CMPs, introducing an π-bridge facilitates charge isolation and enhances electronic delocalization [145]. Thus, incorporating a π–bridge into D-A form CMPs is a viable approach to creating more efficient photocatalysts. Pyrene, being an entirely π-coupled polycyclic aromatic hydrocarbon, facilitates the free flow of charge particles and allows for simple dissociation [146]. The optical properties of pyrene have made it a popular material for use in organic photovoltaics and organic LEDs [147]. Utilizing pyrene-based CMPs for photocatalysis has been a hot topic recently due to their compositional diversity, extended excited-state lifetime, and strong electron-enrich properties [148]. Additionally, anthraquinone has been extensively applied in batteries and optoelectronic systems [149] owing to its renowned reversible redox properties in the dominating H_2O_2 synthesis domain. Anthraquinone can be utilized for photocatalytic hydrogen gas emission and selected organic synthesis due to the significant fluidity of charges facilitated by its aromaticity and rigidity surface [150]. Dong et al. [151] incorporated alkynyl moieties between pyrene and anthraquinone, resulting in Py-π-AQ-CMP. Theoretical calculations suggest that introducing alkynyl groups improves the symmetric π-conjugation and mitigates steric hindrance. Py-π-AQ-CMP exhibits improved distribution of charged particles due to its extended π-conjugation, leading to higher optical reactivity and a narrower band gap. Py-π-AQ-CMP photocatalysis enables the selectivity oxidizing of organic

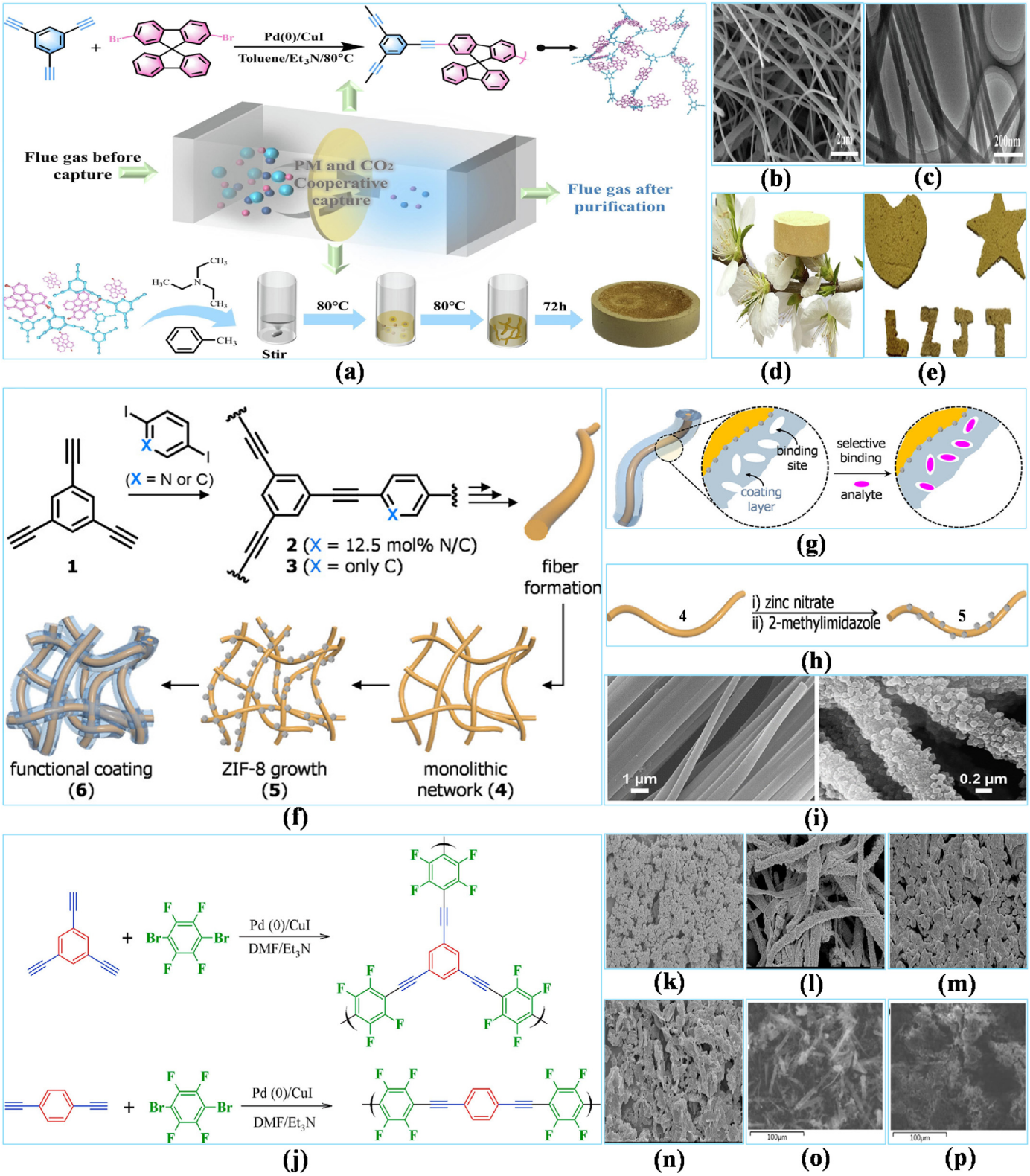

Fig. 16. (a) Synthetic process of DS-CMP; (b) SEM analysis of DS-CMPs (scale: 2 μm); (c) TEM analysis of DS-CMPs (scale: 200 nm); (d) Image of DS-CMPs resting on flowers; (e) Various forms of DS-CMPs [311], Copyright © 2024, Elsevier. (f) A hypothetical illustration of the hierarchical integration of fibrous polymeric monoliths. Monolith 4 is made up of micro-porous composite containing N_2 particles (2), which were generated using (i) bottom-up synthesized from 1 and (ii) an in-situ self-assembled approach; composite 3 is a comparator sample made without any enriched N_2 particles. The hybridized fiber system 5 is formed through encapsulating with ZIF-8 nanocrystals, while the functioning covering on the fibers creates a functional monolith 6 that demonstrates molecular detection properties; (g) Illustration of the binding activities in 6. The functioning, flexible structure in 6 exhibits preferential binding affinity to a particular analyte; (h) ZIF-8 nanocrystals are used to encapsulate a single fiber in 4 to design 5 utilizing zinc nitrate and 2-methylimidazole; (i) Shape of fibers in 4 (left) and 5 (right) determined with SEM at 50, 000 × resolution [312], Copyright © 2021, American Chemical Society. (j) Synthetic process of FCMPs; SEM analysis of FCMP-1 in (k) DMF; (l) toluene and FCMP-2 in (m) DMF; (n) toluene. Scale bar: 1 μm; The SEM/EDX of (o) FCMP-1; (p) FCMP-2. Scale bar: 100 μm [313], Copyright © 2018, Elsevier.

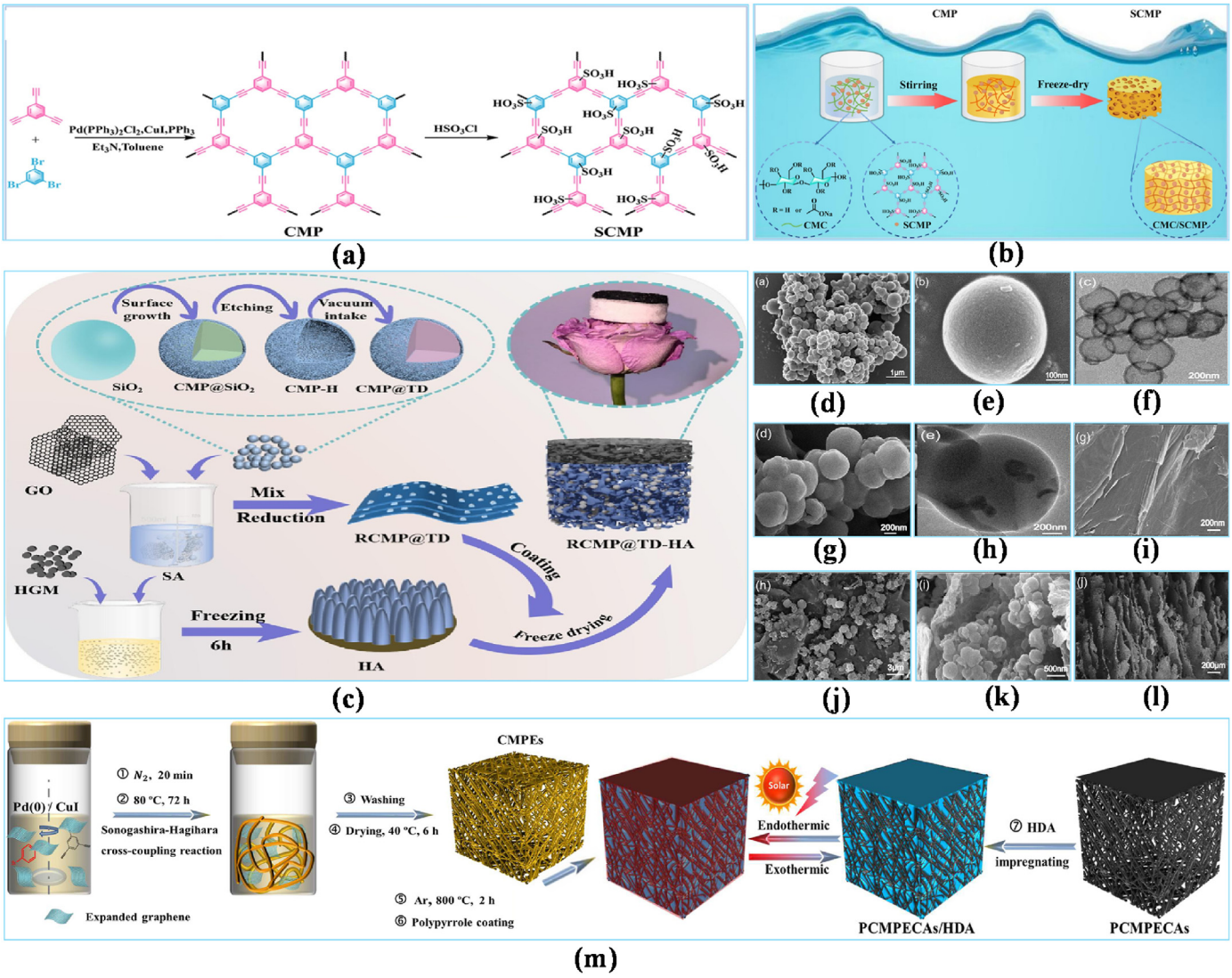

Fig. 17. Schematic mechanism of (a) CMP; SCMP and (b) CMC/SCMP composite hydrogel [334], Copyright © 2023, Elsevier. (c) Graphical illustration of the synthesis of RCMP@TD-HA; Structural analysis of CMP-H, CMP@TD, GO, RCMP@TD, HA, and RCMP@TD-HA. SEM analysis of (d, e) CMP-H at different scales (scale bar: 1 μm; 100 nm), TEM images of (f) CMP-H (scaling size: 200 nm) and (h) CMP@TD; (g) CMP@TD (scaling size: 200 nm), (i) GO nanosheets (scale size: 200 nm); (j, k) RCMP@TD at different scales (scale size: 3 μm; 500 nm); (l) (k) HA at different scales (scale size: 200 μm; 10 μm) [335], Copyright © 2024, Elsevier. (m) Schematic representation of the synthesis of PCMPECA and PCMPECAs/HDA composites [336], Copyright © 2022, Elsevier.

sulfides in methanol. Notably, the performance of Py-π-AQ-CMP, activated by blue light, is almost twice as high as that of Py-AQ-CMP without the alkynyl π-bridge. Mechanical studies demonstrate that electron and energy transitions are involved in the stimulation of dioxygen for sulfide oxidation (Fig. 7c).

2.4.3. *Boranil-based CMPs*

Pristine organic dyes are gaining popularity as effective "non-metallic" photo-redox catalysts, with benefits such as broad photon absorption and tunable structure [152]. Boron-based fluorophores, such as boron-dipyrromethene (BODIPY) and other chelated structures, have evolved as attractive photocatalysts owing to their excellent quantum productivity, variable absorption/emission frequencies, and photostability [153]. However, synthetic dye-based uniform photocatalysts face limitations such as high costs, complex separation methods, and photo-bleaching effects, which hinder their commercial production [154]. Integrating organic pigments into CMPs presents a viable solution to these problems by capitalizing on the tunable structure, controlled porosity, minimal mass, and chemical stability of CMPs [155]. While some CMPs have incorporated boron-based dyes, only those tailoring the BODIPY modification exhibit specific photocatalytic properties. Nevertheless, the light-harvesting properties of BODIPY dyes are limited due to their confined Stokes shifts, which result in significant self-absorption. Consequently, the known organic transformations enhanced by BODIPY-based CMPs are limited to the oxidation of specific molecules [156]. Gong et al. [157] reported the engineering and synthesis of a novel CMP based on a boranil dye, which was used as an effective heterogeneous photocatalyst. Compared to their dye-free variants, the as-synthesized materials demonstrated enhanced photocatalytic efficiency in the aerobic oxidation of amines and sulfides. Additionally, they possessed a small optical bandgap, broad visible-light absorption, and an improved planar π-conjugation, which can be attributed to the boron complexation (Fig. 7d).

2.4.4. *Cyanine-based CMPs*

Metallophthalocyanines (MPcs), macrocyclic polymers with a uniform 18-π electron conjugated structure, have been widely studied as potential photosensitizers due to their exceptional absorption properties in the longer-wavelength visible range [158]. However, their large π-conjugated structures lead to significant π-π stacking interactions,

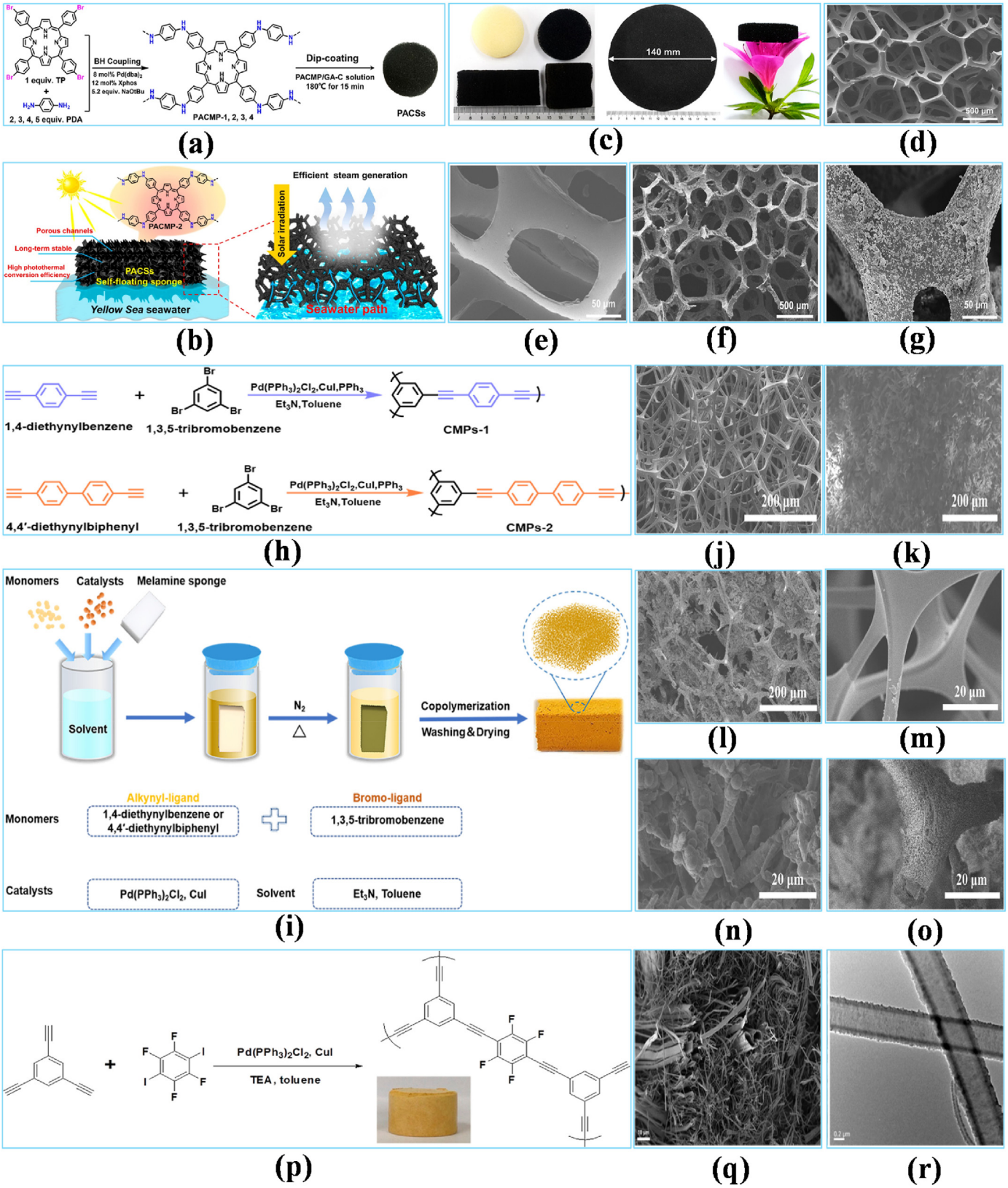

Fig. 18. (a) Synthesis scheme of PACMPs and PACSs; (b) Structural design of PACSs as a solar thermal evaporator; Images of (c) PU sponge and PACS, with PACS in various forms and dimensions; SEM analysis of (d, e) PU sponge; (f, g), PACS-120 [365], Copyright © 2022, American Chemical Society. (h) Synthesis schemes for CMPs; (i) Synthetic process of CMPs@sponges; SEM analysis of the (j, m) Melamine sponge; (k, n) CMPs-1@sponge; (l, o) CMPs-2@sponge [366], Copyright © 2022, John Wiley & Sons. (p) The reaction strategy and photographic representation of the synthesis of MOP sponge; (q) SEM; (r) TEM analysis of MOP sponge [367], Copyright © 2022, American Chemical Society.

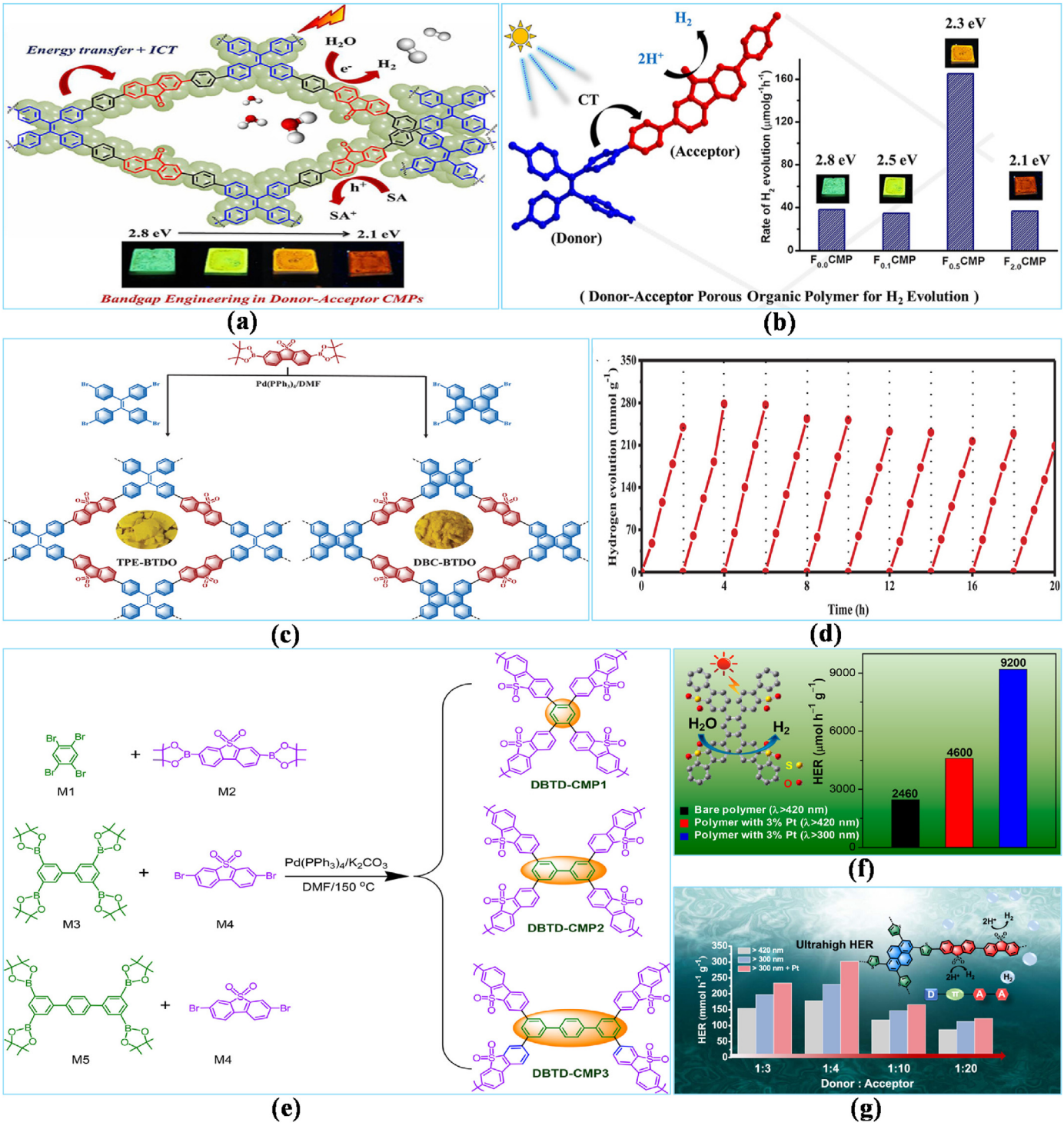

Fig. 19. (a) Schematic illustration of F_xCMPs demonstrating the energy-transfer-based intra-ligands charge-transfer emission that regulates the bandgap over a broad range and permits photocatalytic H_2 production during visible light; (b) D-A porous organic polymer for HER [409], Copyright © 2019, John Wiley & Sons. (c) The synthetic approaches for both of the polymers and the hypothetical configurations (insets: images of the as-prepared polymers); (d) Stabilization assessment of DBC-BTDO containing 1.0 wt% Pt (λ > 300 nm) [410], Copyright © 2022, John Wiley & Sons. (e, f) Synthesis of the CMPs and the related structure [21], Copyright © 2018, American Chemical Society. (g) Synthetic process of the D-π-A-A-type CMPs and associated structure [411], Copyright © 2023, American Chemical Society.

which cause aggregation and limit their singlet oxygen ($^1O_2$) production efficiency by hindering effective interaction with oxygen molecules. Recently, enormous research has been done on microporous polymers derived from organic precursors due to their exceptional efficiency and diverse range of applications. CMPs are a family of porous materials that achieve porosity through cross-linking and π-conjugation [102]. Ding et al. [159] identified new MPc-CMPs as effective photosensitizers for producing $^1O_2$. The rigid microporous design of these MPc-CMPs significantly enhances the contact between most MPc units and oxygen. Additionally, their expanded π-conjugated structures improve light absorption in the far-red spectrum. The microporous structure and superior absorption properties of MPc-CMPs for longer-wavelength radiation result in significant performance for $^1O_2$ production under 700 nm light, as demonstrated using 1,3-diphenylisobenzofuran as a $^1O_2$ trap. Thus,

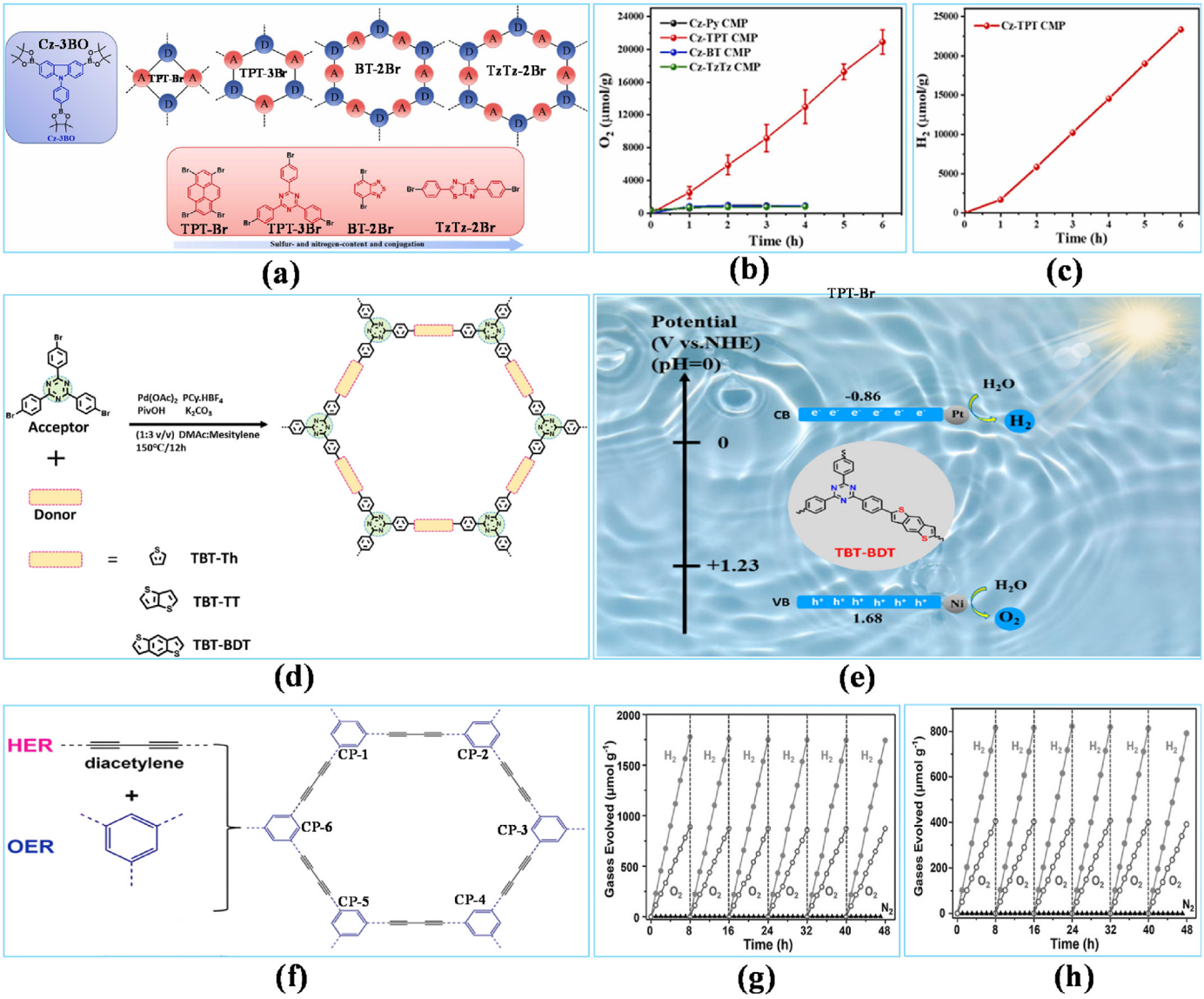

Fig. 20. (a) Synthetic approach for D-A CMPs; (b) The OER of Cz-TPT CMP (2 mg) under visual light in the existence of $AgNO_3$ (0.03 M, 10 mL) and La_2O_3 (8 mg); (c) The HER of Cz-TPT CMP (1 mg) under visible light in the existence of AA (10 mL, 0.1 M) and 2 % Pt [430], Copyright © 2022, Elsevier. (d) The synthesis of TBT-Th, TBT-TT, TBT-BDT; (e) The photocatalytic mechanism of TBT-BDT [431], Copyright © 2023, Elsevier. (f) 2D CPs are synthesized from the molecular linkages that are synthesized from diacetylene and benzene [432], Copyright © 2023, Royal Society of Chemistry. (g, h) Stability performance of HER and OER of PTEPB and PTEB under visible light irradiation [254], Copyright © 2017, John Wiley & Sons.

MPc-CMPs are highly effective photosensitizers for producing $^1O_2$ (Fig. 7e).

2.4.5. Fluorene-based CMPs

CMPs are attractive electrode polymers for electrochemical power generation, but their low redox efficiency and electrical porosity limit their performance [160]. Buchwald-Hartwig (BH) coupling has recently synthesized redox-active N-enriched CMPs by forming C-N bonding via Pd-catalyzed linking of aryl bromides and amines [161]. Because of the elasticity of C-N bonding, it is necessary to carefully choose building blocks of appropriate length and stiffness for synthesizing CMPs with significant surface area via BH coupling [162]. Liao et al. [163] revealed that polyaminoanthraquinone (PAQ) systems produced by BH coupled had a wide surface area and controllable redox response, making it an effective electrode material for both electrically double-layer capacitance and pseudo-capacitive applications. Lyu et al. [164] synthesized CMPs from the Buchwald-Hartwig coupling process, utilizing a spirobifluorene bromide nucleus and p-phenylenediamine precursors (SACMPs), then bonded them onto multi-walled carbon nanotubes (MWCNTs) via one-step in-situ polymerization. The resultant hybrid (MWCNT/SACMP) has a significant surface area (514 $m^2\ g^{-1}$), outstanding redox potential, and suitable conductivity. Significantly, the specific conductivity of MWCNT/SACMP is 594 F g^{-1} at a current intensity of 1.0 A g^{-1}, representing a 252 % enhancement over SACMP solely (236 F g^{-1}) at a MWCNT concentration of approximately 10 wt%. Furthermore, a symmetrical two-electrode supercapacitor made of MWCNT/SACMP has a specific capacity of 254 F g^{-1} and an electricity efficiency of 28.53 W h kg^{-1} at 900 W kg^{-1}, with 84.38 % capacitance retention after 6000 cycles (Fig. 7f and g).

2.4.6. Naphthalene-based CMPs

There is an urgent demand for sustainable energy sources to highlight the environmental degradation produced by using fossil fuels [166]. Supercapacitors combine conventional capacitors and batteries by using electrostatic interactions between electrolyte molecules and carbon electrodes to store and retain energy [167]. Carbon nanotubes (CNTs) are

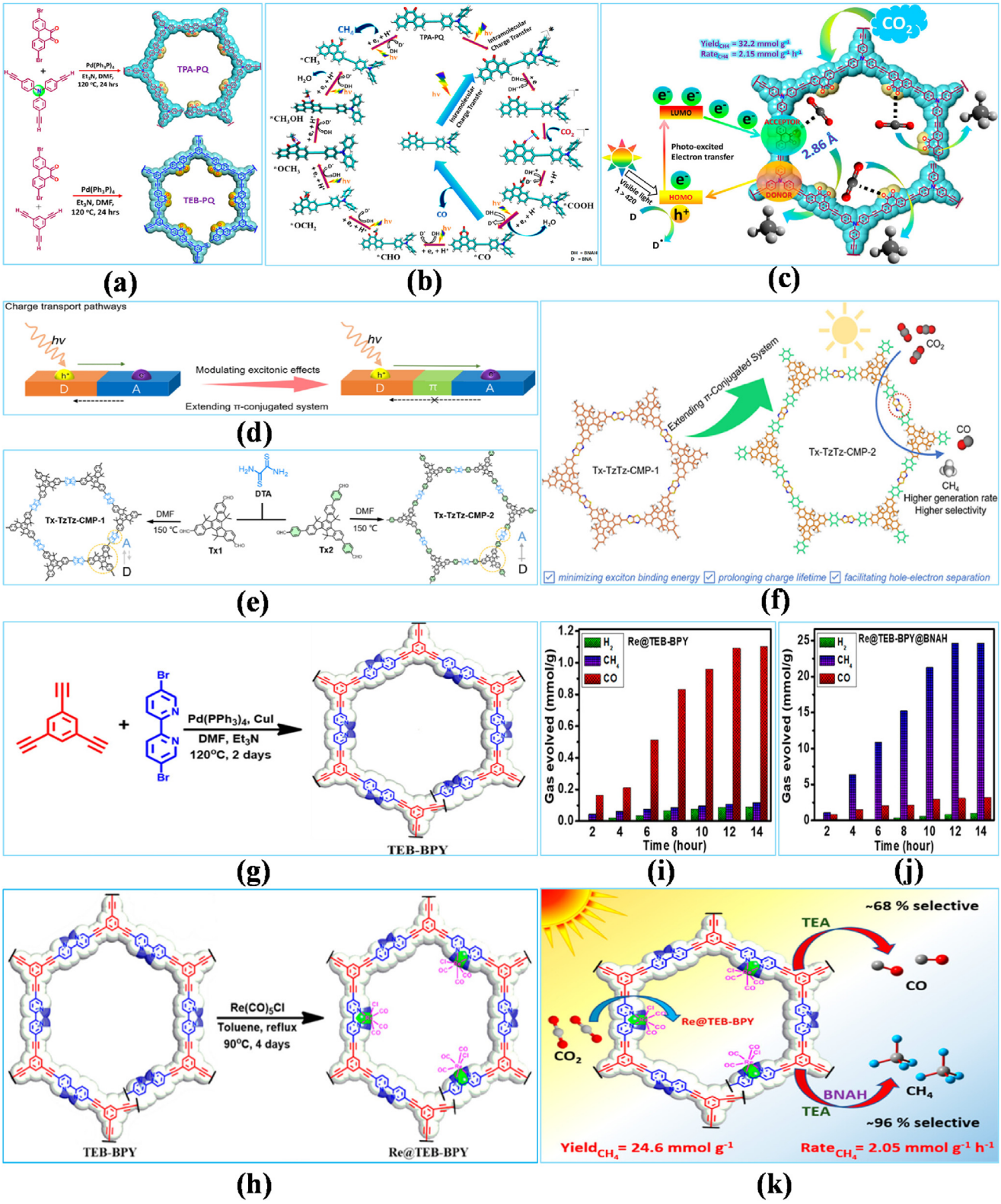

Fig. 21. (a) Synthetic process of TPA-PQ and TEB-PQ using a C-C coupled process; (b) Proposed catalytic cycle using the various reactive intermediates; (c) Graphical representation of photoreduction of CO_2 using a D-A CMP for rapid and effective CH_4 production [449], Copyright © 2021, American Chemical Society. (d) Graphical depiction of photogenerated charge transfer channels in the D-A and D-p-A networks. Prolonged π-conjugated delocalization modulates excitation, increasing charge carrier migration duration; (e) The synthesis of T_x-T_zT_z-CMP-1 and $T_xT_zT_z$-CMP-2 composite; (f) Schematic mechanism of T_x-T_zT_z-CMP-1 and $T_xT_zT_z$-CMP-2 [450], Copyright © 2023, American Chemical Society. Synthetic approach for synthesizing (g) TEB-BPY; (h) Re@TEB-BPY; Photocatalytic activity of Re@TEB-BPY (i) Quantity profile without BNAH; (j) Quantity profile with BNAH; (k) Schematic mechanism of CO_2 reduction based on Re(I)-integrated CMP [451], Copyright © 2023, American Chemical Society.

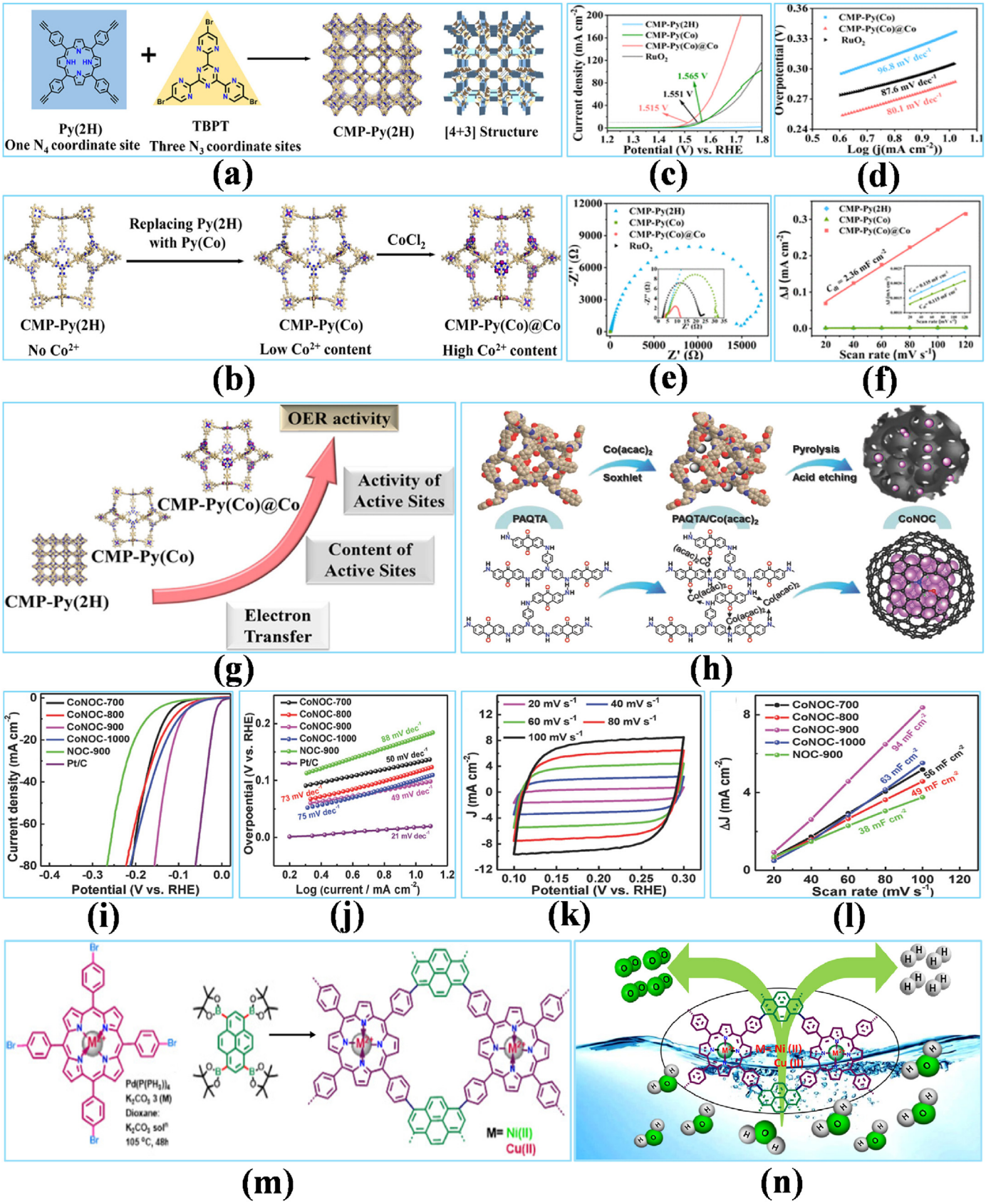

Fig. 22. (a) Graphical illustration of the synthesis of (a) non-metal CMP-Py(2H); (b) metaled CMP-Py(Co) and CMP-Py(Co)@Co containing various Co^{2+} ratios; (c) OER polarized structures; (d) Tafel graphs; (e) Nyquist charts of CMPs and RuO_2; (f) Graphs for determining the C_{dl} of CMPs; (g) Schematic mechanism of CMPs [471], Copyright © 2024, American Chemical Society. (h) Synthesis of CoNOCs; (i) Polarization profiles; (j) Tafel graphs produced in 0.5 m H_2SO_4; (K) CV patterns of CoNOC-900; (l) Scan rate-dependent capacitive current density [472], Copyright © 2018, John Wiley & Sons. (m, n) Synthesis and graphical illustration of Ni-Por-Py and Cu-Por-Py CMP [473], Copyright © 2023, Elsevier.

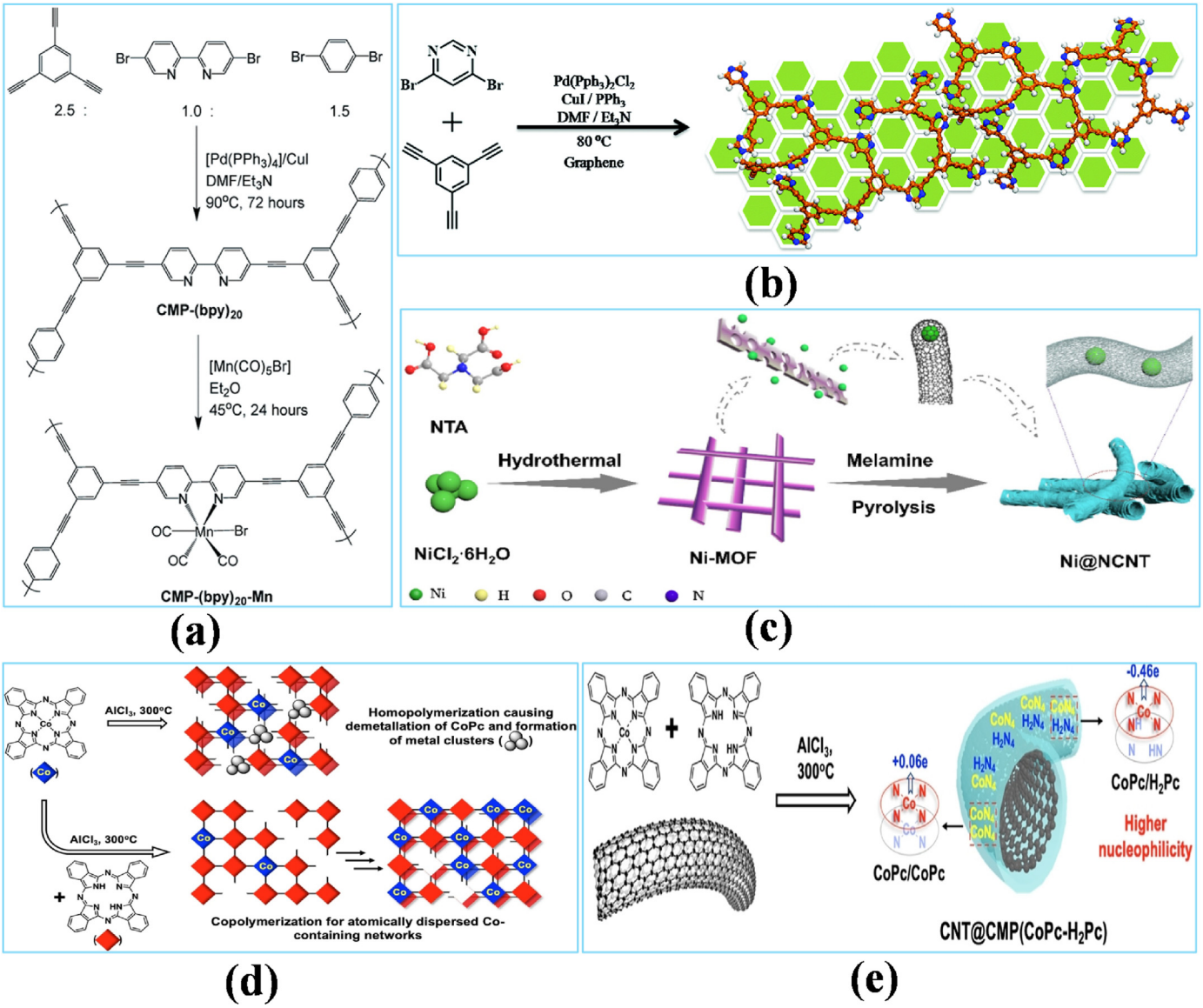

Fig. 23. (a) Synthetic process of CMP-$(bpy)_{20}$-Mn. The notation for the bpy contents of the polymer ascends through the feed percentage of 5,5'-dibromo-2,2'-bipyridine in the polymerization reaction [489], Copyright © 2019, Royal Society of Chemistry. (b) The one-pot, bottom-up preparation of the PyPOP@G. C (orange), N (blue), H (white), G (green hexagons) [490], Copyright © 2016, Royal Society of Chemistry. (c) Synthetic process of Ni@NCNT [491], Copyright © 2019, Elsevier. (d) Schematic demonstration of the structural variations among CMP(CoPc-H_2Pc) and CMP(CoPc) prepared under standard setting; (e) Iono-thermal fabrication of CNT@CMP(CoPc-H_2Pc) comprising the stacked CoPc/CoPc and CoPc/H_2Pc moieties having various Hirshfeld Co atomic charges [492], Copyright © 2019, Elsevier.

known for their higher conductivity and stability [168], and they serve as versatile templates for CMPs to synthesize effective, binder-free electrodes [169]. To improve the electrochemical efficiency of structures such as COFs, MOFs, and CMPs, numerous conductive carbon composites were featured, such as CNTs, graphene, and activated carbons [169]. For example, nanoparticles such as CoPc-CMP/CNTs-2 have excellent capacity retention (89.2 %) and specific capacitance (107.2 F g^{-1}) at 10 A g^{-1} [169]. Previous research has shown that blending CNTs with TBN-based CMPs is a potential technique for synthesizing effective supercapacitor electrodes [170]. Samy et al. [171] synthesized various CMPs using Sonogashira-Hagihara cross-coupling of a tetrabenzonaphthalene (TBN) polymer via pyrene (Py), tetraphenylethylene (TPE), and carbazole (Car) units, and studied their chemical-based structure, heating stabilization, structural properties, crystallinities, and porosity. TBN-TPE-CMP had a larger surface area (1150 m^2 g^{-1}) and better thermal resistance (Td10 = 505 °C; char yield = 68 wt%) than TBN-Py-CMP and TBN-Car-CMP. In order to increase the conductivity of the TBN-CMP material, singular-walled CNTs were incorporated into the composite. The TBN-Py-CMP/SWCNT nanoparticles exhibited exceptional capacitance retention (99.18 %) over 2000 loops and an elevated capacitance (430 F g^{-1}) at a current density of 0.5 A g^{-1}; these properties surpassed those of the TBN-TPE-CMP/SWCNT and TBN-Car-CMP/SWCNT nanoparticles (Fig. 8a).

2.4.7. Phenazine-based CMPs

Recently, there has been considerable attention to the consumption of the p-type dihydrophenazine (Pz) molecule to build polymeric cathodes in Dual-Ion Batteries (DIBs) because of its substantial potential charge storage capacity and continuous redox mechanism [172]. The redox sites in Pz have an estimated capacity of up to 297 mAh g^{-1} and a discharging voltage of more than 3 V vs Li^+/Li [173]. Various approaches were implemented to mitigate the solubility limitation of nano-organic materials in chemical minerals and enhance their flexibility, including utilizing organic salts [174] and planar Pz-based monomers via significant molecular mass [175]. An additional reduction of dissolving challenges has been achieved by using cross-linked structures, resulting in an

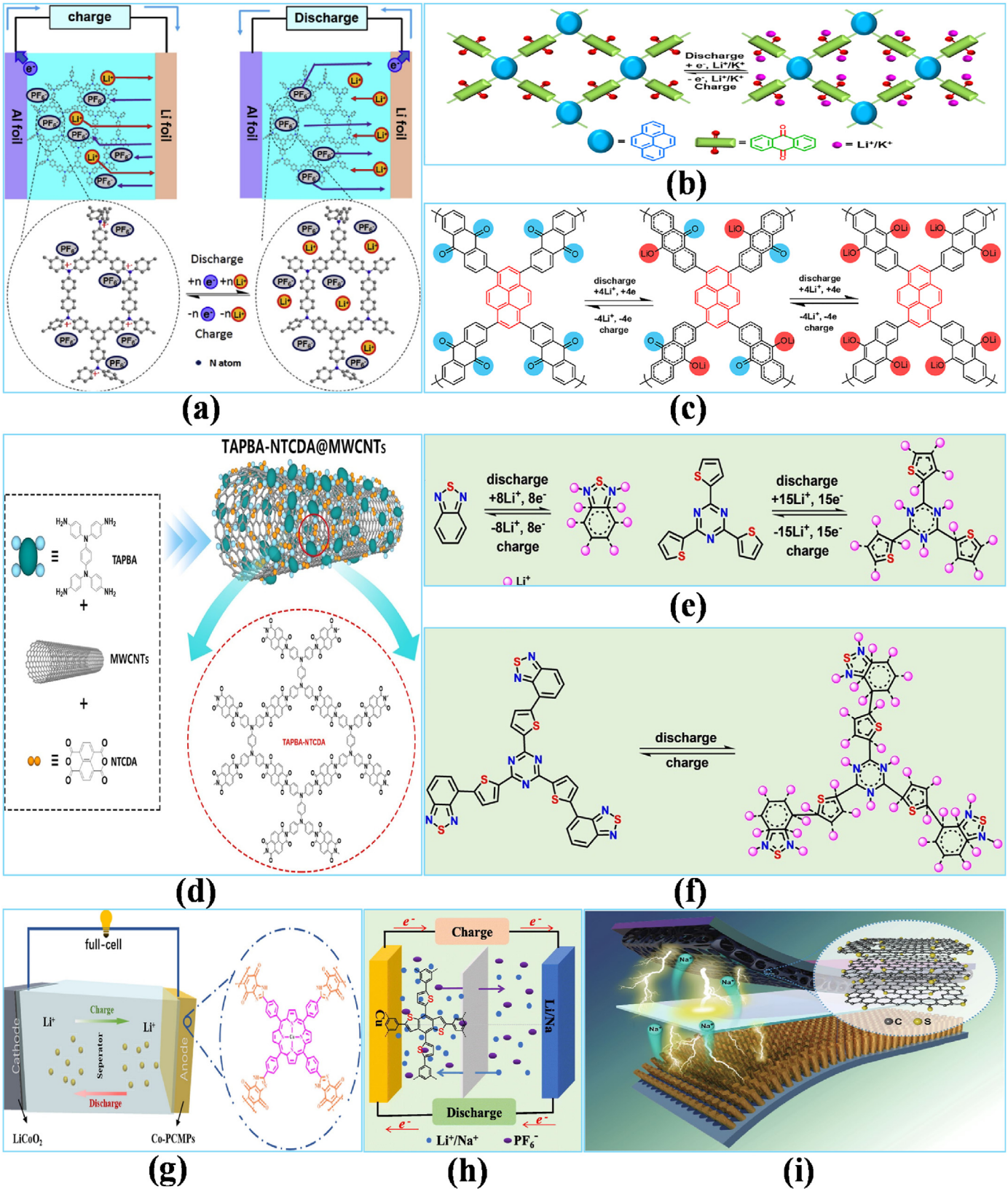

Fig. 24. (a) Synthetic redox reaction of micro-mesoporous polymer PTTPAB [494], Copyright © 2018, Elsevier. (b) The graphical illustration of PyAq for Li^+/K^+ ions storage; (c) Estimated redox method of PyAq [496], Copyright © 2020, Springer Nature. (d) The mechanism for synthesizing TAPBA-NTCDA@MWCNTs via in-situ synthesis [497], Copyright © 2023, Elsevier. (e) Graphical illustration of the projected Li-storage technique for the building units; (f) The segment of the polymer chain for TzThBT [498], Copyright © 2020, John Wiley & Sons. (g) Proposed scheme for Co-PCMPs [499], Copyright © 2022, Elsevier. (h) Proposed mechanism for DBD-CMPs [500], Copyright © 2020, Elsevier. (i) Proposed mechanism for SCMP [501], Copyright © 2019.

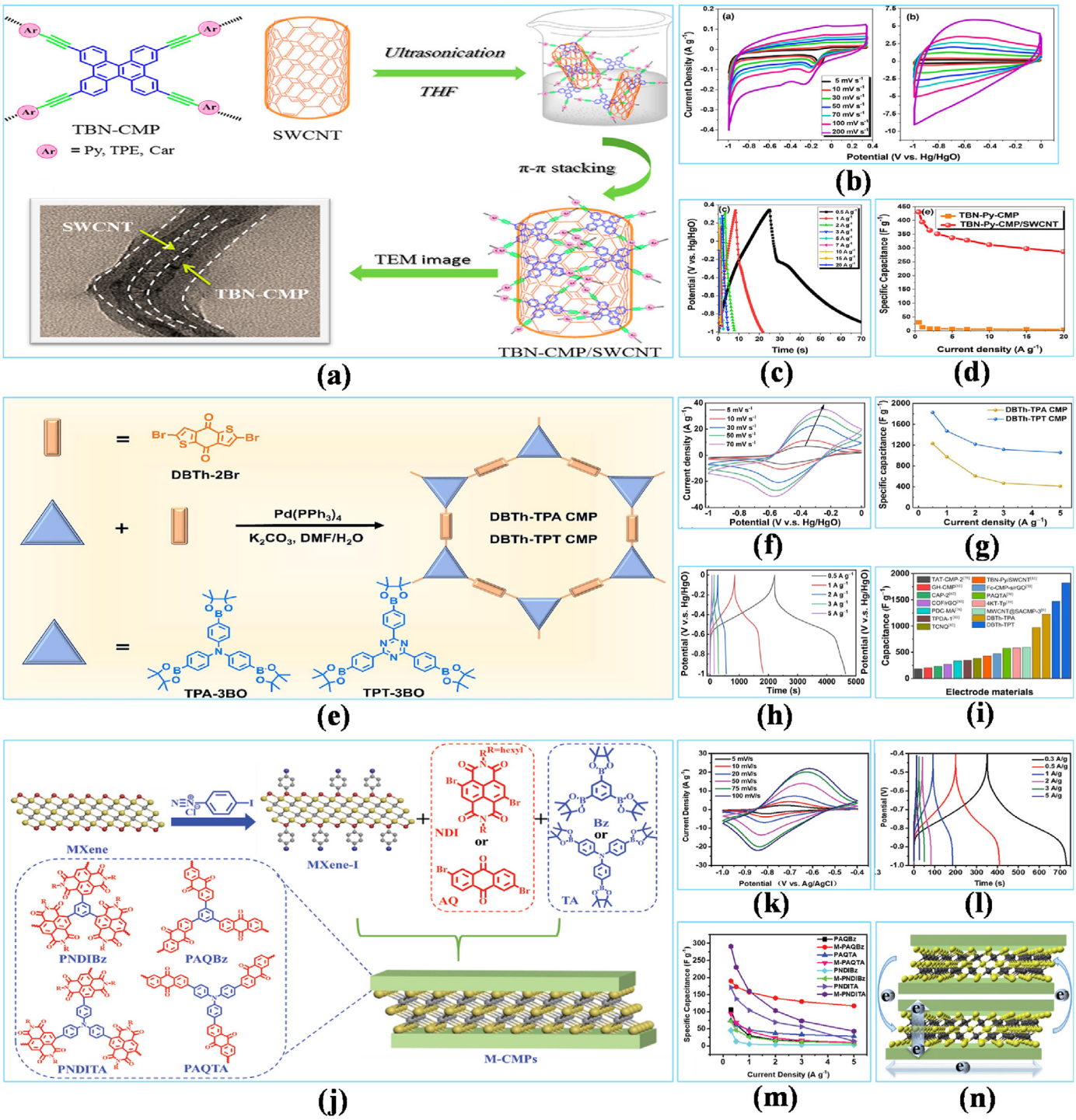

Fig. 25. (a) Synthetic illustration of the formation of TBN-Py-CMP, TBN-TPE-CMP, and TBN- Car-CMP; (b) TBN-Py-CMP and the CV of TBN-Py-CMP/SWCNT material; (c) GCD trends for TBN-Py-CMP; (d) Capacitances specific to TBN-Py-CMP and the TBN-Py-CMP/SWCNT composites as determined by measuring current densities ranging from 0.5 to 20 A g^{-1}; [171], Copyright © 2021, American Chemical Society. (e) Synthesis process for DBTh-TPA and DBTh-TPT CMPs; (f) The CV contours of DBTh-TPA CMP; (g) Estimated specific capacitances for the DBTh-TPA and DBTh-TPT CMPs at various current densities; (h) GCD curves of DBTh-TPT observed at varying current densities; (i) Specific capacitance evaluation between the DBTh-TPA and DBTh-TPT CMPs and redox-active CMP materials [518], Copyright © 2023, Elsevier. (j) Schematic depiction of synthetic processes for M-CMPs; (k) CV contours for M-PAQBz at various scan speeds; (l) GCD trends for M-PAQBz at various current densities; (m) Rate efficiency of M-CMPs and comparable CMPs with current densities varying from 0.3 to 5 A g^{-1}; (n) A schematic depiction of the charging transference channel during charging and discharging [519], Copyright © 2020, John Wiley & Sons.

extended cycling life of around 1000 rounds with no apparent decrease in capacity [176]. Pz-based monomer cathodes have also exhibited improved kinetics when heterogeneous structures consisting of cross-linked polymeric materials were used. However, limitations remain to overcome, such as slow rate efficiency and poor particular strength caused by restricted electron and ion conductivity [177]. Abruna et al. [172] lately showed that copolymerization enhanced the efficiency of cross-linked Pz-based monomers cathodes by maintaining their ionic and electronic conductivities, resulting in a tailored capacity of roughly 195 mAh g^{-1} at 1 A g^{-1} and a cycling life of 500 periods. Ma et al. [178]

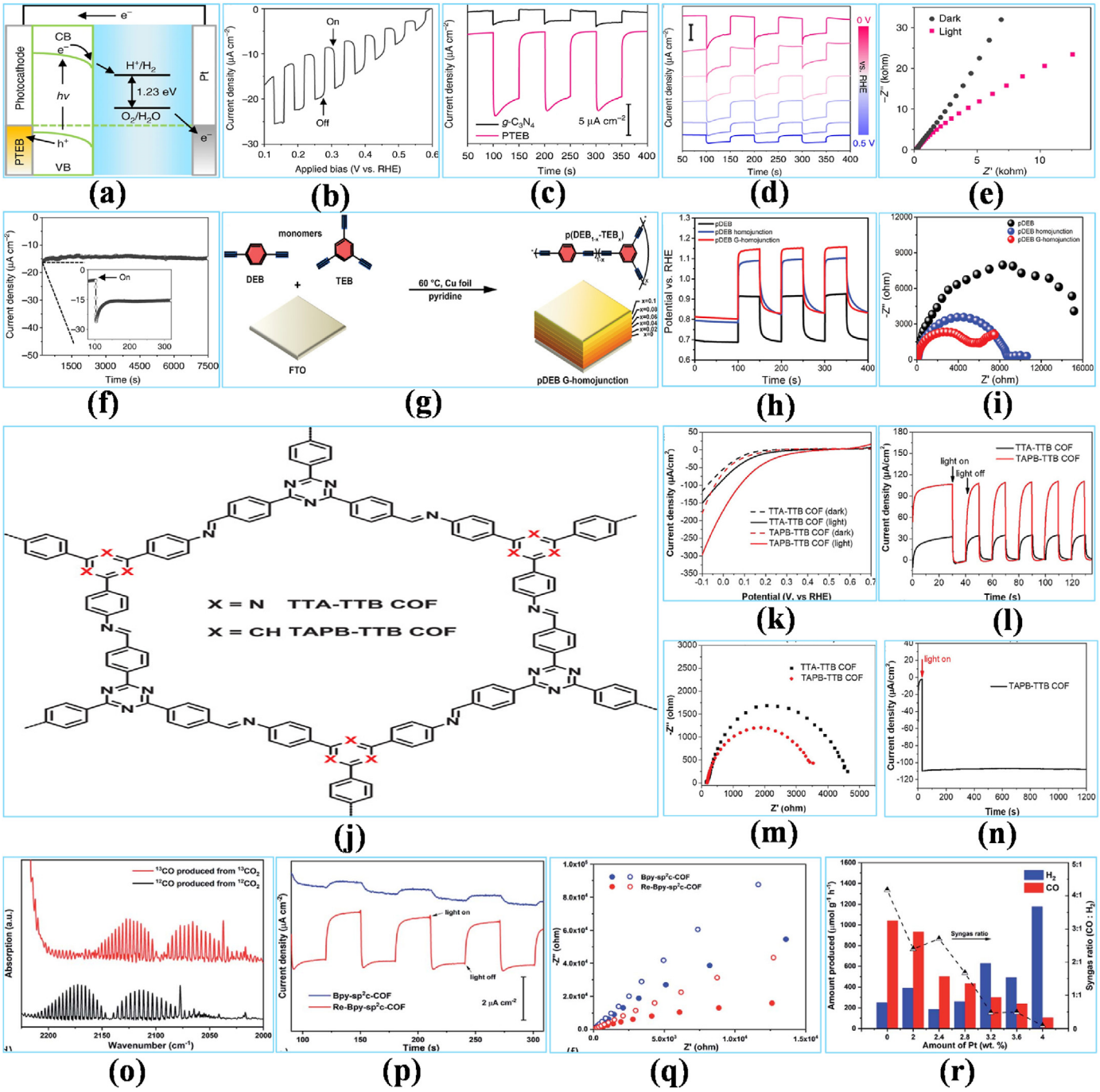

Fig. 26. Performance of the PTEB nanofiber as photocathodes in photoelectrochemistry. (a) Diagram of the PEC cell; (b) Under chopped lighting, linear sweep voltammetry; (c) Chronoamperometries for PTEB (red curve) and g-C_3N_4 at 0.3 V vs RHE under chopped light (black curve); (d) Photocurrent densities in PTEB from 0.5 to 0V in comparison to RHE. 10 μA cm^{-2} scale bar; (e) Under both dark and light conditions, the PTEB Nyquist charts at 0.3V versus RHE; (f) Current density and efficiency of the PTEB electrodes during 7500 s of illumination [529], Copyright © 2018, Nature. (g) An illustration of the synthesis of pDEB G-homojunction on FTO; (h, i) Graphs of the photocurrents for the pDEB and pDEB homojunction and 0.1 m Na_2SO_4 in aqueous solution with pDEB G-homojunction photocathodes exposed to AM 1.5G radiation [525], Copyright © 2019, John Wiley & Sons. (j) Molecular structures of COFs, (k) TTA-TTB COF (black curve) and linear voltammetry curves for TAPB-TTB COF photoelectrodes (red curve) (0.2 m Na_2SO_4 aqueous solution (pH 7) with and without visible light); (l) Under chopped visible light, COFs photocurrents at 0 V vs RHE; (m) COFs at 0 V vs RHE in a Nyquist plot; (n) Current-time of the TAPB/TTB COF photoanode when exposed to visible light (greater than 420 nm) [526], Copyright © 2021, John Wiley & Sons, (o) FT-IR spectra of $^{13}CO_2$ photo-reduced into ^{13}CO. (p) Chronoamperometries for Bpy-sp^{2}c-COF and Re Bpy-sp^{2}c-COF at 0.5 V vs RHE during chopped irradiation; (q) Under both dark and light settings, Bpy-sp^{2}c-COF Nyquist plots (blue) and Re-Bpy-sp^{2}c-COF Nyquist plots (red) at 0.5 V versus RHE, (r) photocatalytic syngas production of Pt modified Re-Bpy-sp^{2}c-COF in the presence of visible light [530], Copyright © 2019, Royal Society of chemistry.

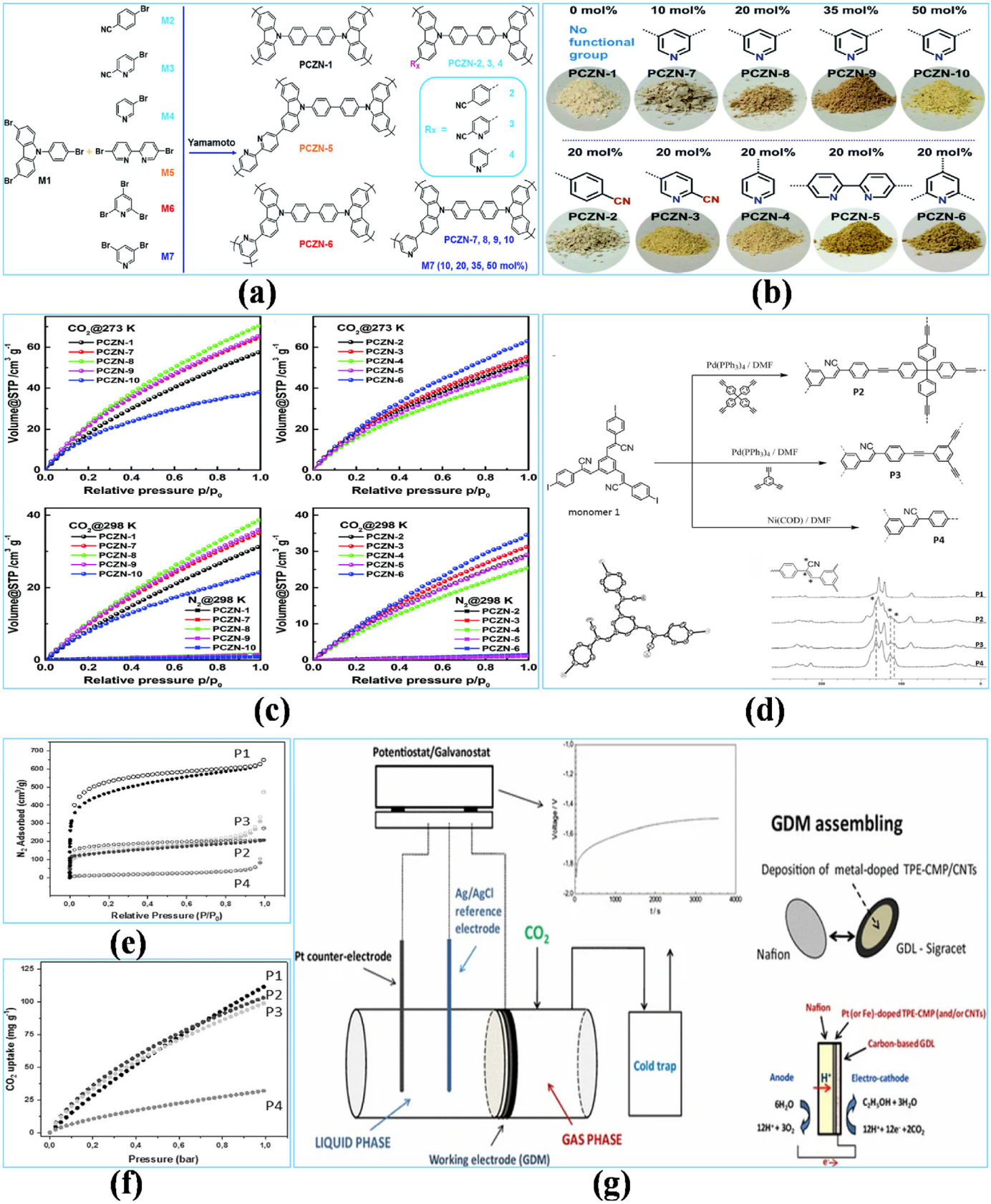

Fig. 27. (a, b) The functionalization path to polycarbazole structure and colors (PCZNs); (c) CO_2 and N_2 adsorption isotherms were tested at 298 K as well as CO_2 adsorption isotherms of PCZNs at 273 K [75], Copyright © 2017, Royal Society of chemistry. (d) P_2, P_3, and P_4 reactions with metal catalysts, as well as structure of single polymer along with XRD pattern; (e, f) The ability of P_1, P_2, P_3, and P_4 to bind CO_2 at 273 K [541], Copyright © 2017, John Wiley & Sons. (g) The design of electrochemical system, for gaseous-phase CO_2 reduction, and assembly of the GDM [549], Copyright © 2015, Springer Nature.

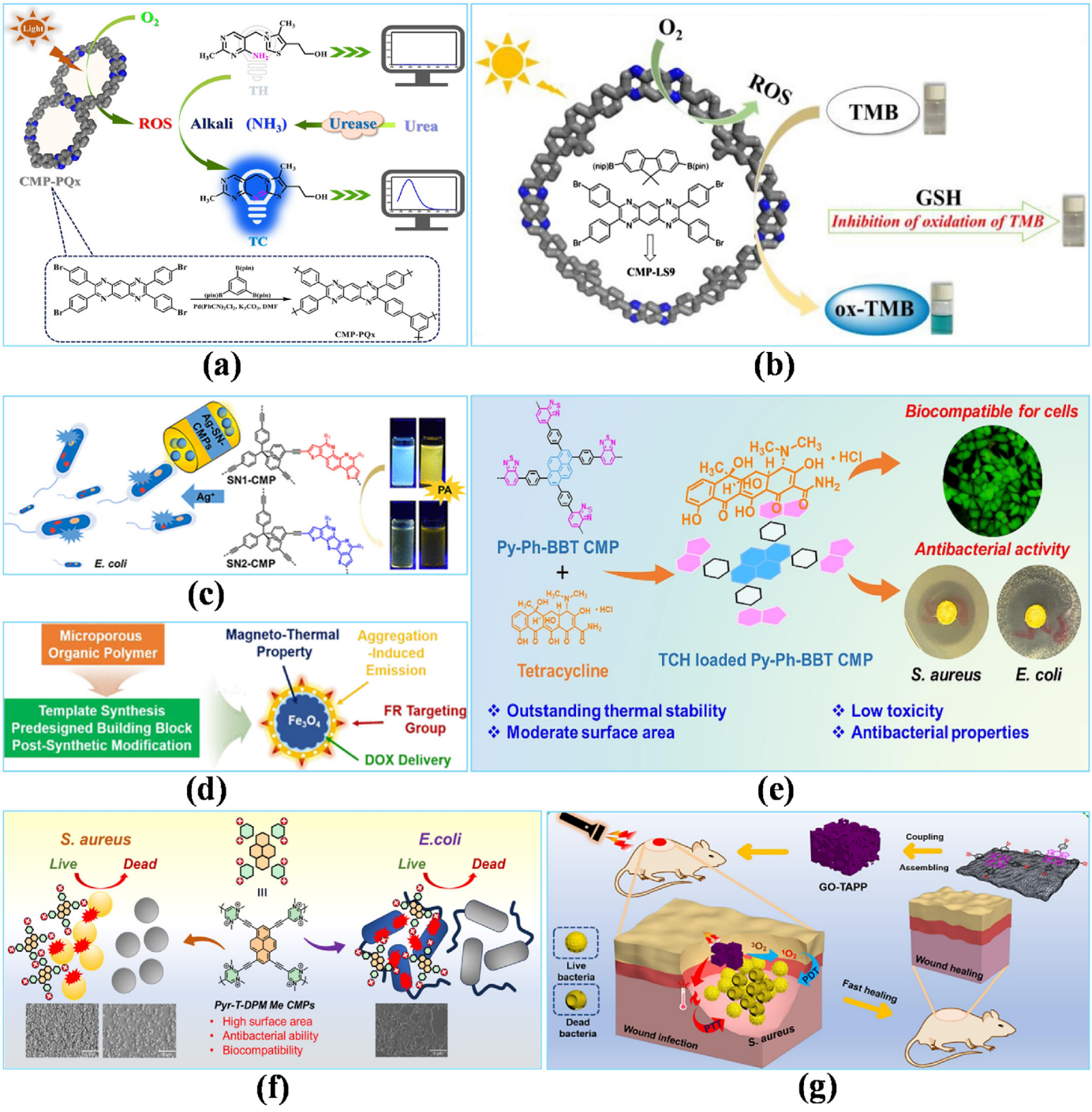

Fig. 28. (a) A fluorescence sensor for urease detection depending on photo-responsive CMP-PQ_x is shown schematically [572], Copyright © 2020, Elsevier. (b) The suggested methodology of light-induced oxidase-like activities of the CMP-LS9 and the detecting method for GSH [573], Copyright © 2021, Elsevier. (c) Schematic mechanism of synthesis SN-CMPs as a fluorescent sensor [574], Copyright © 2018, American Chemical Society. (d) Multifunctional drug delivery device based on Fe_3O_4@Void@MOP-TE-FA [584], Copyright © 2020, American Chemical Society. (e) Schematic mechanism of CMPs as tetracycline antibiotic [585], Copyright © 2023, Elsevier. (f) Graphical illustration of the synthesis process of pyrene-CMP via post-cationic alternation [596], Copyright © 2024, Elsevier. (g) A graphical representation of a hybrid porphyrin-predicated CMP/GO (GO-TAPP) capable of photo-activated combination antibacterial treatment and wound treatment [600], Copyright © 2023, Elsevier.

designed a donor-acceptor (D-A) conjugated microporous polymeric (TzPz) cathode by inserting the electron-donor Pz and D-ATz units into the polymeric ring. The TzPz cathode had a greater conjugation degree and a small bandgap than the related polymeric BzPz, which facilitates electron movements during charging/discharging. The porous design, which had a significant surface area, allowed ionic charge particle movement, leading to an elevated capacity and exceptional rate efficiency. The strongly cross-linked polymeric composition inhibited dissolving into the organic electrolyte, resulting in sustained cyclability for 10,000 cycles. The performance of organic polymeric-based DIBs electrical efficiency may be greatly enhanced by designing a D-A polymer (Fig. 8b).

Table 1
The advantages and disadvantages of different synthesis methods of CMPs.

Synthesis method	Methodology	Advantages	Disadvantages
Templating-methods	Hard templating [81]	The synthesis of particular morphologies at the macroscopic level is simple, and hierarchical porous structures are attainable.	The use of sacrificial templates is necessary; Templates are challenging to eliminate. Scaling up synthesis is constrained.
	Soft templating [82]	Demolding is not necessary; Macroscale structures are readily processable.	It's challenging to regulate synthesis conditions and morphology.
Template-free methods	Surface polymerization [83]	Intense product purification; simplified reaction equipment and conditions.	Excessive use of solvents; the reaction vessel restricts the size of the structure; poor yielding.
	Layer by layer polymerization [84]	Excellent regulation at the nanoscale; enhanced micromorphology.	Restricted reaction types; Complex apparatus for reactions.
Post-synthetic modification [85]	–	Efficient macroscale structural synthesis; broad interface flexibility.	Synthetic constraints; quantitative evaluation challenging; adverse stabilization.
De novo synthesis [86]	–	Possesses the highest degree of grafting.	Oxygen sensitivity caused the formation of unexpected by-products and decomposition of Pd(0) catalyst.
Sonogashira-Hagihara Coupling [87]	–	Broad substrate scope; mild reaction conditions; high selectivity; compatibility with other coupling reactions.	Catalyst sensitivity; formation of side products; toxicity and cost of reagents; long reaction times.
Suzuki-cross Coupling [87]	–	Facile synthesis process; better selectivity; versatility; scalability.	Air and moisture sensitivity; caused undesired reactions or decomposition; high large-scale synthesis cost.
Yamamoto Coupling [87]	–	Broad material protection; superior performance; facile synthesis process and conditions.	Long reaction time; non-friendly environmental behavior; high large-scale synthesis cost.
Heck coupling [87]	–	A higher degree of selectivity; facile synthesis mechanism; broad substrate scope.	Substrate limitations; toxicity and high cost of reagents; massive catalyst loading; complex degradation process.
Other methods	Microwave synthesis [88]	Promotes increased porosity and decreased reactivity period.	Regarding restricted particular conditions.
	Mould-method [89]	Various macroscale structures may be quickly produced.	Weak usability; necessitated elevated temperature.

2.4.8. Porphyrin-based CMPs

CMPs are synthesized using a diverse series of structural elements, ranging from traditional benzene rings to intricate heterocyclic and macrocyclic molecules [179]. Among these, porphyrins have emerged as promising N-based monomers for porphyrin-based CMP production due to their strong π bonding, substantial conjugation design, electron-rich properties, photochemical features, and thermal strength. For example, Xu et al. [180] synthesized two novel CMP composites (Por-TPE-CMP and Por-Py-CMP) using porphyrin as a mediator, which exhibited high selectivity for CO_2 and strong adsorption efficiency for various chemicals. Despite these advancements, the potential of porphyrin-based CMPs as efficient metal-ion sponges remains unexplored mainly [181]. The synthesis of porphyrin-based CMPs has been advanced by investigating their performance, selectivity, and potential for adsorption-based metal ion contamination removal [182]. Hasi et al. [183] developed four porphyrin (Por)-based CMPs, known as Por-CMP-1-4, utilizing a Sonogashira-Hagihara coupling process utilizing porphyrin and acetylene aliphatic elements as structural components. Metal particles were removed from water using these monomers as sponges. The developed Por-CMP-1-4 has a crystalline porosity configuration and good thermal and physicochemical properties. Their significant surface area (541.47, 614.58, 382.38, and 677.90 $m^2\ g^{-1}$ for Por-CMP-1-4) and chelating active sites derived from the porphyrin ring led to their better adsorption capacities for Zn^{2+}, Cu^{2+}, and Pb^{2+} ions. Por-CMP-3 had the maximum adsorption capability for Zn^{2+} particles (640 mg g^{-1}) and an adsorption performance of 80 %, whereas its adsorption rates for Cu^{2+} and Pb^{2+} ions were both 334 mg g^{-1} and 42 %, respectively. The schematic illustration therefore investigating the adsorption rates of Por-CMP-3 revealed Langmuir isotherm patterns and pseudo-first-ordered kinetics for Zn^{2+} ion deposition (Fig. 8c).

2.4.9. Pyrene-based CMPs

Pyrene is a highly effective chromophore, known for its high fluorescence quantum yield and rapid excimer emission, making it suitable for use as a fluorescent sensor [184]. Various pyrene derivative-based polymers were extensively utilized as fluorescence sensors for numerous purposes [185]. Pyrene counterparts were additionally employed in the synthesis of diverse CMPs, which were used as fluorescent resources, gas adsorbents [186], fluorescence sensors [187], and photocatalysts [188]. However, the adsorption capability is low, even though pyrene-based CMPs have been studied for iodine desorption [189]. Recently, the primary constituents utilized in CMPs have been 1,3,6,8-tetrasubstituted pyrene [190]; however, there are a limited 1,3,6,8-tetrasubstituted pyrene-predicated CMPs used as fluorescent sensing material [22], as well as a limited quantity of 2,7-disubstituted,15 1,3-disubstituted pyrene [191]. Geng et al. [192] demonstrated effective iodine capturing and detection using 1,6-dispersed pyrene-based luminescent CMPs synthesized through three distinct methods: Sonogashira-Hagihara polycondensation reaction (TDP), trimerization process of bicyclic materials induced by trifluoromethanesulfonic acid (PCPP), and Friedel-Crafts reactivity stimulated by CH_3SO_3H (TTPDP and TDTPAP). The surface areas of TDP, PCPP, TTPDP, and TDTPAP were 261.9, 43.0, 187.5, and 695.2 m^2/g, respectively. These materials exhibited reversible iodine absorption capacities of 0.61, 3.07, 3.49, and 4.19 g/g in iodine vapor. The reduction in fluorescence indicated that all four CMPs showed higher sensitivity and selectivity towards iodine. PCPP, in particular, was very sensitive to iodine, with a Stern-Volmer constant (KSV) of 1.40×10^5 L/mol and a detection limiting of 3.14×10^{-13} mol/L (Fig. 8d).

2.4.10. Pyridyl-based CMPs

CMPs are potential photon harvesters for photocatalytic H_2 production due to their facile synthesis and wide range of band gaps [193]. To produce CMPs with exceptional photocatalytic performance, selecting the proper design aspects is necessary. Previous investigations have not examined the use of pyridine-based CMPs for the aim of photocatalytic H_2 production, which is achieved by combining co-monomer elements with varying electron densities, planarity, and electronic structures. However, Zhu et al. [194] successfully synthesized pyridyl functionalized CMPs using a fast, non-metal fabrication technique that was used for photocatalytic water splitting. In contrast to pyrene (Py) and triphenylamine (TPA), which have a lower charge concentration than benzene (BZ) or TPP [195], Py and TPA have more excellent planarity than BZ, respectively. The photo-luminescent materials, such as those included in photochromic systems, are in great demand. For example, photosensors [196] and solar cells [197] utilize photo-luminescent materials, which are classified as such because they emit cationic radicals during oxidation, resulting in distinguishable color changes [198]. Kotp et al. [199] designed a pyridyl-based boronic ester, 2,4,6-tris(4-(4,4,5,5-tetramethyl-1,3,2-dioxaborolan-2-yl)phenyl) pyridine (TPP-3BO), which served as a precursor for synthesizing four distinct CMPs (TPP-Py, TPP-TPA, TPP-TPP, TPP-BZ CMPs) with varying planarities and charge

concentrations for photocatalytic H_2 evolution. Their study explored the configuration-function interactions of these pyridyl-based CMPs by altering their precursors and analyzing the resulting electronic configurations and morphologies. These materials demonstrated the ability to adjust their emission spectra and optical gaps over a broad range. All four CMPs exhibited excellent luminescence stability, higher surface area, and outstanding thermal stability. Consequently, they effectively facilitated the photocatalytic production of H_2 from water within a sacrificial electron donor (Fig. 8e).

2.4.11. Pyrimidine-based CMPs

Ion-functionalized CMPs exhibit unique features suitable for real-world applications due to their diverse synthetic methods and ionic structures [200]. These composites were utilized in different domains like catalysis, adsorption, separation, detection, and sensing, owing to the high ionic volume, polarization, and electric field intensity of porous materials synthesized without templates [201]. Research on ionic porous synthetic monomers and multipurpose ion-functionalized CMPs is gaining increasing attention [202]. These nanostructured adsorbents can rapidly and selectively capture ionized dyes through fast absorption and ion exchange processes, showing significant potential in practical applications [203]. Several synthesis techniques, including cross-coupling processes and PSM, have been explored for synthesizing ion-functionalized CMPs. While traditional cross-coupling methods face challenges with organic substrates, PSM offers advantages such as high yield, reliable functional group incorporation, and excellent selectivity, making it a preferred approach. PSM has been excessively employed in various porous materials, like MOFs, for various applications [204]. Liu et al. [205] utilized the Sonogashira reaction to synthesize 1,3,5-triethynylbenzene with 2,5-dibromo-pyrimidine, resulting in CMP-PM, a porous organic monomer with a surface area of 416 m^2/g and a CO_2 uptake of 44.5 cm^3/g at 273 K and 760 mmHg. Through PSM, CMP-PM was methylated with CH_3I to produce CMP-PM-Me, which had an surface area of 241 m^2/g. CMP-PM-Me exhibited remarkable fast absorption of ionized dyes such as methyl orange (MO) and Congo red (CR), adsorbing 292.4 mg g^{-1} of CR in just 2 min from an initial 226.4 mg/L concentration. Additionally, CMP-PM-Me demonstrated favorable selectivity in the deposition of dyes from binary mixtures containing both anionic and non-anionic dyes in water, enabling efficient separation of anionic dyes through simple filtration. This performance highlights the potential of ionic pyrimidine-linked CMPs for effective dye adsorption and separation (Fig. 8f).

2.4.12. Tetraphenylenthene-based CMPs

Aggregation-induced emission (AIE) is the higher visibility of particles caused by confined intramolecular movement, phases, and actions [206]. AIE has applications in various fields, including Bioprobes [207], bioelectrochemicals [208], biosensor devices [209], photo-dynamic treatment [210], and tissue visualization [211]. The twisting of phenyl chains around tetraphenylethylene (TPE) facilitates electron transfer through POPs, resulting in AIE rather than aggregation-caused quenching (ACQ) [212]. Incorporating holes into dense AIE polymers can improve the performance of assays by enhancing the dispersion of detecting reagents [213]. TPE-based AIE-reactive polymers have been intensively researched for monitoring small molecules, peptides, and photodynamic treatment, with CMPs gaining popularity [214]. The use of CMPs with TPE as a structural component has allowed for the detection of hazardous compounds [215]. Electrochemiluminescence (ECL) caused by CMP-mediated AIE has not been investigated yet, even though there have been advancements in ECL luminophores that are AIE-active and have improved visibility in aggregation phases [216]. Cui et al. [217] introduced TBPE-CMPs as effective AIECL transmitters for the first time, demonstrating an ECL efficiency of 1.72 % within tri-n-propylamine (TPrA) as a co-reactant. This efficiency is attributed to improved electron-hole interactions and effective control of non-radiative processes, leading to increased fluorescence at the anode during ECL. TBPE can be combined with various ligands, such as TEPA, DEP, and TEPT, to form TBPE-CMPs, which reduce the energy barrier for electron insertion into the polymeric structure and allow for tuning of the ECL properties. For one-step dopamine detection, researchers developed an ECL detector based on TBPE-CMP-1, utilizing its electro-oxidation intermediates as energy acceptors. The sensors exhibited exceptional sensitivity and remarkable anti-interference capabilities against ascorbic acid and uric acid, making them promising tools for clinical diagnostics and biological research (Fig. 9a).

2.4.13. Thiophene-based CMPs

Thiophene-based adsorbents and catalysts, particularly thiophene-based polymers, have recently gained popularity due to their unique properties [218]. The easy modification of thiophene molecules allows for the synthesis of various derivatives with diverse features and potential applications. Thiophene-derived microporous materials are synthesized cost-effectively and sustainably. These materials exhibit a substantial charge volume, high active sites, and a high surface area for optimal interaction with pollutants, making them excellent adsorbents [219]. Thiophene-based CMPs possess optical properties, stability, and longevity, making them suitable for many applications. However, there is limited information on the safe disposal of hazardous Cr(VI) ions associated with these materials [220]. Kotp et al. [221] synthesized three CMPs via one-pot poly-condensation linkages of boronated triphenylpyridine (TPP-3Bor) with 4,7-bis(5-bromothien-2-yl)benzo[c] [1,2,5] thiadiazole (ThZ-2Br), 2,5-dibromothiophene (Th-2Br), and 1,4-dibromobenzene (Bz-2Br), resulting in TPP-ThZ, TPP-Th, and TPP-Bz CMPs. These TPP-based CMPs were characterized by their cylindrical morphology, adjustable porous size, and excellent thermal and chemical stabilities. Among them, TPP-ThZ CMP exhibited the excellent absorption potential for Cr(VI) ions (209 mg g^{-1}). Additionally, TPP-based CMPs demonstrated high recyclability for Cr(VI) ion conductivity and absorption, showcasing their potential as dynamic materials for Cr(VI) absorption and conductivity. These findings also highlight the potential of thiophene intermediates for developing future Cr(VI) adsorbents (Fig. 9b). Han et al. [222] synthesized three thiophene-based CMPs using benzo[1,2-b:3,4-b':5,6-b"]trithiophene units (BTT-CMP1, BTT-CMP2, and BTT-CMP3) employing a similar methodology. These materials exhibited excellent efficiency and high surface area for photocatalytic applications. Among them, BTT-CMP2 demonstrated the highest catalytic efficiency for light-driven benzimidazole production. Notably, BTT-CMP2 also showed various usages, effective reusability, and photocatalytic properties without metal catalysts (Fig. 9c).

2.4.14. Triazine-based CMPs

CTFs, also identified as 1,3,5-triazine-based CMPs (TCMPs), are an interesting family of N-rich polymers that blend the properties of inorganic carbon nitride (CN_x) polymers with those of organic CMPs [223, 224]. Integrating strong, electron-withdrawing triazine molecules into CMP systems enhances the stabilization and modulation of electronic states [225]. Amorphous transition metallic dichalcogenides (TCMPs) are utilized in various fields such as metals ion monitoring, electronic batteries, luminescence detection of nitroaromatic compounds (NACs) [226], catalytic activity [227], separation [228], and absorption [223], due to their advantageous π-electron movement. TCMPs exhibit significant iodine absorption properties at normal atmospheric pressure due to nitrogen-rich heterocyclic molecules, which enhance interaction with adsorbates. However, TCMPs are rarely used for iodine collection, and their overall absorption capacity is generally low [229]. Hao et al. [230] developed two triazine-based CMPs with varying triazine molecule ratios. This small compositional change caused a substantial variance in photocatalytic efficiency. T-CMP-1 demonstrated a hydrogen evolution rate (HER) of 3214.3 μmol h^{-1} g^{-1} under visual illumination, whereas T-CMP-2 achieved only 242.1 μmol h^{-1} g^{-1}. This suggests that increasing the concentration of triazine molecules in CMPs can significantly enhance their photocatalytic activity (Fig. 9d). Geng et al. [231] utilized

the Friedel-Crafts polymerization reaction to synthesized three new fluorescent triazine-based CMPs (TCMPs) using electron-rich N,N,N',N'-tetraphenyl-1,4-phenylenediamine (TPPA), 1,3,5-tris(diphenylamino) benzene (TDAB), and 1,3,5-tris[(3-methylphenyl)phenylamino]benzene (mMTDAB). Among these, TTPPA had a very high iodine uptake capacity of 4.90 g/g. Their study revealed that TCMPs' superior porosity, efficient adsorption sites, distorted propeller-like structure, and charge-transfer couplings were responsible for their significant iodine desorption potential. Both TTDAB and Tm-MTDAB exhibited remarkable efficiency for adsorbing iodine in both vapor and solution phases, which was unexpected given their low porosity. Both the sorbents and the absorbed iodine from TCMPs were readily recyclable. Additionally, all three TCMPs demonstrated excellent detection sensitivity and selectivity for o-nitrophenol (Fig. 9e). Zhang et al. [232] synthesized three CMPs based on thiophenes and triazine and studied the influences of cross-linkering length on their photocatalytic efficiency. BTPT-CMP1 showed a blue-shifting optical reflection than BTPT-CMP2 and BTPT-CMP3, which had longer crossed-linkage. BTPT-CMP1 also exhibited a larger photocurrent due to its substantial surface area and low surface charge transfer impedance. The results indicated that the photocatalytic efficiency of BTPT-CMP1 (5561.87 mmol g^{-1} h^{-1}) with smaller cross-linkage was superior to that of BTPT-CMP2 (1840.86 mmol g^{-1} h^{-1}) and BTPT-CMP3 (1600.48 mmol g^{-1} h^{-1}). Furthermore, BTPT-CMP1 demonstrated a remarkable HER rate, surpassing most other 1,3,5-triazine-based CMPs (Fig. 9f).

2.5. Dimensionality of CMPs

2.5.1. One-dimension (1D) CMPs

Porous polymers (PPs) have garnered substantial attention owing to their significant surface area and prospective uses in various fields, including sensing, catalysis, optoelectronics, and energy production [102]. Although previous studies have mainly focused on developing PPs using new chemical methods and tunable pore structures, achieving exact control over their morphology remains challenging [233]. Although graphene [234] and MoS_2 [235] have been used as templates for synthesizing 2D PPs, research on 1D PPs is limited. Current methods for producing 1D PPs often result in uncontrolled mixtures and sizes, hindering their application in eco-friendly power systems like fuel cells and metallic-air batteries, which require controlled production methods [236]. To develop eco-friendly power systems like gasoline tanks and metal-air batteries, it is essential to discover methods for the controlled production of 1D PPs. These techniques depend on efficient catalysts in the ORR [237]. The performance and stability catalysts based on conventional valuable metals, such as Pt and Pd, are limited by their high price and lack of stability [238,239]. The electrocatalytic properties of several porous carbon materials doped with heteroatoms for ORR show promising results [240]. While heteroatoms-dopant carbon structures have been widely studied, developing ternary-doped porous carbons, specifically those doped with B/N/S, has not been reported due to the challenges in regulating their production. A limitation in the synthesis of efficient carbon-based catalysts for ORR is the limited accessibility of precursor materials and the relatively small surface area. Porous carbons synthesized by CMP provide a potential solution. 1D CMPs are appealing substitutes for ORR catalysts because of their significant surface area, microporous patterns, and unique chemical structure. Consequently, there has been growing scientific attention towards analyzing CMPs for their use in renewable energy sources [241,242]. He et al. [243] presented a methodology that synthesized core-shaped 1D CMPs layered by layered using structurally directed precursors made of single-walled carbon nanotubes (SWNTs). CNT cores operate as electron receivers (n-type), whereas CMP shells function as electron donors (p-type) in 1D CMPs. The as-synthesized 1D CMPs have significant surface area of 623 m^2 g^{-1} and apparent electronic interaction in the p/n heterojunctions, exhibiting efficient inverted decay rates (π_{eff}) of 164 and 354 ps for three-layered and randomized CMPs. 1D CMPs that include heteroatoms and have carbon efficiencies ranging from 58 % to 73 % are ideal to synthesize 1D porous carbons that are doped with heteroatoms. Direct pyrolysis was used to yield porous carbons with a hierarchical structure infused with ternary heteroatoms (B/N/S). These carbon materials have a porous structure and a substantial surface area (up to 753 m^2 g^{-1}). The catalytic ORR efficiency of 1D porosity carbons synthesized via three-layered 1D CMP was better than that of 1D porous carbons using non-layer 1D CMP. The results suggest that the layered-by-layered process for carbon materials derived from 1D CMPs provides a unique and regulated method for developing electron push-pulled linkages, heteroatom loading, and porosity designs for various applications (Fig. 10a–i). Hwang et al. [244] synthesized semiconductive 1D conjugated polymers (1D CP) of specific lengths by using coordinated self-assembly during the polymerization process. An initial achievement was the successful continuous polymerization of interlinked poly(3,4-dihexylthiophene), which exhibits outstanding water solubility. Subsequently, a widely dispersed 1D crystalline polythiophene core, with sizes ranging from 15 to 282 nm, was spontaneously assembled through the block copolymerization of poly(3,4-dihexylthiophene)-block-polythiophene. To obtain optimal performance and accurate control of dimensions, it is essential to have a core that performs moderate polymerization and a highly soluble shell. This will promote nucleation expansion rather than isodesmic growth. The authors use a unique method that combines kinetics and high-resolution imaging to achieve in-situ nanoparticulation of coupled polymers by crystallization (CD-INCP). During this process, the formation of seeds occurs naturally, which are then enlarged in micelle units by the process of seeding proliferation. In addition, the achievement of “living” CD-INCP was shown using a chain elongation test. The structure of 1D-CP with certain lengths were obtained by simplifying the CD-INCP that was achieved by mixing both monomers in a single-step co-polymerization (Fig. 10j to m).

2.5.2. Two-dimension (2D) CMPs

Microporous polymers are a class of organic materials with high surface area and smaller pores of 2 nm, including the HCP [245], PIMs [191], COFs [246], MOFs [247], PAFs [248], and CMPs [87]. The PIMs have a constant presence of small pores and can be easily processed into films, making them highly suitable for film production [249,250]. Despite their elevated porosity, MOFs exhibit inadequate thermal and hydrothermal stabilization [251]. COFs have strong covalent bonding and high stability [252]. CMPs are a new kind of material with interesting optoelectronic properties because they combine persistent porosity with prolonged conjugation [194]. While CMPs have many potential uses, they have certain drawbacks, such as not being soluble in solutions [253]. A potential solution to this problem is the formation of 2D CMP films using on-surface crosslinking [254]. The films exhibit noticeable properties, such as a structure resembling a sheet or film, irregular repeating units, larger horizontal dimensions, and stability due to covalent cross-linking. The 2D CMP films have distinctive mechanical, physical, and electronic properties, proving them useful for various purposes. Novel techniques have been developed for developing 2D CMP films, which exhibit distinct properties such as ordered structures, strong structures, uniform surfaces, and tunable layers. 2D CMP films have more potential uses than powder CMPs in areas such as energy preservation, gas/molecular separation, chemical sensing, and optoelectronic technologies. An comprehensive evaluation of the techniques and applications for synthesizing 2D CMP films, particularly inoptoelectronics, is important despite existing research on powder CMPs [50,255]. Their research presented a summary of novel advancements in on-surface preparation techniques and the application of 2D CMP. Hardian et al. [256] synthesized four independent microporous 2D polymeric membranes with a stiff benzobisoxazole connection to enable long-term organic solvent nanofiltration (OSN). The membranes possessed chemical strength, rigidity, and elasticity due to the benzobisoxazole chemistry and 2D composition. The membranes with varying pore sizes have been prepared utilizing a flexible two-step solvothermal polymerization

method. These membranes were called B-BOP, TPPy-BOP, TPB-BOP, and TPB-F-BOP. The hydrophobicity of the TPB-F-BOP membrane was enhanced by fluorinating the phenolic node. The structured pore diameters influenced the filtration performance, which in turn influenced the molecular sieving properties. The values of molecular weight cutoff (MWCO) increased with larger pores size: 676, 760, and 1759 g mol^{-1} for BBOP, TPPy-BOP, and TPB-BOP membranes, respectively (pore sizes: 1.4, 1.6, and 2.8 nm). TPB-F-BOP exhibited a lower MWCO of 1402 g mol^{-1} compared to TPB-BOP. Although performing continuous filtration for 120 h, none of the membranes exhibited any indications of compression in terms of acetone flow or rejection of rose bengal. The experiments conducted on all membranes confirmed the results obtained from the pore flow simulation, assuming that liquid penetration occurs via the inherent porosity of the CMP membrane. This suggests that although while CMP membranes are composed of up of different components, they nevertheless maintain a certain arrangement that helps liquids pass through. This statement challenges the prevailing method that suggests solute molecules move through organized materials via defined pathways. Their study emphasizes the need of combining nanofiltration experiments with transfer modeling for understanding how operation factors and material composition affect the performace of OSN (Fig. 11a–c). Liang et al. [257] synthesized a new type of OSN membrane based on all-rigid porosity structures made of chemically stable C-C and C-H bonding. Unlike the frequently used polyamide or polyarylate composites, which lack interconnected pores, 2D CMPs have many linked, interconnected micropores in 3D systems made up of all-rigid π-conjugated structures. The molecular synthesis of interlinked 2D CMP structures might potentially provide exact control of sahpe and structure of the pores. In addition to their microporous properties, 2D CMPs have the potential to effectively retain solutes and exhibit high solvent porosity when used as OSN membranes. This allows them to effectively resist structural relaxation in many liquids (Fig. 11d–f). For the first time, Liu et al. [258] presented the mixture-based all-polymer one diode–one resistor (1D1R) crossed-bar memory broad, which consists of a sequentially layered P_3HT diode and a 2D CMP storage cell. These materials are very attractive due to their multi-element designs, exceptional mechanical strength, larger-area adaptable nanoscale dimensions, and 2D CMP layers formed from surface-bounded Schiff-base reaction during ambient temperature. The sandwich-structure CMP system exhibits non-volatile flash properties, utilizing the CMP layer obtained as the resistant switching substrate. These properties include a sustained cycling persistence of more than 25 cycles, a moderate set voltage of around 1.65 V, and an extended retention period of 104 s. An all-polymer 1D1R array was designed by directly mixing a P_3HT diode onto the CMP storage mechanism. The simultaneous development of bilayer structures comprising of 2D permissive polymer and traditional composites gives promising potential for storage devices, as it offers a simpler alternative to the existing all-polymer 1D1R systems. The 1D1R device enhances memory restoration and suppresses sneaky routes more effectively than the 1R-only storage cell, addressing the issue of interference in crossed-bar storage design. The advancement of 2D memristive polymerization and emergent-coupled all-polymeric systems has opened up opportunities for the convenient and precise production of CMPs films with heterostructures, which may be used in integrated polymer memory systems (Fig. 11g–i). Liu et al. [259] effectively designed a generic technique for synthesizing wafer-scaled extremely-thin 2D CMP films on any substrate using $FeCl_3$-stimulated surface-based oxidative polymerization. Various monomeric carbazole-like monomers were used to synthesized three types of 2D carbazole films on SiO_2/Si substrates: 2D CMP-1, which is about 1.5 nm thick, 2D CMP-2, which is approximately 3.6 nm thick, and 2D CMP-3, which is approximately 1.7 nm thick. These 2D CMP coatings exhibited distinct surface composition and variable semiconductor properties. Furthermore, a cost-effective chemical synthesis technique was used to acquire a larger-area 2D CMP-1/rGO heterogeneous structures by rapidly synthesizing 2D CMP-1 on rGO film. A 2D CMP/rGO heterostructure-based organic field-effected transistor was effectively synthesized. The transistor demonstrated normal p-type conductor, had a good repeatability, and an on/off current ratio of 4.82×10^3. The potential practical application of 2D CMP films is greatly assisted by the ability to yield these films over enormous areas and various substrates by bulk fabrication in a standard semiconductor assembly process (Fig. 11j to p).

2.5.3. Three-dimension (3D) CMPs

The increasing environmental concerns associated with conventional petroleum and natural gas usage have driven efforts toward efficient energy conservation and implementing sustainable energy supplies. Supercapacitors have developed as promising technologies due to their fast charging and discharging ability, higher energy density, and prolonged cycle lifespan [260,261]. These capacitors utilize electrochemical pseudo-capacitance (EDLCs) and electromagnetic double-layer capacitance to effectively store electrical energy [262]. Maximizing the capacitance of EDLCs requires materials with specific mechanical features such as a surface area, ordered pore sizes, and a high pore ratio. Pseudo-capacitors facilitate a reversible redox process between the electrode composite and the electrolyte, enhancing overall energy storage capabilities [263]. POPs have attracted attention for their flexibility, particularly in energy preservation and gas absorption activities [264]. The porous structures of these composites can be categorized as macroporous (>50 nm), mesoporous (2–50 nm), or microporous (<2 nm). They are synthesized using different methods, including COFs, CTFs, HCPs, and CMPs [166,265–267]. In addition, CMPs are remarkable because of their non-crystalline structure and interconnected π-conjugated units, which are synthesized using techniques including Sonogashira-Hagihara, Suzuki-Miyaura, and Yamamoto coupling. The capacity to change structural elements and synthetic methodologies enables customizing of the structures, skeletons, and properties of 3D CMP [167,179]. Its unique paddle wheel structure distinguishes Triptycene (Try) and consists of three benzene units connected by sp^3-hybridized carbon atoms. It exhibits outstanding thermodynamic performance, mechanical properties, and porosity [268]. The unique structure of Try makes it an excellent component for 3D CMP designs, as it has the potential to enhance energy preservation performance. Weng et al. [269] synthesized three 3D CMPs featuring triptycene (Try) groups linked to thiophene (Th), pyrene (Py), and tetraphenylethene (TPE) units using one-pot poly-condensation via Suzuki cross-coupling reaction. Thermal gradient analysis (TGA) showed that compared to Try-Ph-Th CMP (Td10 = 471 °C; char yield = 65 wt %) and other CMP composites, Try-Ph-Py and Try-Ph-TPE CMP had greater thermal stability (Td10 = 605 °C; char yielded = 80 wt %). The Try-Ph-TPE CMP materials showed substantial electrochemical efficiency, with a specified capacity of 245 F g^{-1} at a current density of 0.5 A g^{-1} than to a large surface area (up to 700 m^2 g^{-1}) and pore size (0.45 cm^3 g^{-1}), as determined by N_2 adsorption/desorption evaluations. The Try-Ph-Th, Try-Ph-Py, and Try-Ph-TPE CMPs exhibited impressive capacity retentions of 75.00 %, 85.71 %, and 92.85 %. These 3D CMPs not only demonstrated outstanding efficiency with three electrodes, but when utilized as actual supercapacitors, they achieved very significant specific capacitances of 53, 84.2, and 166 F g^{-1} (Fig. 12a–c). Qi et al. [270] effectively synthesized TFPM-EP-Br, a highly fluorescent 3D ionic olefin-linked CMP. The fully conjugated structure of TFPM-EP-Br has better fluorescence properties and stability. TFPM-EP-Br effectively captured and extracted TcO_4^-/ReO_4^- in real-time by its 3D design, abundant binding sites, and fast mass transfer. This technique might be expanded to identify and detect the additional environmental toxins due to the abundance of functionalized ligands that are particular to certain pollutants (Fig. 12d and e). Weng et al. [271] effectively prepared four Try-based 3D CMPs utilizing a one-step Sonogashira-coupled process that included PyT, TPET, and $BTBr_2$ materials. These CMPs have outstanding heat stability and porosity features. Significantly, the Try-PyT CMP exhibited a surface area of 613 m^2 g^{-1}, which surpassed the surface area of all alternative CMPs. However, with a Td10 value at 400 °C and a char

yielding of 70 wt %, the Try-TPET CMP showed the best thermal stability. In terms of electrochemical properties, the maximum capacitance analysis of 157 F g^{-1} for Try-TPET-BT, 66 F g^{-1} for Try-PyT, 116 F g^{-1} for Try-PyT-BT, and 100 F g^{-1} for Try-TPET have been determined at 0.5 A g^{-1} for each CMP. These data indicate a significant correlation between the surface area and the overall performace of these porosity Try-CMPs. Notably, there was an apparent change in the relationship between electrochemical efficiency and BET surface area. This suggests that the presence of heteroatoms mostly influences the electrochemical features of these composites. These electrode composites exhibited exceptional capacity retention and sustained thermal stability across 2000 charging-discharging cycles, making them an excellent choice for energy conservation. These findings emphasize the potential of Try-based 3DCMPs as very effective composites for power conservation in supercapacitors, highlighting good prospects for their use in practical applications (Fig. 12f and n).

2.6. Morphology aspects of CMPs

CMPs are typically synthesized from homogeneous powders that are insoluble, non-fusible, and highly effective in various applications. Additional types of CMP composites include nano-spherical, nano-tubular, thin-film, monolithic, aerogel, and sponge patterns, which can be sequentially integrated using diverse synthetic techniques. These structural variations enable CMPs to be employed in large-scale applications in the energy sector [272]. CMP films exhibit excellent quality and are ideal polymers in renewable energy applications, mainly as efficient hole conductors due to their substantial thickness, making them suitable for innovative device designs [273,274].

2.6.1. CMPs nanospheres and nanotubes

CMPs nanotubes and nanospheres are used in gas detection, fuel storage, and sustainable energy conversion [274,275]. The morphology of CMPs can be tailored by regulating the reaction conditions and co-monomer composition. Extensive research has focused on optimizing methods to control the micromorphology of CMPs and understanding how different reaction parameters influence their structural properties. Hollow spheres present superior electrochemical and photocatalytic properties compared to solid spheres, making them essential in forming porous composites [276]. Many feasible strategies, namely noble metal-catalyzed formation, composite repeating efficiency [277–279], and layered-by-layered methodology [280] are all effective ways to design CMP structures with hollow structures. A microporous polymer configuration with a semi-zero-dimensional structure was synthesized utilizing a complex lattice method that relies on silicon dioxide [281]. Silicon dioxide may be easily removed by chemically etching it using hydrofluoric acid (HF) or sodium hydroxide (NaOH). Thus, using chemical etching of the silica complex has become a significant technique for designing hollow polymeric structures. Kang et al. [282] used the silicon hemispheres technology to synthesize a highly significant hollow microporous organic network (HMON). The Stober approach involved the addition of silica microspheres to the polymerization process. Subsequently, the combination was treated with HF solutions to remove the silicon structure and get the H/MONs. By changing the processing parameters, it is possible to entirely modify the shell diameter of H/MONs. The Sonogashira coupling process was used to prepare zinc porphyrin (TP/Zn) by reacting 5,10,15,20-tetrakis(4-ethynylphenyl)porphyrin-Zn(II) with deaminated co-monomers. The resulting zinc porphyrin (TP/Zn) was then used to form symmetrically distributed spheres in solutions by the incorporation of bidentate bipyridine (BP)-type substituents [283]. Tan et al. [284] synthesized 2D-CMPs by cross-linking polymer chains of 1,3,5-triethynylbenzene and 1,3,5-tribromobenzene, including alternating phenylene and ethynylene groups. Various liquids were used in the synthesis process. Their research results demonstrate that the solvents used in the synthesis process substantially influence the morphology of CMPs. Toluene, p-xylene, and mesitylene liquids are used to yield spherical, tubular, and plate-like structures, respectively. Their research indicates that the morphology of CMPs substantially influences the capacity to store organic phases, with the plate-like CMP exhibiting the highest performance. Li et al. [285] synthesized nanotubes (hPorBDP NTs) by using Sonogashira-Hagihara cross-coupling polycondensation via silica nanorods as protective substrates, and then scraping the inner centers. Their study demonstrated that the highly porous hPorBDP nanotubes (NTs), characterized by a hollow nanojunction, facilitated the purification process and enhanced the visibility of the active sites of photocatalytic reaction. The hPorBDP NTs were used as mixed catalysts in both batch and continuous flow systems to induce photoexcited electron/energy transfer-reversible addition-fragmentation chain transfer (PET-RAFT) polymerization. The catalyst-bound NTs may be conveniently isolated and recycled using centrifugation. This method minimizes leaching and preserves the catalytic activity of the catalyst, even after many polymerization processes (Fig. 13a–e). Mohammad et al. [286] synthesized three CMPs by Sonogashira coupling brominated-oxadiazole (OXD-Br_2) structural units with TPA, TPE, and Py molecules. These three OXD-CMPs were subsequently combined with CNTs to form OXD-CMP/CNT nanoparticles, which were assessed as supercapacitor electrode materials. The Py-OXD-CMP/CNT electrode exhibited high specific capacitance (504 F g^{-1}) and cycle stability (91.1 % capacitance retention). The OXD-CMPs/CNT nanoparticles exhibit the potential for enhanced charge energy consumption (Fig. 13f–h). Ma et al. [287] developed flame-resistant polymers based on CMPs hollow nanospheres (CMPs-HNS) utilizing a facile immersion technique. Whereas CMPs-HNS-BSb has excellent thermal strength (thermal breakdown temperature was 285 and 320 °C, respective), CMPs-HNS demonstrates an elevated surface area (327.6 and 483.5 m^2 g^{-1}) and super-hydrophobicity (164.2° and 166.8°). CMPs-HNS-BSb exhibited immense peak heat releases (PHRR) of 76.5 and 73.05 W g^{-1} as measured by a microscale combustion colorimeter (MCC). The addition of just 0.5 g of CMP_2-HNS-BSb to EP resulted in a pHRR value of 645.03 kW m^{-2} as assessed by conical calorimetry (CC). The flame-retardant efficiency of the composite is much greater than that of pure EP. The starting process of CMPs-HNS-BSb results in the production of water, phosphoric acid, and PO· free radicals. These components reduce the concentration of oxygen and inhibit the combustion of the polymer. Thus, CMPs might be used as an innovative flame-retardant material (Fig. 13i to q).

2.6.2. Hierarchy porous CMPs

The geometry and structure of CMPs are pivotal in optimizing renewable energy harvesting and storage. For example, phase-changing materials (PCMs) offer significant energy storage properties for applications like greenhouse energy management. However, PCMs leakage during phase transitions poses a challenge. Integrating porous materials with large surface area, well-defined pore configurations, and higher storage efficiencies with PCMs has proven to be an effective strategy to mitigate PCMs leakage during phase transitions [288]. Yan et al. [161] demonstrated that unique hierarchical porosity hollow N-doped carbon spheres (HCSPs) were synthesized and applied as supplementary composites for 1-octadecanol (ODA) to yield HCSP/ODA materials with better basic properties. The small pore size, high porosity, and large surface area of HCSPs enable efficient absorption of ODA, leading to increased hydrophilicity of the HCSP surfaces and reduced porosity of ODA. The intensively specified route for synthesizing SiO_2/SA-CMPs, HCSPs, and their solutions has previously been synthesized. The SEM and TEM morphology of SA-CMP, SiO_2, and SiO_2/SA-CMPs are depicted in Fig. 14a–e. The purity of SA/CMP is shown by its powdered structure, which has a size of around 2 nm (Fig. 14b). SA-CMP emerges on the surface of SiO_2 nanostructures in SiO_2/SA/CMPs, as shown by the interior encasing designs recognized by TEM analysis of SiO_2/SA/CMPs. The average sizes of as-prepared materials are 338, 323, and 318 nm, indicating that the varied concentrations of SA-CMP granule layers on the surface of SiO_2 cores and the size of SA-CMPs layer were improved by

varying the SiO_2 concentration. As the amount of SiO_2 increased, the diameter of shells decreased. Similarly, the morphology of HCSPs exhibits a perfect hollow sphere structure, as indicated by the difference among the center and shells in TEM analysis, and is corroborated by some fractured hemispheres in the SEM data. With increasing SiO_2 content, the layer of HCSPs progressively gets smaller, suggesting a reduction in SiO_2 deposition in the polymeric structure. Under identical composition conditions, the shell size of HCSP-2 (SiO_2 pattern size: 300 nm) is less than that of HCSP-4 (SiO_2 pattern size: 90 nm). Consequently, the content and structure of silica might regulate the shell size of HCSPs, hence optimizing their radiant heat retention capabilities. The XRD analysis was conducted by analyzing the composition of HCSPs. Furthermore, there seem to be two distinctive diffraction patterns at 2ɵ ¼ 39.9° (111) and 2q ¼ 46.4° (200) that are attributable to the remaining Pd nanoparticles and are comparable with the black particles found in TEM images. Moreover, the wide diffraction pattern at 2ɵ ¼ 26° was assigned to the (002) graphite planes, showing that such composites were graphitized during calcinations [289]. The SEM and TEM analyses were utilized to study the geometries of HCSP/ODA hybrids while preserving the structure of HCSPs. In addition, ODA was injected into the porosity and hollow structure. The porous hollow graphite microspheres with tunable porous morphologies and interfacial areas were successfully designed by using silicon nanoparticles as precursors and CMPs as shells. Graphite microspheres with high porosity are efficient transporters for PCMs like ODA. As a result of the different pore sizes and surfaces, the dense hollow graphite showed variable ODA effects. Gao et al. [290] developed an exceptionally CMP structure with a hierarchically linked porous structure by using 4,7-dibromo-2,1,3-benzothiadiazole (BT) and 1,3,5-triacetylene benzene as acceptor and donor. The excellent planarity and strong p-electron decentralization of BT units increase the conductivity of BT-CMP. The coordination behavior of the active sites of C-N is enhanced, and the fast interaction and discharge of K^+ ions is made possible by the synergistic linking of S and N. Furthermore, porous systems coupled in a hierarchical shape allow for simple access to active sites and easily sustain volumetric increase, allowing K-ions to be preserved throughout time. Hence, the BT-CMP anode exhibits an elevated specific capacity (462 mAh/g^{-1}) at 30 mA g^{-1} following 100 cycles and an ultra-longer stability (226.2 mAh g^{-1}) at 1000 mA g^{-1} following 2000 cycles without noticeable modification (Fig. 14f–j). Zhang et al. [291] successfully integrated the micro and mesopore-based CMP (Por-CMP) onto the surface of a 3D interlinked macroporous graphene hydrogel (GH). The as-synthesized GH-CMP included the properties of both CMP and GH, with micro-, meso-, and macroporous patterns and an increased surface area. This method makes it possible to easily develop various graphene-based composites with hierarchical porous properties, as well as POP-based composites with good conductivity. The resultant GH-CMP demonstrated superior capacitive efficiency, including strong specific capacitance and outstanding cycle stability (Fig. 14k to o).

2.6.3. Thin films CMPs

CMP thin films exhibit exceptional physicochemical properties such as porosity, expanded π-conjugation, delocalization of excitons, and efficient electron transfer due to well-defined hole conduction pathways with tunable size [292]. These properties make CMP thin films highly promising for applications in renewable energy technologies and device design [281]. In 2015, the Jiang group mentioned the performance of electropolymerized thiophene-based CMP films at the surface of solution electrodes and characterized the conducting properties of CMP composites [293]. Thus, the electropolymerization of the C-C bond facilitated the arranging of each thiophene subunit in the reaction, creating a thin film. Estimations achieve the optimal configuration of a single hole, and this multi-limbed design optimizes the fabrication of a porosity π-skeleton [294–296]. Additional porosity polythiophene membranes, which were employed in solar equipment on a large scale, could further enhance this capability. The sequencing process may similarly be used for developing CMP nanofilms. Mi et al. [297] described the surface molecular layer deposition (MLD) approach for synthesizing the CMP thin films and their exceptional molecular screening properties as nanofiltration membranes. The deposition of larger-area CMP thin films on porosity substrates is made possible by the gas-phased self-limited interactions among volatile monomers during MLD, which result in films devoid of defects. Through progressively deploying MLD cycle values, the width of the CMP films may be precisely modified; for example, using 100 MLD cycles resulted in a CMP thin film with a width of less than 70 nm. The mixed membranes, which include MLD thin films as chosen layers, exhibited improved molecular screening features compared to other CMP membranes. This is supported by their penetration rate of 134 L $m^{-2}h^{-1}$ bar^{-1}. Moreover, modifying the MLD cycle frequency ranges makes it possible to finely tune the permed selectivity of the CMP membrane. The improvement of the deposition process, namely by selecting suitable precursors, enables the successful deposition of CMP thin films onto polymer substrates that are sensitive to temperature, with dimensions of up to 10 cm × 10 cm. Their work demonstrates the potential and optimistic prospects of MLD CMP thin films, allowing enhanced membranes with controllable thickness and diverse applications (Fig. 15a and b) [297]. Lindemann et al. [298] used orthogonal click chemistry to investigate the surface modification of CMP thin films and nanofilms. The surface modification reaction scheme of the Cu(I) active alkyne-azide cycloaddition (CuAAC) reaction is utilized for the layer-by-layer introduction of the CMP nanofilms, and then the thiolyne reaction is used to amend the alkyne molecules of the interface of final coating of the CMP sheets to perceive the surface alteration. This post-prepared analysis for the external surface of CMP nanofilms is important in increasing their changeability and simplifying their use in some optics/electronics, catalysis, or sensing applications. The etching process is also an excellent performance for CMP films [299]. Their work demonstrates the potential and optimistic prospects of MLD CMP thin films, which allow the synthesis of enhanced membranes with tunable thickness and diverse applications [300]. Moreover, the additional approach is non-standard and can potentially damage the extended π-linked structure of CMPs [49]. As a result, further research is needed to improve an effective exfoliation process for introducing CMP sheets. Wang et al. [301] subsequently revealed an exfoliation method for synthesizing a sequence of fragile CMP layers with improved ORR that could be applied in fuel cells. Similarly, Fig. 15c depicts the process of introducing ultra-thin CMP films, while Fig. 15d depicts the phthalocyanine monomer with four isomers. When employing D_4h and D_2h as two examples, it is possible to achieve nine conjugated structures in an irrational manner (Fig. 15e). The presence of defects and modifications in a single layered decreases the interaction between layers in a polymer made of ethynyl-coupled phthalocyanine combined with a polymer (MPc/CP). This breakdown decreases the connections between layers while significantly increasing the strength required to separate them by more than 50 %. These materials, which are composed of thin sheets and have a high level of dispersion, exhibit a greater number of catalytic active sites and possess enhanced material transshipment capabilities. The primary indication that the main $Fe_{0.5}Co_{0.5}$Pc-CP composite was successfully exfoliated into ultrathin $Fe_{0.5}Co_{0.5}$Pc-CP NSs was the detection of a distinct Tyndall impact, whenever a laser pointer was passed across the solution formed by the supersonic exfoliation technique **(inset in** Fig. 15f). The synthesis of ultrathin $Fe_{0.5}Co_{0.5}$Pc/CP NSs is significantly supported by the TEM analysis, which shows a carbon materials structure of translucent $Fe_{0.5}Co_{0.5}$Pc/CP NSs with horizontal sizes of many 100 μm (Fig. 15f). The size of the $Fe_{0.5}Co_{0.5}$Pc/CP NSs was evaluated using atomic force microscopes (AFM). Similarly, Fig. 15g and h shows that the $Fe_{0.5}Co_{0.5}$Pc/CP NSs have a uniform flat surface with a size of 1.05 ± 0.05 nm, or three layered. Despite this, no noticeable structural patterns are seen in aberrations correction scanning transmissions electrons microscope (AC-STEM) images (Fig. 15i), indicating that the boundary surface of CP are porous due to weaker symmetric isoforms in Fe[Pc(I)$_4$] and Co[Pc(ethynyl)$_4$]. Furthermore, luminous lights (outlined by red dots) are visible in the aberration-corrected

high-angle annulus dark-field S-TEM (AC HAADF-S-TEM) depicted in Fig. 15j, which corresponds to individual Fe/Co particles situated in N_4-coordination positions of phthalocyanine complexes. The unpredictable distribution of such Fe/Co particles, in particular, reveals the disorganized structure of the $Fe_{0.5}Co_{0.5}Pc$/CP NSs. According to the EDS and XPS data, the $Fe_{0.5}Co_{0.5}Pc$/CP NSs are constituted of C, N, O, I, Fe, and Co, as well as the pure $Fe_{0.5}Co_{0.5}Pc$/CP composite. The constituent analysis confirms the uniform surface dispersion of Co, Fe, C, and N across the entire $Fe_{0.5}Co_{0.5}Pc$/CP NSs (Fig. 15k).

2.6.4. Monoliths CMPs

Fiber structures are pivotal in various technologies because they impart specific properties and offer exceptional surface-to-volume ratios [302–304]. These structures serve as foundational elements in synthetic and biological systems, enhancing functionalities in smart materials and connective tissues [305]. Organic polymeric composites enable the development of patterns with diverse properties along specific directions through processes such as extrusion, spinning, and drawing [306]. By incorporating molecular-level modifications, these composites can self-organize into complex fiber systems with desired attributes such as conductivity, shape adaptability, and biological functionality [307]. Non-covalent interactions facilitate the spontaneous formation of asymmetric supramolecular structures from small particles possessing chiral centers or specific solubility properties. Conversely, polymers with covalent networks can synthesize fibrous structures through self-assembly processes [308]. CMPs offer a promising approach to designing fiber structure monoliths due to their strong physicochemical properties, versatile chemical compositions, and large surface areas. These materials have demonstrated performance in various applications, including sensing, storage, separation, and catalysis, thereby supporting advancements in renewable technologies [309,310]. Zhao et al. [311] developed monolithic spiro-bi-fluorene-coupled CMPs (DS-CMPs) for efficiently capturing PM and CO_2 from flue gas emissions. These DS-CMPs are synthesized by coupling 1,3,5-triethynylbenzene with 2,7-dibromo-9, 9'-spirobifluorene (DS-Br_2) using the Sonogashira-Hagihara reaction. The CMPs feature spiro-bi-fluorene units aligned in a precise orientation within the structure, creating centralized holes that enhance surface transfer efficiency. The monolithic DS-CMPs consist of cylindrical nanotube modules with open 3D hierarchical pores and smooth surface layers. They exhibit a notable "slip effect," reducing aerodynamic friction and achieving a limited penetration impedance of 8 Pa. ESP simulation analysis identified key factors contributing to their high capture efficiency and low penetration resistance. The rigid covalent molecular structure ensures DS-CMPs maintain excellent physicochemical strength under high humidity and calcination conditions, preserving their capture capacity. These CMPs also exhibit strong structural stiffness, allowing them to endure multiple regeneration cycles while maintaining cyclic stability. Thermodynamic analysis of three adsorbed systems revealed that a higher micropore-to-mesopore ratio and significant surface charge differences enhance CO_2 adsorption efficiency. Compared to powdered adsorbents, monolithic DS-CMPs offer three distinct advantages in co-capturing PM and CO_2 in commercial bed circulation systems: improved sample evaporation, reduced gas tension drop, and enhanced cycle efficiency (Fig. 16a–e). Jeong et al. [312] synthesized hierarchical effective, flexible, and microporous polymeric monoliths with molecular sensing capabilities. The synthesis of these composites involved the incorporation of integrated heterostructures and inherent micropores into conjugated polymer systems. Nitrogen-doped porous filaments were evenly integrated with ZIF-8 nanoparticles, producing composite monoliths suitable for accelerating the thiol-epoxy process and forming an operational coated surface. The surface had been produced via this process, which included the formation of binding pores with molecular shapes. The fibrous composition of monoliths allowed mass movement, which increased DES sensing efficiency. The authors proposed that using various substrates or chemistry might result in specialized functionality in fibrous monoliths. Furthermore, transforming these polymers into threads or textiles may accelerate the design of textile-based pass--through devices for bio-signal purposes (Fig. 16f–i). Wei et al. [313] demonstrate a unique approach for synthesizing fluorine-enrich CMP monolithic nanofoams using a Pd-stimulated Sonogashira-Hagihara cross-coupling hydration process. The resultant nanofoam was very porous and had a significant surface area of 1194 $m^2\ g^{-1}$ and superhydrophobic properties. Experimental results demonstrated its remarkable insulation ability (heating conductance of 0.02 $W\ m^{-1}\ K^{-1}$) and flame retardance (lower peaking heat emission rate of 10.4–11.2 $W\ g^{-1}$). The FCMPs monolithic nanofoams possess appealing properties, making them an attractive option for improving thermal insulation in modern designs or energy-efficient applications. This is particularly apparent due to their exceptional flame-retardant properties and superhydrophilicity. Moreover, the ability to modify CMPs allows for the design of versatile CMP-based composites that can be adjusted to have desired thermal conductivity and flame-retardant properties, making them suitable for various applications (Fig. 16j to p).

2.6.5. Aerogels CMPs

Fast global economic growth in recent decades has intensified environmental challenges, particularly concerning water pollution [314–316]. Industrial wastewater discharge containing harmful organic pollutants poses significant environmental and health risks [317,318]. The most hazardous heavier metals include Pb^{2+}, which represents an irreversible danger to human health and the environment [319]. Additionally, organic pigments like methylene blue (MB) destabilize ecosystem balance and impede light transmission via water [320]. As a result, hazardous materials, including organic dyes must be removed from wastewater instantly [321]. A range of techniques was investigated, such as absorption [322], membrane isolation [323], and catalysis [324] has proven to be the most practical and effective process [183]. For this reason, various porous polymers have been synthesized, including nanoparticles [325], biochar [326], and composites [327]. Comparatively, CMPs stand out from other materials because of their outstanding durability and large surface area [86,87]. The hydrophobic nature of most CMPs, however, inhibits their solubility in water and, consequently, their ability to adsorb pollutants [328]. Sulfonation is one of the post-processing processes that has been studied. Its goal is to make materials more hydrophilic and increase their adsorption properties [329]. Yu et al. [330] revealed that sulfonated CMPs have demonstrated superior properties in adsorbing molecular dyes and heavier metal particles. Shi et al. [331] and Park et al. [332] discovered that while these methods are effective, their practical use is hindered by challenges such as recovering the materials and the risk of further contaminants after adsorption. These problems highlight the urgent need for further progress in this field [333]. Guo et al. [334] synthesized an unique composite aerogel (CMC/SCMP) by using a sulfonation technique, physical integration, and freeze-drying. Their design focused on attaching CMP nanocomposites onto carboxymethyl cellulose aerogel to increased adsorption performance and facilitate the recovery of nanocomposites. The aerogel that developed demonstrated exceptional properties like porosity, hydrophilicity, tensile stability, and temperature tolerance. They conducted studies to determine its adsorption capability for heavier metal particles (Pb^{2+}) and cationic dyes (MB) in water, and the results were outstanding. Moreover, the hydrophilic composition and porous structure of the CMC/SCMP allowed for efficient water transfer and enhanced light absorption when coated with polypyrrole. This suggests that it has the potential to be used as a unique method for obtaining renewable steam energy with outstanding efficiency (Fig. 17a and b). Zhou et al. [335] synthesized a new aerogel composite by inserting the phase transition material TD into CMP-H hollow spheres, combining it with decreased graphene oxide, and depositing it on an aerogel formed of hollow glass microspheres. This material exhibits remarkable photon absorption, excellent porosity, and effective thermal resistance. To accomplish efficient vaporization in all weather conditions, the material that endures a phase transition was successfully absorbed by the

CMP-H-based material. This is because the material has high porosity and a large surface area. The RCMP@TD-HA exhibited evaporation rates of 1.68 kg m^{-2} h^{-1} and 2.95 kg m^{-2} h^{-1}, under light frequencies of 1 kW m^{-2} and 2 kW m^{-2}. In addition, when there was no sunlight, RCMP@TD-HA used the TD as exceptional heat retention properties to sustain evaporation. Furthermore, the oil resistance of the aerogel composite was enhanced by putting an oleophobic coating to its minimal interface, hence expanding its potential applications. The presence of oil pollution and limitations of water flow led to an increase in the evaporation performance of the O-RCMP@TD-HA from 21.3 % to 90.2 % in water contaminated with oil, attributed to the oleophobic coating. Their research presents a technique to enhance the evaporation of surfaces caused by solar energy, particularly in regions with fluctuating sunlight. It also introduces potential applications in practical situations, such as the purification of oil waste products (Fig. 17c to l). Ye et al. [336] revealed a unique technique for synthesizing three types of PCM nanocomposite using PCMPECAs as carbon-based supportive materials integrated with HDA for solar/electrically-to-thermally power transformation and preservation. They examined the capacity of CMPs carbon aerogels to efficiently convert and store solar or electrical energy into heat based on their unique structure and carbon composition. The PCMPECAs/HDA hybrids exhibited enhanced photo- and electro-thermal efficiency and superior conductivity compared to pure HDA. These hybrid materials demonstrated outstanding thermal conductivity (reaching 0.344 W/m K at 25 °C), significant power storing efficiency (up to 205.0 kJ/kg), structural and thermal stability, and excellent light conversation and retention performance (up to 93.5 %). Despite undergoing 300 cycles of warming and cooling, the PCMPECAs/HDA composites maintained a substantial amount of absorbed heat, measuring at 150.20 kJ/kg. In addition, the composites exhibited exceptional electric-thermal properties at low voltage levels (Fig. 17m).

2.6.6. CMPs sponges

The importance of desalinating industrial, aquatic, and oceanic waters has increased due to the growing scarcity of global freshwater resources [337]. Various techniques proposed for this purpose include electrodialysis [338], reversal osmosis [339], membrane filtering [340], and thermal distillation [341]. An innovative and sustainable approach to harnessing photovoltaic energy involves solar-thermal conversion for steam generation without additional power sources [342]. Conventional solar evaporators have limited performance due to their poor sunlight absorption and fast heat loss [343]. Materials with exceptional conversion potential and high light-absorption capacity are necessary to enhance the performance of solar-thermal conversion [344]. Polymers derived from metal materials, particularly plasmonic metals like Au [345] and Ag [346], exhibit a significant absorption of near-infrared (NIR) light, leading to their development as water evaporators [347]. Carbon-based polymers have also been considered [348–350], but they are often expensive and lack recyclability. Graphene oxide (GO), carbon nanotubes (CNTs), and amorphous carbon are examples of carbon-based materials that possess broad lighting absorption area but are afflicted with elevated heating conducivity, which results in accelerated heat dissipation and reduced evaporation rates [351–353]. Effective and practical methods are required to generate solar-thermal transition polymers with high light absorption and limited heat waste for dehydration. Coupled polymerization is a potential new class of composites with tunable bandgap and strong NIR absorption for photothermal synthesis [354]. CMPs, characterized by their strong π-coupling and inherent porosity, provide an ideal platform for solar steam generation [355]. The large surface area, high porosity, and strong NIR light absorption of CMPs enable efficient use of solar fuel, enough fluid channels for energy transmission, and the capacity for managing steam overflow [356]. CMPs may be used for photovoltaic thermal transformation because of the addition of porphyrin and aniline-based monomers, which improve their photosensitivity, affordability, superior conductivity, and capacity to absorb near-infrared radiation [357]. Optimizing the evaporator structure is essential to improve the properties of solar heating production. Through the reduction of heat conduction and dispersion of light in cavities, macropore structures, including consistent, disrupted, or multilayer channels, effectively utilize light and provide thermal insulation [358]. Various porous materials, both biological and synthetic, may be used to design solar evaporators to extract fresh water. These materials include sugar cane [359], straw [360], loofah [361], extended polyethylene bubbles [362], nickel bubbles [363], and polymer formation [364]. Shi et al. [365] described porphyrin-based CMPs as innovative solar thermoelectric illumination absorbents. Initially, porphyrin/aniline-based CMPs (PACMPs) had been synthesized using a Buchwald-Hartwig (BH) cross-coupling reaction among para-phenylenediamine (PDA) and meso-tetra(pbromophenyl)porphine (TP), which exhibited an effective solar-thermal converting feature. The PACMPs were then inserted into the polyurethane (PU) sponge structure using a dip-coating process that included a green cross-coupling reagent derived from glucaric acid chitosan. The PACMP-mixed sponges (PACSs) attained an elevated evaporation amount (1.31 kg m^{-2} h^{-1}) and solar-thermal converting performance (86.3 %) beneath a single sun radiation (1 kW m^{-2}). In addition, PACSs demonstrated remarkable desalination and dye decolorization capabilities, effectively removing over 99.9 % of the saline and more than 99.2 % of the dye, from the seawater of the Yellow Sea. The potential uses for PACSs include sterilizing, sewage treatment, and saltwater desalination because to their inherent lightness and enduring solar-thermal evaporation capability (Fig. 18a–g). Hasi et al. [366] synthesized two types of hydrophobic CMP sponges (CMPs-1@sponge and CMPs-2@sponge) by polymerizing a specially designed monomer on melamine sponges using the Sonogashira-Hagihara coupling reaction. These sponges exhibited exceptional strength, increased hydrophobicity, and enhanced structural integrity. Both CMPs, namely sponges, effectively eliminated small concentrations of organic benzene from water, as well as oils and other organic compounds like floating oil and denser oil (Fig. 18h to o). Kim et al. [367] presented a single-piece catalyst based on a MOP sponge. The MOP sponge has a 3D network structure composed of tubular polymeric fibers. The material displayed a hierarchical porosity and variable compression. After functionalizing the sponge with sulfur couples, silver nanoparticles were used as a decorating agent. The performance of the monolithic catalyst was evaluated by its involvement in the elimination of 4-nitrophenol. The flexibility of the catalyst was used to enhance the rate of reaction (Fig. 18p to r).

3. Application of CMPs

3.1. Photocatalytic water splitting (WS)

An effective strategy for achieving a carbon-free world involves using photoactive semiconductor catalysts to convert abundant solar energy into sustainable and environmentally beneficial hydrogen energy [368–371]. The efficiency of a photocatalyst plays an important part in extracting the efficiency of the conversion of solar energy into chemical energy [372]. A range of photoactive catalysts, including inorganic [373], organic [288], and organic-inorganic composites [374], have been developed for the purpose of yielding H_2 from sunlight. The performance of photocatalytic HER is primarily determined by the properties of the photocatalysts, such as their molecular configuration, electrical properties, bandgap, and surface composition [375–381]. Therefore, it is essential to enhance the performance of H_2 by developing efficient photocatalysts [382–384]. Organic semiconductive photocatalysts include many desired properties, including a broad range of visual-illumination adoption, the ability to respond quickly to different carriers, multiple synthetic processes, and the capacity for tunable electronic designs. These features have raised interest in organic semiconductive photocatalysts, which are comparable to inorganic semiconductor and metal-based photocatalysts [385–387]. Graphitic carbon nitrides (g-C_3N_4) have been extensively studied for their potential

use in HER. Similarly, optimizing the synthesis technique might significantly enhance their efficiency [388–393]. Moreover, organic photocatalysts provide a multitude of renewable advantages, flexible structural methods, and tunable energy spectrum configurations, which are just a few of their distinctive benefits [394–396]. The process of HER has been thoroughly investigated utilizing photocatalysts that have organic semiconductor properties and are characterized by linked molecular structures. These include small molecules [397], g-C_3N_4 [398,399], crystallized porous organic polymers [400], and amorphous CMPs [401–403]. The CMP photocatalysts have advantages, including the capacity to elongate polymer structures, a significant surface area, and long-lasting composition, which enhance the speed of photocatalytic HER [404]. Significant progress has been achieved with CMP photocatalysts, specifically in the efficient production of H_2 using natural sunlight [405]. Several designing methodologies were revealed to enhance the efficiency of CMP photocatalysts for producing H_2 via photocatalysis. For example, Cooper et al. [188] demonstrated the capacity to accurately modify the organic composition and bandgap of CMP photocatalysts via sequential copolymerization. Thomas et al. [406] designed polymeric structures, including heptazine donors and acceptors (D-A) that demonstrated superior photocatalytic activity compared to g-C_3N_4 composites. This was due to the efficient separation of charge carriers generated by light. Yu et al. [407] demonstrated that designing a D-A polymer structure is an operative method to improve the photocatalytic efficiency of CMPs. Wang et al. [408] prepared benzothiadiazole-containing CMPs, and analyzed the impact of polymer structure on photocatalytic performance, and observed that linear polymers demonstrated superior photocatalytic efficiency compared to cross-linked polymers. Mothika et al. [409] developed a series of microporous CMPs that are linked to a D-A system. In this system, 9-fluorenone (F) is the acceptor, while tetraphenylethylene (TPE) is the donor. The synthesized CMPs, namely $F_{0.1}$CMP, $F_{0.5}$CMP, and $F_{2.0}$CMP, possess tunable band gaps and demonstrate the ability to produce H_2 via photocatalytic WS. The CMPs showed intramolecular charge transfer (ICT) absorption in the visual range, with the highest absorption appearing at a wavelength of 480 nm. The bandgap may be precisely controlled between 2.8 and 2.1 eV by adjusting the quantity of 9-fluorenone. The color of the material exhibits an obvious transformation from green to red as the amount of 9-fluorenone increases. This change occurs because energy is transferred from locations in the material that are not involved in carrying electrical charge. These regions emit photons in the range of 540–580 nm. The D-A CMPs have higher photocatalytic efficiency compared to the 9-fluorenone-free polymer ($F_{0.0}$CMP) due to their lower bandgap and increased absorption of visible light. The $F_{0.5}$CMP material exhibits the most H_2 production under visible light, owing to its optimal band gap of 2.3 eV. Additionally, each polymer has exceptional solubility properties in organic combinations and may be easily used as coatings on solid substrates (Fig. 19a and b). Han et al. [410] investigated the use of two-electron donors, tetraphenylethylene (TPE) and dibenzo [g,p]chrysene (DBC), together with the BTDO acceptor, to synthesize two D-A CMP photocatalysts for H_2 formation. According to their study, the arrangement of the electron donor has a substantial impact on the photocatalytic performance of the consequent materials. The distorted molecular structure of TPE hinders the alignment of the composite, therefore inhibiting the movement of charge particles. However, the extended π-conjugated planar structure of DBC allows it to facilitate the movement of charges and separate electrons and holes under light. The unmodified DBC-BTDO polymer, derived from the DBC donor, has an outstanding photocatalytic HER of 104.86 mmol h^{-1} g^{-1} under UV–Vis irradiation ($\lambda > 300$ nm). This HER is much higher than the TPE-BTDO polymer, which is only 1.80 mmol h^{-1} g^{-1}. Furthermore, the addition of 1.0 wt% Pt as a co-catalyst enhances the HER of DBC-BTDO to 126.81 mmol h^{-1} g^{-1}. Their study revealed the importance of the electron donor's structure in determining photocatalysis's efficiency. Additionally, it suggests that dibenzo[g,p]chrysene might be a promising substitute electron donor for producing high-performance D-A polymer photocatalysts (Fig. 19c and d). Wang et al. [21] presented a CMP consisting of dibenzothiophene superoxide as an effective molecular photocatalyst for generating H_2 using visible light. The experiment analyzed whether the elongation of a helix, caused by a cross-linker with four polymerizable functional groups, ranging from benzene to biphenyl to p-terphenyl, effected the performance of the catalyst. The photocatalytic efficiency of the developed CMPs reduces as the size of the cross-linker increases. The interference of coupling and consistency, which impedes the propagation and dissociation of light-excited charge carriers, may be ascribed to the twisted polymer structure. Notably, the benzene cross-linker allows DBTD-CMP1 to demonstrate exceptional photocatalytic performance. Without a Pt co-catalyst, it obtains a median HER of 2460 μmol h^{-1} g^{-1} during visual light ($\lambda > 420$ nm). In addition, when DBTD-CMP1 is doped with 3 wt% Pt, it's HER significantly rises to 9200 μmol h^{-1} g^{-1} under broad-spectrum visible light ($\lambda > 300$ nm). Their findings suggest that CMPs containing dibenzothiophene dioxide have the capability to act as photocatalysts for generating H_2 from photocatalytic WS (Fig. 19e and f). Han et al. [411] prepared a series of D-π-A-A-type CMPs using a threefold sequential copolymerization method. They used pyrene, thiophene, and BTDO as electron donors, π-bridges, and electron acceptors. The purpose of this structure was to include a substantial amount of photoactive acceptors, so increasing the number of active sites accessible for H^+ reduction and subsequently promoting the production of H_2. In order to prevent direct bonding between pyrene and BTDO, a tetra-functional bromine-activated group monomer was designed by pre-coupling the pyrene donor with the thiophene π-bridge. Pyrene units and bromine/borate-functionalized BTDO were used in a precise ratio to promote polymerization, ensuring accurate control over the composition (Fig. 19g).

3.2. Photocatalytic overall water splitting (OWS)

According to photocatalytic water reduction or oxidation, the cost of stoichiometry WS into HER and OER without adding a loss factor is low due to the employment of both photogenerated electrons/holes [250, 412–423]. The investigations of active CMPs for PWS are currently new. In 2016, Wang et al. [424] observed that the structure of g-C_3N_4 had a substantial effect on its catalytic activity and that Pt-doped g-C_3N_4 was an effective catalyst for OWS. The urea-based g-C_3N_4 represents a 2D nanosheet structure and a consolidated layer-like structure, resulting in superior charge transfer compared to the other two materials synthesized from the precursors of dicyandiamide and ammonium thiocyanate [425–427]. None of the three pure forms of g-C_3N_4 without any Pt display any photocatalytic activity. Similarly, after the deposition of Pt as a cocatalyst within these materials demonstrated superior performance, corresponding to HER and OER of 1.2 and 0.6 mmol h^{-1} ($\lambda = 420$ nm). Recently, Zhang et al. [428] synthesized 3D g-C_3N_4 with significant crystallinity. The large surface area of such material (130 m^2g^{-1}) was superior to that of pristine g-C_3N_4 (10.83 m^2g^{-1}) and g-C_3N_4 nanofilms (93.84 m^2g^{-1}). Interestingly, the 3D g-C_3N_4 exhibited HER and OER values of 101.4 and 49.1 mmol $h^{-1}g^{-1}$ after adding 1 wt% Pt and 3 wt% IrO_2. Such materials exhibited that the inclusion of co-catalysts plays an essential function, therefore dominating the surface shape of g-C_3N_4 for photocatalytic WS. In 2017, Xu et al. [429] synthesized 1,3,5-tris-(4-ethynylphenyl)-benzene (TEPB) and 1,3,5-triethylbenzene (TEB) by Glaser oxidative linking of terminal alkynes. Saber et al. [430] prepared a series of semiconductor D-A CMPs with varying S and N_2 ratios and degrees of conjugation for effective photocatalytic H_2 and O_2 formation via photocatalytic WS. They employed a carbazole (Cz) group as the donor, while acceptors included pyrene (Py), triphenyltriazine (TPT), benzothiadiazole (BT), and thiazolylthiazole (TzTz). The obtained D-A CMPs have a substantial surface area (up to 1530 m^2 g^{-1}) and strong thermal stability (T_{d10}: up to 623 °C; char yielded: up to 83 wt%). Furthermore, the Cz-TzTz CMP demonstrated an exceptional HER of 15.3 mmol g^{-1} h^{-1} with the ascorbic acidic as the sacrificial agent, avoiding the requirement for an extra Pt co-catalyst. Interestingly, when $AgNO_3$ was

used as a sacrificial agent, the Cz-TPT CMP produced an outstanding OER of 3.38 mmol g^{-1} h^{-1} (Fig. 20a–c). Yi et al. [431] synthesized a new D-A type CMP called TBT-BDT using Pd-catalyzed directed C-H arylation. The TBT-BDT has excellent thermal stability and photoelectric properties because of its extremely symmetric and elongated interlinked structure, especially the electrons-donated group BDT. Similarly, the TBT-BDT exhibited a superior HER performance under visible light to maintain the photocatalytic OWS. Their study emphasizes the synthesis of effective photocatalysts by demonstrating how electron-enrich monomers may be easily modified to alter the photoelectric properties, band arrangement, and photocatalytic performance of CMPs (Fig. 20d and e). Wang et al. [432] developed a set of eight 2D conjugated polymers (CPs) through the assembly of molecular precursors synthesized from diacetylene and benzene. These precursors were active sites for HER and OER. They investigated the photocatalytic, fundamental, electrical, and optical properties of OWS using first-principles calculations. The electrical topologies and absorption spectrum of CPs were substantially changed by adding benzo-heterocyclic rings, which made them ideal for visible light-induced OWS. In contrast to sacrificial reagents and cocatalysts, CP-4, which is composed of benzotrifuran and diacetylene, was distinguished by its ability to activate OWS in a stable condition under the influence of its own light-excited bias. The behavior of HER was mainly attributed to diacetylene units, whereas OER behavior was focused on benzo-heterocyclic rings. The photocatalyst CP-4 demonstrated an optimal solar-to-hydrogen (STH) efficiency of 13.87 %, indicating its applicability as a viable option for massive commercial OWS (Fig. 20f). Wang et al. [254] showed that polymer structures connected by 1, 3-diyne bonds accelerate oxidative OWS with estimated quantum yields of up to 10 % at a wavelength of 420 nm. Their exceptional photocatalytic efficiency is attributed to their different porous, sheet-like structures that exhibit extended conjugation. This arrangement enhances the displacement of charges over greater distances and facilitates surface interactions that successfully minimize significant charge recombination. First-principles simulations may provide a better understanding of OWS processes by identifying active sites on polymeric photocatalysts and potential four-electron reaction pathways (Fig. 20g and h).

3.3. Photocatalytic CO_2 reduction reaction (CO_2RR)

The extensive consumption of fossil fuels has led to a substantial increase in the levels of CO_2 in the atmosphere over time, resulting in significant ecological and conservation concerns [433–438]. Among the most efficient solutions to these problems is to use sunlight radiation to convert CO_2 into hydrocarbons [439,440]. The technique could provide significant economic and ecological benefits by lowering greenhouse gas emissions while simultaneously addressing the fuel constraint issue [441–443]. Moreover, CO_2 molecules are exceptionally linear and stable. The conversion of CO_2 sources is challenging due to the need for extra energy to break the bonds between carbon and oxygen [444]. Water is required to provide H_2 in a standard photoreduction process of CO_2 to reduce. During this method, catalysts facilitated the absorption and subsequent release of CO_2. Polymer materials are discouraged from use in a liquid-solid structure for photocatalytic CO_2 reduction in entirely saturated aqueous media [445]. The CO_2 reduction process occurred when the solid and liquid phases were exposed to light at their contact. Triethanolamine, an organic solvent, is necessary to remove undesired holes. However, the process of reducing CO_2 by photocatalysis in a gas-solid system is relatively simpler, despite water vapor being the primary source of electrons. Subsequently, the photocatalysts were uniformly distributed at the base of the reactor. While photoexcitation led to a decrease in CO_2, a porous composites chemisorbed and enhanced the reduction of CO_2. The majority of catalysts used for photocatalytic CO_2 reduction are inorganic compounds, namely metallic oxides or sulfates such as TiO_2, CdS, $BiVO_4$, and others [446–448]. Organic polymers have received less attention until recently. To achieve optimal photochemical substitutes with enhanced results, it is necessary to consider various factors such as band gaps, surface area, CO_2 absorption spectrum, energy layer straights, and photoexcited charges separation when developing highly efficient porous CPs for photocatalytic CO_2 reduction. Furthermore, the performance and options of the reactions may be influenced by external variables and operational parameters, such as the intensity of catalysts, the pH of solutions, the pressure of CO_2, and the temperature. The main obstacle to attaining high efficiency in photocatalytic CO_2 reduction in a liquid-solid system is the very low solubility of CO_2 in the reaction environment. Barman et al. [449] synthesized a redox-active CMP named TPA-PQ by combining an electron-donor (tris(4-ethynylphenyl)amine, TPA) with a redox-active acceptor (phenanthraquinone, PQ). The non-metal photocatalyst TPA-PQ was used to induce under visible light to convert CO_2 into CH_4, demonstrating exceptional efficiency (32.2 mmol g^{-1} in 16 h) and high selectivity (>97 %). The analysis of the photophysical, electrical, and computational properties showed that TPA-PQ yields stable charge particles under UV light. These particles gather electrons at the PQ cell and successfully facilitate the reduction of CO_2 (CO_2RR). In order to demonstrate the importance of the semiconductor donors-acceptors property, another material (TEB-PQ) was designed by replacing TPA with triethynylbenzene (TEB). This substitution resulted in a significantly lower efficiency of photoreduction of CO_2 into CH_4 (4.3 mmol g^{-1}) compared to TPA-PQ. The closest keto group of the photocatalyst acted as a site for the interaction between deposited CO_2 and chemical intermediates, thereby facilitating the eight-electron reduction process. A catalytic chain has been developed to study the mechanical properties of CH_4 production in TPA-PQ. Through in-situ DRIFTS observation and DFT studies, a chemical intermediate was identified (Fig. 21a–c). Meng et al. [450] synthesized two redox-active CPMs based on a surface connected by thiazolo[5,4-d]thiazole, which were utilized as non-metal photocatalysts to selectively reduce CO_2 into CH_4. Similarly, the CMP named Tx-TzTz-CMP-2 exhibited remarkable photocatalytic performance, thus producing 300.6 μmol g^{-1} h^{-1} of CH_4 with a selectivity of 71.2 % by featuring an improved π-conjugated structure. The use of phenyl incorporation as a π-bridge has been shown to enhance electron delocalization, leading to improved intramolecular charge transfer and dissociation capabilities. This is achieved by reducing the exciton binding energy. The quantitative and analytical studies into the action mechanism revealed that the N-site of the thiazole unit served as both a catalytic core and an electron reservoir, enabling the hydrogenation of CO_2 and the subsequent synthesis of CH_4. In addition, the incorporation of the thiazole unit enhanced the confinement of photoexcited electrons, resulting in a reduction in the energy required for *CHO formation and an increase in the selectivity towards CH_4 (Fig. 21d–f). Rahimi et al. [451] developed a bipyridine-based CMP (TEB-BPY) with exceptional mechanical and physical stability with a surface area of 430 m^2 g^{-1}. The reagent [$Re(CO)_5Cl$] was deposited onto TEB-BPY, producing the Re@TEB-BPY. The material exhibited efficient catalytic ability for the reductivity of CO_2 during visual light, producing CO at a rate of 90.8 μmol g^{-1} h^{-1} with a selectivity of around 68 %. Triethylamine (TEA) served as a sacrificial electron donor. The use of 1-benzyl-1,4-dihydronicotinamide (BNAH) as a sacrificial source of electrons, together with TEA as a base, led to a significant change in selectivity towards CH_4, with a rate of 2.05 mmol g^{-1} h^{-1} and a selectivity of around 96 %. The capability of catalysts to absorb light allowed for its recycling and showed remarkable stability without the need for an extra photosensitizer. A highly efficient photocatalyst for reducing CO_2 has been invented and designed. This catalyst utilizes intense visible light and selectively yields desired products by utilizing sacrificial electron donors. Their study used DFT simulations to get a detailed understanding of the mechanism, highlighting the importance of BNAH in selectively producing CH_4 rather than CO. Theoretical calculations, confirmed by experimental tests, showed the unique interaction between BNAH and TEA that enhances the efficiency of synthesis (Fig. 21g–k).

3.4. Electrocatalytic overall water splitting (OWS)

The unregulated consumption of fossil fuels constitutes a significant risk to global ecological systems and modern society since it emits greenhouse gases, which cause global warming and the greenhouse effect [452–454]. The Paris indicate of the worldwide society in 2015 emphasized the essential requirement of investigating renewable energy materials in order to satisfy the rising needs effectively [455]. Electrocatalytic OWS via bifunctional electrocatalysts during the HER [456] and OER [457] is considered an optimized approach for the current energy crisis, as it provides renewable energy. The OER is essential in many energy-converting devices, whereas H_2 is expected to be widely used as a fuel due to its high energy efficiency and lack of emissions [458]. IrO_2, Ir_2O_3, RuO_2, and Pt were identified as exceptional catalysts for achieving high performance in OER and HER. Nevertheless, their limited availability and excessively high cost hinder their widespread application [459]. Researchers are now developing cost-effective bifunctional electrocatalysts that address this problem by using porous nanocomposites and abundant non-noble elements [460,461]. The potential for optimal OWS is demonstrated through the utilization of porous systems, including MOFs [462], metal-modified COFs [463], and metal-grafted CMPs [464]. In addition, mixed synthesis techniques that combine transition metal oxides with materials like amorphous carbon [465], graphene [466], and carbon nanotubes (CNTs) [467] have demonstrated effective HER and OER performance. However, certain challenges remain, such as the difficulty of designing COF structures on a large scale and the limited capacity of MOFs to endure hydrothermal conditions. CMPs have recently gained interest due to their many functional properties, such as their low production costs, higher metals-doped capability, functioning flexibility, and facile synthesis. CMPs feature properties that make them suitable candidates for several applications, including gas storage [186], energy applications [468], sensing [469], and catalysis [470]. Li et al. [471] effectively synthesized an innovative organic monomer known as 1,3,5-triazine (TBPT), which is 2,4,6-tris(5-bromopyrimidin-2-yl) and possesses N-rich and 3-associated pyridine coordination sites. Using the Sonogashira reaction and TBPT, researchers synthesized two new composite materials, CMP-Py(2H) and CMP-Py(Co), by connecting them with Py(2H) or Co(II) porphyrin. CMPPy(Co)@Co was synthesized by further metalizing CMP-Py(Co) with $CoCl_2$ resulting in Co-N_2Cl_2 structures. Electrochemical and theoretical studies have shown that CMPPy(Co)@Co has improved efficiency for the OER because of its abundant and easily accessible Co^{2+}-pyridine sites (Fig. 22a–g). Wang et al. [472] deployed a pyrolysis method to yield cobalt nanoparticles (CoNPs) enclosed in N, O-dual-doped carbons (CoNOCs). This electrocatalyst, derived from CMPs, is both cost-effective and stable for the process of HER. The PAQTA precursor was used in this technique. The precursor was chemically applied onto carbon fiber fabric (CFC) to yield membrane-like HER electrodes, which possess the potential for use in deeper electrolyzed units. To synthesize a significant amount of CoNOC-x catalysts, PAQTA was fully infused with $Co(acac)_2$ and then subjected to pyrolysis in a nitrogen environment at four specific temperatures (x = 700, 800, 900, and 1000 °C). In a loose manner linked metal species were later removed using sulfonic acid etching (Fig. 22h to l). Das et al. [473] used the Suzuki cross-coupling reaction to synthesize co-polymers of porphyrin and pyrene, including transition metal ions (Ni^{2+}, Cu^{2+}), into CMPs. The resulting materials have significant specific surface areas, measuring 1400 m^2g^{-1} and 1350 m^2g^{-1} for the nickel and copper alternatives, respectively. Additionally, they possess considerable microporosity and extensive π-coupling. The use of polymers coated on nickel foam in continuous sweeping voltammetry exhibited remarkable overpotential rates for both the HER and the OER. The catalyst Cu-POR-Py exhibited lower overpotential values of 170 mV for OER and 213 mV for HER, compared to Ni-POR-Py, which had values of 250 mV for HER and 163 mV for OER. These overpotential values were used to achieve a current density of 10 mA/cm^2. Studies on the performance of Ni-Por-Py and Cu-Por-Py composites, along with further analysis of the associated electrochemical properties using drop casted materials on glassy carbon electrodes, have demonstrated that transition metal materials with an abundance of porphyrin holes in CMPs enhance OWS in alkaline systems (Fig. 22m and n).

3.5. Electrocatalytic CO_2RR

The electrochemical conversion of CO_2 to fuels and chemicals is regarded as an effective approach for exploiting CO_2 in sustainable energy sources [474–476]. Electrocatalysts are required to reduce energy storage and enhance performance due to the very stable and unreactive properties of CO_2 and the complex processes involving multiple electrons and protons. Considerable efforts have been conducted to transform CO_2 into CO and other significant compounds by using various electrocatalysts, including metallic materials [477], metallic oxides [478], MOFs [479], carbon resources POPs [480], and metallurgy [481]. CMPs are distinguished from POPs because of their prolonged network-like recombination, stable micropores, and chemical stability. As a result, they have the potential to be an ideal photosensitizer. An electrocatalyst is a composite that increases the amount of an electrochemical reaction by reducing the formation energy required for the reaction to occur [87]. Like MOFs, inserting individual metal atoms into CMPs may enhance catalytic efficiency, although their electrocatalytic conductivity is inefficient [482]. A viable solution to this issue is to use carbons like graphene and CNTs as substrates for CMPs instead of reducing them into carbon entities by pyrolysis [483]. However, the electrocatalytic efficiency of these heterogeneous catalysts is only sufficient and seldom attains its complete ability for practical purposes [484,485]. Due to the challenges in precisely controlling the dimensions, shape, and composition during synthesis to effectively expose catalytic sites and enhance charge transference kinetics, showed that CMPs are amorphous structures. Molecular catalysts, such as metals phthalocyanines (MePcs) and their counterparts, have a higher selectivity for molecules with a single carbon atom, mainly CO, to reduce CO_2. Integrating molecular catalysts into nanoscale structures is a promising method to yield solid electrodes in functioning technology and improve their stability and selectivity [486]. The simplest approach for inserting MePc groups onto CNTs is by either covalent or non-covalent incorporation [487]. In addition, the polymerization of benzene-1,2,4,5-tetracarbonitrile via metallic centers allows for the formation of an extremely thin poly-MePc, including surrounding CNTs [488]. Smith et al. [489] synthesized an electrocatalyst for the electrocatalytic reduction of CO_2 by incorporating a fac-[Mn(bpy)$(CO)_3$-Br] unit into a CMP structure. The SH cross-coupling technique were utilized to yield CMP-(bpy)20, which was then mixed with [$Mn(CO)_5$Br] to form CMP-(bpy)20-Mn. The material had a surface area of 549 m^2 g^{-1}. CMP-(bpy)20-Mn absorbed an only 4.7 % of CO_2 by weight at a temperature of 298K and pressure of 1 bar. This is lower than the 8.4 % by weight of BPL carbon, which serves as a commonly utilized reference material (Fig. 23a). Soliman et al. [490] synthesized the microporous composite material PyPOP@G via the SH cross-coupling reaction. This material exhibited substantial electrocatalytic efficiency for electrocatalytic CO_2 reduction (5 mA cm^{-2} at −1.0 V vs RHE), which was utilized to increase the electronic transference potential in CMPs (Fig. 23b). Zhu et al. [491] proposed an innovative method for enhancing the electrocatalytic CO_2 reduction by synergistically integrating a CMP with a supportive polymer. A sandwich-shaped CMP has been synthesized by directly polymerizing the CMP onto an extremely thinner exfoliating nickel phosphorus trisulfide ($NiPS_3$) 2D structure that contained Ni sites coupled in N and S. A porous carbon nanosheet (CNS) reagent was synthesized subsequent to pyrolysis and disintegration, featuring singular diffused Ni atoms and S and P doping agents. The larger proportions of elements and surface areas in these porous CNS, as compared to typical porous CNS, allow for the exposure of single-atom sites and improved conductance. This leads to the exceptional

electrocatalytic performance of the porous CNS (Fig. 23c). Wang et al. [492] deployed a solid-state iono-thermal technique for obtaining a fragile CMP coating on CNTs by controlled Scholl-linked reaction of non-metallic H_2Pc and CoPc. A 2D system with a high degree of cross-linking was achieved by copolymerizing H_2Pc and CoPc using $AlCl_3$ as the catalyst. When CoII metal compounds were present together, these systems experienced a significant change and formed an extremely thin layer that resembled CNTs. H_2Pc units served two roles by enhancing the nucleophilicity of Co sites for CO_2 coupling and acting as proton sources via pyrrolyl moieties to enhance the reaction capacity of CO_2 molecules via H-linking reactions. The CNT@CMP (CoPc-H_2Pc) samples exhibited exceptional stability and selectivity in their capacity to convert CO_2 into CO. Their study presents a novel and untested approach to copolymerization, which enhances electrocatalytic performace by increasing the quantity of uniformly distributed CoN_4 sites by the use of proton/electron double donation (Fig. 23d and e).

3.6. Batteries

CMPs have recently garnered attention as promising materials for various energy storage applications, including batteries. High-performance batteries require cathode materials that have particular capacities and a stable redox voltage [493]. However, synthesizing organic electrodes with a redox voltage greater than 2.5 V against Li/Li^+ is quite difficult. Chen et al. [494] synthesized a unique monomer based on triphenylamine, which was then transformed into the CMP poly[1,3,5-tris(4-diphenylamino-phenyl)benzene] (PTTPAB) using chemical oxidizing polymerization [495]. As anticipated, the surface area of PTTPAB is much higher at 595 m^2/g compared to the usual PTPAn, which has a surface area of 11 m^2/g. In comparison to the cell performance of PTPAn, the PTTPAB synthesized in its initial state showed enhanced rate efficiency, longer cycle life, and superior coulomb performance. As a result, it is a viable cathode composite for batteries (Fig. 24a). Luo et al. [496] synthesized a cathode material called poly(pyrene-co-anthraquinone) (PyAq) using chemical methods. This material was designed by combining co-anthraquinone and pyrene materials. The synthesized PyAq has a large surface area, a significant π-conjugated structure, and several redox-active areas. These areas are formed from the carbonyl family of the anthraquinone group. Therefore, the PyAq cathode shows exceptional electrochemical performance for both lithium-ion batteries (LIBs) and potassium-ion batteries (KIBs). LIBs assembled using a PyAq cathode exhibit a significant reversible capacity of up to 169 mAh g^{-1} when operated at a current density of 20 mA g^{-1}. These batteries also demonstrate a higher rate capacity of 142 mAh g^{-1} when operated at a current density of 1000 mA g^{-1}. Additionally, they possess exceptional flexibility, retaining 92.9 % of their capacity after 350 cycles at 20 mA g^{-1} and 79.6 % of their capacity after 4000 cycles at a higher current density of 1000 mA g^{-1}. In addition, the PyAq cathode used in KIBs has an exceptionally long cycling durability of more than 800 cycles and a substantial reversible capacity of 143 mAh g^{-1}. The ex-situ FTIR spectroscopy investigation demonstrated that the PyAq cathode displays notable reversible lithiation/delithiation activities due to its large redox activities and the reversibility of carbonyl groups (Fig. 24b and c). Chen et al. [497] used the conventional polycondensation method to synthesize a novel CMP that is adsorbed onto the surface of multi-walled CNTs. TAPBANTCDA@MWCNTs demonstrate remarkable efficiency in both sodium-ion batteries (SIBs) and LIBs. Specifically, when the mixture is consumed in SIBs, it yields an initial reversible defined capacity of 98.4 mA h g^{-1} at a rate of 0.1 A g^{-1}, together with an active site consumption of 86.4 %. In addition, the cathode has outstanding rate capacity (56.3 mA h g^{-1} at 5.0 A g^{-1}) and long-term cycling stability (51.4 mA h g^{-1} at 2.0 A g-1) for 10,000 cycles. A comprehensive electrochemical finding demonstrates that the use of MWCNTs is essential for achieving exceptional electrochemical efficiency. In addition, ex-situ XPS and FT-IR spectroscopy investigations demonstrate that the carbonyl groups of TAPBANTCDA@MWCNTs undergo a reversible reaction. Hence, their research might provide a feasible approach to achieving novel, exceptional, and efficient electrode materials for energy conservation systems (Fig. 24d). Ren et al. [498] synthesized a TzThBT CMP anode by combining triazine (Tz), thiophene (Th), and benzothiadiazole (BT) molecules into a polymeric structure. They next evaluated the capacity of polymer to store Li^+ ions. The TzThBT anode for LIBs has a remarkable capacity to store Li^+ ions, reaching up to 1599 mAh g^{-1} at a current of 50 mA g^{-1}. It also demonstrates improved performance at higher rates, with a capacity of 363 mAh g^{-1} at 5 A g^{-1}. Furthermore, it shows extraordinary endurance, maintaining a capacity of 326 mAh g-1 after 1500 cycles at 5 A g^{-1}. This is a result of the extremely tightly π-bonded structures, fully accessible surface area, and many redox-responsive groups (Tz, Th, and BT). The enhanced electrochemical efficiency of TzThBT makes it a very appealing potential as an anode for enhancing Li-organic batteries (Fig. 24e and f). Shu et al. [499] synthesized a novel Co-PCMPs (porphyrin-based CMP) by combining a porphyrin unit (CoTCPP, [5,10,15,20-tetrakis (4-carboxyphenyl) porphyrinato]-Co (II)) with carbonyl chemical molecules (TABQ, tetraminobenzoquinone) in a properly designed structure. Both CoTCPP and TABQ may serve as redox-active sites and connecting components in this arrangement. As a result, they not only enhance the overall capacity but also build links with each other. When used as the anode material for LIBs, Co-PCMPs have impressive capabilities, with a capacity of 700 mAh g^{-1} at a current density of 0.05 A g^{-1} and a precise rate capacity of 400 mAh g^{-1} at a current density of 1.0 A g^{-1}. These properties are attributed to the unique molecular structure and well-designed composition of Co-PCMPs. Co-PCMPs have superior electrochemical stability in comparison to PCMPs. Their finding suggests that the addition of metal ions within the N_4 linked macrocycle is significant. Moreover, the practical use of this technique in batteries is shown by synthesizing whole cells using coordinated Co-PCMPs as the anode and $LiCoO_2$ as the cathode composite (Fig. 24g). Yang et al. [500] developed two CMPs (DBD-CMPs) based on 4,8-di(thiophen-2-yl)benzo[1,2-b:4,5-b']dithiophene. These CMPs include a large number of redox-active thiophene groups and were used as n-type dopants for both LIBs and SIBs. The newly developed DBD-CMPs possess an entirely interlinked polymeric structure, several nanoporous configurations, and a higher concentration of thiophene units with redox reaction, resulting in the polymers exhibiting exceptional capacity for storing Li^+/Na^+ ions. The DBD-CMP2 material has a remarkable lithium-ion storage capability, reaching a maximum capacity of 1167 mAh g^{-1} at a current density of 50 mA g^{-1}. Furthermore, it has a specific capacity of 414 mAh g^{-1} at a current density of 50 mA g^{-1} for sodium ion storage, which may be attributed to its significant level of crossed-coupling and concentration of thiophene (Fig. 24h). Li et al. [501] used the traditional infused phase reaction technique to yield an S-shaped thiophene-based CMP (SCMP), which was then utilized as both a precursor and a source of dopant for in situ SC synthesis. The carbon skeletons were efficiently impregnated with sulfur owing to the arrangement and uniform clustering of sulfur atoms in the SCMP precursor. The synthetic supercapacitors showed outstanding sodium-ion storage efficiency, showing their ability to be used in more efficient sodium-ion batteries (Fig. 24i).

3.7. Supercapacitor

It is essential to develop sustainable energy solutions rapidly in order to address the environmental damage induced by the use of fossil fuels [166,502,503]. Supercapacitors are becoming more significant as essential energy storage technologies, serving as an intermediary between traditional capacitors and batteries [167,504]. These systems use electrostatic interactions between composite conductors and electrolytic ions, resulting in several advantages, including small size, high density, wide temperature range, fast charge and discharge cycles, and high power generation [505]. The efficiency of supercapacitors, which are already integrated into industries like electric vehicles and continuous energy-generating devices, depends extensively on their selection of

electrode materials [506,507]. Organic electroactive materials, particularly CMPs, have attracted interest due to their environmentally friendly nature, easy availability of resources, and capacity to remain active, as opposed to the environmental concerns linked to inorganic resources. CMPs, which have a microporous structure with π-conjugation, display different structures and properties as a result of the varied synthesis processes used [508,509]. Their positive properties include simple synthesis, high porosity, large surface area, strong luminescent activity, heat sensitivity, and optoelectronic properties. Consequently, they show significant promise as catalysts for producing photocatalytic H_2, energy storage, separating gases, and production of solar fuel [152,510–512]. However, the low conductive properties of CMP materials presented challenges, consequently limiting their potential use in the area of energy conservation [513,514]. Mohamed et al. [515] revealed that a hyper cross-coupling POPs material based on DPT had a specific capacitance of 110 F g^{-1}. Additionally, An-CPOP-1 and An-CPOP-2, which were derived from tetraphenylanthraquinone materials, showed specific capacitances of 72.75 F g^{-1} and 98.40 F g^{-1}, respectively. Khattak et al. [516] synthesized a DAP-TFP COF with a specific capacitance of 98 F g^{-1}. The specific capacitances with an applied current density of 0.2 A g^{-1} was measured for TPA-COF-1, TPA-COF-2, TPA-COF-3, TPT-COF-4, TPT-COF-5, and TPT-COF-6. The maximum specific capacitance values obtained were 51.3, 14.4, 5.1, 2.4, 0.34, and 0.24 F g^{-1}, respectively [517]. Samy et al. [171] synthesized three new CMPs by combining Sonogashira linkage with brominated TBN. The TGA and BET analyses demonstrated that TBN-TPE-CMP exhibited remarkable properties, including a high decomposition temperature of 505 °C, a char yielding of 68 %, a significant surface area of 1150 m^{-2} g^{-1}, and an aggregate pore volume of 1426 cm^{-3} g^{-1} with pore sizes measuring 1.04 and 2.00 nm. The TBN-CMP composites were used as electrode materials for supercapacitors and were coupled with SWCNTs resulting in TBN-CMP/SWCNT nanoparticles. The TBN-Py-CMP and SWCNT composite material exhibited remarkable capacitance retention of 99.18 % over 2000 cycles at a current density of 10 A g^{-1}, along with a high specific capacitance of 430 F g^{-1}. The exceptional efficiency of the TBN-Py-CMP/SWCNT supercapacitor cathode was attributed to the strong π-coupling between the highly conductive SWCNTs and TBN-Py-CMP (Fig. 25a–d). In 2011, the Jiang group [49] designed aza-fused CMPs specifically for supercapacitor energy storage devices. The CMPs were synthesized by reacting a phenazine ring with 1,2,4, 5-benzenetetramine tetrahydrochloride and triquinoyl hydrate in the presence of $AlCl_3$ in a sealed container under high temperature conditions ranging from 300 to 500 °C. The N-rich, black CMP powder exhibits a BET surface area varying from 24 to 1227 m^2 g^{-1} at higher temperatures. The composites possess conductivity due to the presence of aza groups that facilitate dipolar interactions with the electrolyte cations. This allows for the deposition of protons on the surface and enhances the porosity of the electrolyte, offering a favorable interface for EDLC. The CV pattern have an inclined form, particularly at higher scan speeds of up to 200 mVs^{-1}. The inclination is caused by variations in electrode potential across both positive and negative slips over the whole voltage range. This phenomenon may be attributed to the electric resistivity of Aza-high CMPs. Zhan et al. [518] synthesized two redox-active CMPs, DBTh-TPA and DBThTPT, by performing a one-pot Suzuki coupling polymerization of DBTh-2Br with TPA-3BO and TPT-3BO. The polymers exhibited surface area about equal to 551 m^2/g. Spectroscopic techniques, including solid-state ^{13}C NMR and FTIR, have been utilized to confirm the atomic structures of the DBTh-CMPs. The possibility of using these DBTh-based CMPs in supercapacitors was evaluated by assessing their conductance, faradaic power preservation, and quick charge transmission. The capacitors exhibited exceptional stability, retaining 81.75 % of their original capacitance even after performing 10,000 cycles. At a current density of 0.5 A/g, the three electrodes achieved a specified capacitance of 1823 F g^{-1}, which is the maximum efficiency reported for a CMP. In addition, the DBTh-TPT CMP was used in a supercapacitor system with two electrodes. It functioned at a power density of 500 W k g^{-1} and a voltage of 1.0 V. It showed a capacitance of 609 F g^{-1} and an energy density of 84.5 Wh k g^{-1}. Furthermore, it retained 73.2 % of its original capacitance after 10,000 cycles (Fig. 25e–i). Yang et al. [519] prepared a series of MXene-based CMP nanosheets arranged in a sandwich-like structure by chemically embedding MXene between CMPs. This approach has the ability to prevent both the reassembling and breakdown of MXene nanosheets. Moreover, the M-CMPs obtained in their original state possess the same 2D structure, high electrical conductivity, and the hierarchical granular design and large effective surface area characteristic of MXene and CMPs. M-CMPs exhibited a higher capacitance compared to their predecessors, including both MXene and MXene-free materials, when used as supercapacitor electrodes. The significantly enhanced efficiency of M-CMPs may be attributed to the compositional advantages, together with the greater electrical conductivity of MXene and the quantity of accessible CMP activation sites (Fig. 25j to n).

3.8. Photoelectrochemical cells (PEC)

Recently, PEC WS has been aggressively studied as a viable solution for enhancing solar energy storage. A PEC cell is a technology that efficiently transforms renewable energy into chemical energy [520–522]. The primary factor contributing to changes in photochemical reactors is the presence of localized reduction and oxidation processes, namely at the anodic and cathodic surfaces. The operation of splitting provides an electromagnetic potential inside the photoelectrode, which assists in the separation of charges and decreases the ratio of interaction between electrons and holes. The optimum situation occurs when the photoelectrodes effectively collect and absorb enough renewable energy to power both semi-processes. Additionally, a higher voltage is frequently required to maximize the reactions [523]. Zhang et al. [524] demonstrated the addition of nanosheets using acetylenic C abundance, but they excluded the copper layer while using Triethynylbenzene 1,3,5-Glazer polycondensation. As a result, they used the same PTEB technique to a copper conducting template that can be converted into many non-conducting templates. They successfully synthesized PTEB nanofibers with an optical bandgap energy of 2.51 eV. They used these nanofibers to demonstrate the photocatalytic process in PEC cells, resulting in a cathodic photocurrent of 10 Acm^2 at various applied voltages (Fig. 26a–f). The photocurrent obtained from the process of copolymerizing 1,3,5-triethynylbenzene with thieno[3,2-b] thiophene monomer resulted in a novel polymer increased to 21 A cm^2 (PDET). In 2019, Sun et al. [525] presented their research deploying a similar approach. They used a poly(1,4-diethynylbenzene) descending homostructure (pDEB G-homostructure) on fluorine-coupled tin oxide (FTO), which was then covered with readily accessible copper foil. The combination of 1,4-diethynylbenzene (DEB) and 1,3,5-triethylbenzene (TEB) by co-polymerization, in different proportions ranging from 100:0 to 90:10, resulted in the formation of pDEB G-homojunction. The electrochemical performance of resulting material was also evaluated. Through the use of electrochemical impedance spectroscopy (EIS), they observed a significant enhancement in charge transfer due to the constant twisting of the band in the pDEB G-homostructure (Fig. 26g–i). Consequently, the measured photocurrent densities of the pDEB G-homostructure were higher compared to those of pure pDEB, pDEB homostructure, and newly developed organic photocathodes composed of g-C_3N_4. These findings emphasize the significance of acetylenic networks in PEC devices as polymeric photocathodes for the infusion of hydrogen. According to COFs, Bein's team [526] pioneered the use of a 2D-COF as a photocathodic composite for HER, as shown in Fig. 26j to n. They used tetraphenylethylene with a higher level of amine functionalization (1,1, 2, 2′-tetra-p-aminophenylethylene) and dialdehyde benzo[1,2-b:4, 5-b]-dithiophene- 2,6-dicarboxaldehyde (BDT) to include the COF (ETTA). The COF forms were used to accumulate the coupled polyimine films, which were derived from the fundamental structure of aromatic amine-functionating tetraphenylethylene and thiophene-predicated

dialdehyde, with the intention of creating photoactive porous systems. They investigated the optoelectronic features of BDT/ETTA COF sheets and discovered that the maximum occupied molecular orbital and minimum unoccupied molecular orbital sites, together with the energy difference between them (bandgap energy), may be efficiently used for applications related to HER. Silk et al. [527] recently presented an innovative approach to yield a unique porous 2D sp^2c-COF by performing the Knoevenagel condensation of 1,3,6,8-tetrakis(4-formylphenyl) pyrene (TFPPy) and 5,50-bis(cyanomethyl)-2,20-bipyridine in a mixture of 1,2-dichlorobenzene and 1-butanol (Fig. 26o to r). After the addition, a rhenium material, namely Re-Bpy-sp^2c-COF, was included to enhance the efficiency of the photocatalytic CO_2 reduction process. This system was previously mentioned, but they have incorporated it in this section because to its achievement of certain PEC requirements. The COF was dispersed in acetonitrile and the solution was coated with an FTO layer glass to produce the photoelectrodes. This method might help in describing the material, as shown by the researchers, but it is improbable to develop a thin layer that is stable, ideal in quality, and easily accessible for conducting a thorough PEC analysis. Re-Bpy-sp^2cCOF, as determined by the photocatalyst, exhibited a CO/H_2 selectivity of 86 % and a CO introduction rate of 1400 mmol g^{-1} h^{-1}. The presence of crystallinity and porosity was evident, except these materials had a defined structure and had pores, which was associated with low photocatalytic activity. Liu et al. [528] recently revealed a photoelectrochemical H_2 production process using a 2,4,6-triphenyl-1,3,5-triazine-based COF. Compared to the TTA/TTB COF with a photocurrent of 35 Acm^2, the TAPB/TTB COF showed a greatly improved visible light photocurrent of 110 Acm^2 when 2,4,6-triphenyl-1,3,5-triazine was included. This enhancement was achieved without the need for a huge organic loss factor or metal co-catalysts.

3.9. CO_2 adsorption/conversion

The research focuses on the capability of materials to collect and respond to their high porosity and pores surface [417,531,532]. Certain polar chains, including -NO_2 [533], arylamines [534], -OH [535], -COOH [536], -SO_3H [535,537,538], and heterocyclic N molecules, could considerably change the layer of porous materials, by increasing the binding energy of CO_2, to increase the absorption efficiency of CO_2 and selectivity of photocatalyst. Zhu et al. [539] explored how -COOH, -NH_2, and -OH affected the structure capability of the polymer to adsorb the CO_2. Surprisingly, in comparison to "bare" PAFs, PAF-33-NH_2 with -NH_2 demonstrates excellent CO_2 isosteric heat (32.9 kJ mol^{-1}), while PAF-33-COOH with -COOH demonstrates the most CO_2 imposition per unit areas (4.37 and 2.71 μmolm^{-2}) at 273 and 298 K. This demonstrates the efficiency of combining series in enhancing the interaction between PAF structures and CO_2 molecules, hence boosting the adsorption features. In addition, post-metallization has the potential to modify PAFs (i.e., Mg, K, Na, and Li) [540]. The isosteric temperatures of adsorption of CO_2 vary depending on the type of thin metal ions, complying with the sequence PAF-26-COOMg < PAF-26-COOLi < PAF-26-COOK < PAF-26-COONa. Significantly, an enlarged modular design and subsequent assembly of chemical applications of CMPs might enhance their ability to be more responsive and absorptive in their CO_2 absorption. Thomas et al. [75] synthesized a set of secondary building units by using PCZNs after introducing them via the Yamamomo reaction (Fig. 27a and b). The N content and porosity of polymers are believed to have a substantial influence on the amount of CO_2 that is absorbed. Both of these measurements are susceptible to variations in the chemical composition and concentration of secondary monomers. In this state, the properties are improved by the formation of advantageous groups by post-applications, namely PCZN-8. This material has the potential to accomplish a substantial CO_2 absorption capacity and a strong CO_2/N_2 separation (the green line in Fig. 27c). The length and shape of the bonds may be modified to considerably affect the pore properties of polymer structures to boost the adsorption properties of CO_2. Thomas et al. investigated the relation between the CO_2 adsorption capacity of CMPs and the extent of the functionality series [541,542]. To capture CO_2, they inserted a chain of nitrogen-rich microporous polymers based on cyanovinyl and also depicted the structure of a single polymer along with an XRD pattern (Fig. 27d–f). A point diagram illustrates the correlation between the absorbability of a structure and its capacity to adsorb CO_2 based on the quantity of operating groups. The capacity of the functional chain to adsorb CO_2 increases gradually from P_4 to P_1, achieving concentrations of 32, 99, 103, and 111 mg g^{-1} at 1 bar and 273 K, respectively. Renewable energy technology assists in effectively containing global warming by the conversion of CO_2 into valuable chemicals or enhanced thermal energy. The composite materials that collect and convert CO_2 may be developed by adding metal-organic particles to CMP structure. The use of Salen-Co/Al as a standardized catalyst for the synthesis of cyclic carbonates from CO_2 and epoxides at low pressures and temperatures was reported for the first time [543,544]. A series of Co/Al-coordinated CMPs have been synthesized by including this component into CMP structure. These CMPs have superior CO_2 capture and transformation features in terms of the environment, and their adsorption capability is related to certain widely used inorganic catalysts [545,546]. Meanwhile, under ambient conditions, such CMPs might also be used as standardized catalysts for the CO_2 and propylene oxide (PO) process for generating propylene carbonate (PC). The Co/CMP and Al/CMP showed notably large catalyst processes in the transformation of CO_2 in the presence of the fourfold ammonium salt nBu_4NBr (TBAB). The Co/CMP single catalysts have exceptional stability and can be used repeatedly 22 times without noticeably decreasing their catalytic efficiency. This proposal integrates the functions of gas storage and catalysis and proposes a recent concept for a cost-effective, one-step approach for lowering CO_2 emissions, which requires additional research. Similarly, it focused on the design features of 2D CMPs and the highly efficient catalytic process of metalloporphyrin catalysts for the conversion of CO_2. Chen et al. [547,548] developed a novel 2D CMP with metalloporphyrin as a key structure along with a practical unit as well as thiophene as a relationship towards the reduction of CO_2 emission. Furthermore, a group of metals (Cu, Mn, Mg, and Fe) was incorporated into CMP structures to modify the electrical properties of metalloporphyrin groups, enhancing the CMPs' ability to facilitate CO_2 conversion. The results show that these CMPs possess catalytic properties, a stable electronic structure, and tunable electrical properties. Among them, the Fe-altered thiophene-coupling metalloporphyrin (Fe/TMP) demonstrated the highest catalytic performance in CO_2 reduction. The single homogeneous catalytic method faces several challenges, including catalyst segregation, sample purification difficulties, challenging catalyst recovery, and hazardous residual materials, which could pose significant environmental risks. To address these issues, embedding a homogeneous catalyst on a solid porous support has proven effective. Under optimal conditions, CMPs combined with evenly distributed metal nanocomposites as electrocatalysts can selectively capture CO_2 and convert it into liquid fuel. Claudio et al. [549] used the Yamamoto process to prepare tetrakis-phenylethylene CMPs (TPE/CMPs). The Pt (or Fe) nanocomposites were then applied to their surface using the sol immobilization method in order to modify the TPE/CMP to yield an effective catalytic CO_2 reduction site on the CO_2 adsorption site of polymers. An electrochemical system for the conversion of CO_2 into liquefied fuels employs a gaseous dispersion membrane (GDM) composed of metal-doped CMPs. Fig. 27g depicts a representation of the experimental equipment and the GDM structure. In the gaseous phase, the cathode is linked to the unoccupied region of the gas diffusion interface, whereas in the liquid phase, the anode is connected to a portion of the Nafion membrane (GDL). The process to yield liquid fuel involves the passage of CO_2 via a GDL, where it is absorbed into the metal-coupled TPE/CMS interface. Subsequently, the CO_2 interacts with nanocomposites containing either Pt or Fe components. A simple apparatus located between the functioning and opposing electrodes was used to illuminate and analyze electrocatalytic components. This electrocatalyst scheme offers

advantages over conventional liquid-phase electrochemical methods as it eliminates the need for CO_2 dissolution and the recovery of liquid samples. Additionally, it exhibits superior selectivity towards complex hydrocarbons and oxygen-containing materials. The addition of polymer electrocatalysts, including appropriate metal catalysts, is one factor contributing to the growth of highly efficient electrode materials. Installing multilayer complex electrode composites that preserve high proton mobility and conductivity is another way to enhance the overall performance of electrocatalytic equipment. While the operational conditions and sample portions for electrochemical systems may differ significantly, it is crucial to examine the essential factors to enhance the system's performance. Furthermore, the specific phases of the CO_2 reduction strategy that include distinguishing rates are unknown due to the preceding variables [550]. Increasing the number of CO_2 absorption sites might be an effective approach to accelerate the reduction process. These sites distinguish between activating and adsorbing carbon dioxide, which demands additional research.

3.10. Biological applications

The number of CMP publications focused on biological applications is significantly lower than research in other fields. While MOFs have been extensively studied for their ability to incorporate heavy metal ions, CMPs offer distinct advantages: they are non-toxic, compatible with living organisms, and composed of organic materials [551]. The usage of CMPs in recent years has expanded to include biosensing [552], drug delivery and bioimaging [553,554], the synthesis of singlet oxygen [555], antibacterial [556], and phototherapy [557]. However, CMPs have yet to be explored for other bioapplications, such as DNA detection, enzyme immobilization, and colorimetric immunoassays [558].

3.10.1. Biosensing

Natural enzymes, despite their efficient catalytic properties, have limited practical applications due to their high production costs, low stability, and short lifespan [559]. Therefore, other materials that possess enzyme-like properties have been investigated. These include magnetic nanoparticles [560], noble metal nanoparticles [561], MOFs [562], manganese dioxide nanosheets [563], and graphene dots [564]. These options provide exceptional stability, low cost, and a facile synthesis process [565,566]. Enzyme-like materials have several applications in medical treatment [567], biosensing [568], bioimaging [569], and environmental protection [570]. The materials presented are oxidase simulates, which are well recognized for their ability to catalyze redox reactions in analytical investigations. Various methods have been developed to regulate the catalytic efficiency of enzyme-like reactions, such as synthesizing hybrid nanomaterials, modifying the size and shape, and modifying the surface [571]. Wang et al. [572] used the Suzuki cross-coupling process to synthesize a new photo-sensitized porous composite known as CMP-PQ_x. This material, which is distinct from others in its category, showed promising potential as an oxidase mimic that is activated by visible light. The performance of CMP-PQ_x may be easily controlled by changing the light source, which is not the case with normal oxidase mimics. The porous design of this material enhances the oxidative activities of catalysts by facilitating increased interaction with reagents and enabling efficient charge transfer. CMP-PQ_x effectively oxidizes a variety of materials, including thiamine, TMB, PPD, ABTS, and OPD, under UV light. More precisely, a biosensor that is sensitive to changes in pH and can detect the presence of urease may be designed by transforming the nonfluorescent thiamine into the fluorescent thiochrome. This transformation exhibits a significant ability for responding to changes in pH. CMP-PQ_x has exceptional stability and may be efficiently recycled in catalytic oxidation processes. Furthermore, its effectiveness for biological detection has been shown by urease testing carried out on saliva materials (Fig. 28a). Liang et al. [573] effectively designed an illumination-responsive D-p-A CMP-LS9 by using Suzuki cross-coupling techniques. The material has remarkable oxidase-like properties and can efficiently catalyze the oxidation of ABTS, TMB, and OPD within dispersed oxygen under UV light. Moreover, GSH significantly inhibits the oxidation of TMB. Based on these results, a systematic design for an extremely sensitive and selective colorimetric detection tool for GSH has been developed. Their research will provide the foundation for advanced CMP materials that operate as imitative enzymes in sensing technologies. Furthermore, a unique methodology for developing illumination-responsive CMPs was presented (Fig. 28b). Wu et al. [574] synthesized two unique CMP systems using phenanthroline-shape S, N-heteroarenes as repetitive units, resulting in micropores with larger surface area than polymers synthesized from pure phenanthroline polymers. These SN-CMPs showed flexibility in applications such as fluorescence sensing and better efficient antibacterial agents. Their capacity to recognize PA in a targeted and responsive manner was facilitated by their high electron content and fluorescence. Furthermore, the incorporation and stability of Ag nanocomposites were further enhanced by the homogenous and porous system, wherein Ag^0 and Ag^+ exhibited the greatest dispersion. These CMPs have potential for producing exploding detectors and various antimicrobial materials. Their finding represents the first use of CMPs to precisely control the thickness of silver nanoparticles in order to improve their effectiveness in destroying microorganisms (Fig. 28c).

3.10.2. Bioimaging and drug delivery

Multifunctionality is a complex subject in material engineering [575–577]. The primary goal of material engineering, from an economic perspective, is to achieve multifunctionality. Functional composites are often developed by combining inorganic and organic elements [578–580]. In addition, microporous materials have been actively studied due to their potential for having several functions [581–583]. Kim et al. [584] synthesized multifunctional drug delivery devices by integrating reactive inorganic nanoparticles with metallic-organic polyhedra (MOP) synthesis. The Fe_3O_4@SiO_2 nanomaterials were used as building blocks for the Fe_3O_4@Void@MOP composites. Aggregation-Induced Emission (AIE) capability was inserted into the MOP materials using a pre-prepared assembly block technique. In addition, foliate groups were formed by a post-synthetic modification technique. Floxorubicin (DOX) was effectively transported to KB cancer cells using Fe_3O_4@-Void@MOP-TE-FA, which could precisely enter the cells by FR-specific internalization. Furthermore, Fe_3O_4@Void@MOP-TEFA exhibited hyperthermal activation inside a magnetic field and displayed considerable fluorescence based on AIE. This combination resulted in a remarkable anticancer effect when used in conjunction with chemotherapy and hyperthermal treatment (Fig. 28d). Mousa et al. [585] used the Suzuki coupling method to synthesize three distinct CMPs based on the BBT moiety: TPA-Ph-BBT, TPE-Ph-BBT, and Py-Ph-BBT CMPs. The unique BBT-CMPs were thoroughly examined and showed adjustable properties, such as thermodynamic stability and porosity. As an example, based on the TGA evaluation, the TPE-Ph-BBT and TPA-Ph-BBT CMPs exhibited Td10 values of 554 and 491 °C, respectively, and a maximum char yield of 71 wt%. The biocompatibility tests done on L929 cells demonstrated that these CMPs exhibited a high level of protection and few adverse effects. In addition, they demonstrated antibacterial performance against *S. aureus* and *E. coli* using the inhibition method, and they were used as carriers for the antibiotic TCH. Their findings demonstrated that the TCH-TPE-Ph-BBT, TCH-Py-Ph-BBT, and TCH-TPA-Ph-BBT CMPs effectively inhibited the growth of both bacterial species. Py-Ph-BBT CMP showed superior antibacterial activity compared to other assessed CMPs due to its remarkably flat structure (Fig. 28e).

3.10.3. Antibacterial materials

Cationic chemicals are becoming more popular as effective antibacterial agents due to their decreased susceptibility to the development of resistance. These materials include cationic surfactants [586], carbon-based materials [587], lipids, antimicrobial peptides, and natural and artificial polymers [588]. Cation-based polymers containing various

cations, such as imidazolium [589], pyridinium [590], quaternary ammonium [591], pyrrolidinium [592], and phosphonium [593]. An extensive investigation has been conducted on these polymers because of their potential to avoid the development of drug resistance in microorganisms, unlike antibiotics [594]. Their antibacterial process involves the use of cationic moieties, which help the antibacterial agent stick to the surfaces of bacterial cells. This is followed by the penetration of hydrophobic components into the cell membrane, which leads to its degradation and ultimately results in the destruction of the microorganisms. The capacity of conjugated polymers to interact with the negatively charge bacterial membrane is contingent upon their positive charges [595]. Mousa et al. [596] used the Sonogashira-polycondensation process of Pyrimidine-Br_2 via ethynyl pyrene (Pyr-T) to synthesize pyrene-T-coupled CMP, leading to the formation of Pyr-T-DPM CMP. A novel antibacterial molecule, PyrT-DPM Me CMP, was synthesized by a further modification with iodomethane, resulting in the formation of a cationic CMP. The properties of the Pyr-T-coupled CMP composites were analyzed utilizing a range of quantitative techniques, including as FTIR, solid-state NMR, BET, TGA, SEM, TEM, and XPS investigations. The original Td10 and SBET values for Pyr-TDPM CMP were 397 °C and 178 $m^2\ g^{-1}$, respectively. However, after modification, these values decreased to 190 °C and 46 $m^2\ g^{-1}$, respectively. The antibacterial efficacy of these materials was evaluated in respect to *S. aureus* and *E. coli*. SEM revealed that Pyr-T-DPM Me CMP, which includes N-methylpyrimidinium salts, successfully inhibited the growth of *S. aureus* bacteria. The bacterial sustainability decreased as the quantity of Pyr-T-DPM Me CMP increased, with a concentration of 5 mg ml^{-1} showing the greatest antibacterial efficiency (Fig. 28f).

3.10.4. Phototherapy

A significant aspect of graphene-based materials is their extensive conjugated framework, which exhibits an aromatic surface. This structure facilitates the effective loading of aromatic materials by using strong π-π bonding [597]. Graphene oxide (GO) has made significant progress as a material-based therapeutic agent for antibacterial and wound treatment purposes. Hou et al. [598] investigated the photo-transformation capacity and microbiological toxicity of GO under laser light. Furthermore, Liu et al. [599] revealed the antibacterial and pro-healing properties of nanocomposites composed of graphene oxide-quaternary ammonium salt (GO-QAS). Chen et al. [600] deployed a distinct composite approach to enhance the antibacterial properties of graphene-based composites. The GO-TAPP composite was formed by precisely maintaining a CMP on a graphene oxidation lattice. In comparison to pure graphene oxide, this combination exhibited superior physicochemical properties and demonstrated efficient photo-synergistic antibacterial activity against both Gram-positive and Gram-negative bacteria. Compared to vitro and in vivo analyses, including *Staphylococcus aureus* and *E. coli*, the GO-TAPP hybrid effectively suppressed bacterial growth and reproduction, surpassing the performance of both bare TAPP and graphene oxide. In addition, the GO-TAPP combination showed low levels of toxicity and accelerated the healing of damaged wounds. The increased effectiveness against microbes may be attributed to the synergistic combination of the two components. Their findings indicated a promising approach for the production of versatile antimicrobial agents in the future, using graphene (Fig. 28g).

4. Conclusion and future prospective

This review paper highlights an overview of the latest advancements and ongoing challenges in the field of microporous polymers, a class of materials that is now gaining attention. Our study provides a comprehensive overview of CMPs. It covers their fundamental design concepts, building blocks, recent advancements in fabrication and synthesis processes, post-synthetic functionalization methods, morphologies, dimensions aspects, and their use in various applications. We also explore the limitations of their functioning and discuss the potential implications of these unique organic porous materials. Furthermore, CMPs are a stimulating area of research in materials chemistry, explicitly addressing their design approaches. Numerous doping strategies enable the synthesis of various structures, resulting in porous solids similar to metal-organic structures (MOFs) and porous coordination polymers (PCPs). Nevertheless, it is important to note that not all MOF incorporation is automatically advantageous when used with other composites. It is essential to take into consideration the comparison of properties between CMPs and other porous solids such as activated carbon. CMPs have a distinct and improved level of interaction, which sets them out as a distinctive material, especially when considering their position as the first microporous organic semiconductors. The advantages of cross-linking in CMPs, particularly in photocatalysis, are clear, yet there is still an enormous amount of unexplored potential. The mix-and-match features of CMPs allow the advancement of various capabilities, providing a distinctive platform for innovation in areas such as renewable energy technologies and optoelectronic applications. In order to maximize the capabilities of CMPs and ensure their viability against other advanced materials, it is essential to participate in research and development continuously. In this article, we provide an overview of the potential and challenges in the field, as well as future directions. We address topics such as design and preparation, characterization, practical applications, and the significance of these achievements.

- The synthesis of CMP often depends on carbon-carbon cross-coupling processes catalyzed by metals. However, there is a need for polymerization processes that do not need metals in order to achieve scalability and sustainability. Although CMPs do not possess long-term molecular ordering, they however provide flexibility and reliability in molecular design and synthesis techniques, resulting in diverse properties such as pore properties and electronic structure. Recent progress has enhanced the understanding of the structural pattern of CMP, hence enabling the synthesis of porous composites. Significant difficulties persist, especially when interacting with CMP composites that have specific surface areas higher than 5000 m^2g^{-1}. In recognition of adsorption and storage applications, it is essential to thoroughly evaluate the optimum shape, size distribution, and practical applicability of pores. CMPs have the potential to improve 3D polymer structures for optoelectronic technologies. However, there are still hurdles to the synthesis of CMPs with narrow bandgaps and an extensively understanding of their systematic interaction with electronic structure. Further research is required to obtain the potential of CMPs in these areas effectively.
- Although CMPs have shown promise in photochemical reactions and catalyzing hydrogen evolution, their use in chemical conversions has not been thoroughly investigated. A great deal of photoactive catalysis exploits homogeneous systems that include non-traditional materials. The use of microporous nanostructure materials in heterogeneous photochemical catalysis reduces costs and accelerates the process of recycling. The results obtained from photochemical HER, such as optimizing performance in the visible spectrum, have immediate significance and ought to be quickly implemented into action.
- Limited mass conductivity of CMPs imposes constraints on their use in energy production applications such as batteries and capacitors. Typically, this requires the inclusion of carbon, which contributes weight to the device and may possibly decrease the total storage capacity. Understanding the development of CMPs that are both extremely porous and functionalized while also improving conductivity, is a promising field of study. The findings from current research on sp^2 carbon-based COFs have the potential to lead toward significant progress in this field of study.
- CMPs composites have potential as energy storage materials, presenting benefits over other porous materials. The doping approach can improve the stability and catalytic activity of conventional CMPs catalysts. Integrating different elements such as photoinduced

particles, redox-active particles, and catalytic centers into CMP structures may be used as a foundation for coordinated catalytic processes in energy conversion devices. Nevertheless, further research is needed to fully understand the particular association between the composition and properties of CMPs in order to enhance their catalytic capabilities.

- Additional research into the correlation between the qualities and structures of CMPs might lead to the synthesis and production of CMPs with specific attributes optimized for certain purposes. The combination of experimental findings and computer simulations, together with rational design techniques, could assist in the development of CMPs that demonstrate enhanced performance.
- Additional research might focus on the development of CMPs with multifunctional properties. These features may include the ability to accumulate gas and exhibit catalytic activity or possess conductive properties together with porosity, enabling novel applications in energy storage, sensing, electronics, and catalysis.
- CMPs have significant potential for several applications beyond gas storage and separation, including photovoltaics, light-emitting diodes (LEDs), sensors, and electrochemistry. The contribution of exploring novel application areas and developing materials based on CMP for cutting-edge technologies might potentially provide remarkable opportunities.
- Surface functionalization and post-synthetic modifications of CMPs provide possibilities to enhance their properties and offer unique advantages such as improved chemical stability, catalytic activity, or selective molecular detection.
- The progress in scalability and the development of environmentally friendly synthesis techniques for CMPs, which include the use of green chemistry principles and sustainable and renewable raw materials, may greatly enhance the long-term potential of CMPs applications and research.
- Incorporating CMPs into mixed materials that include nanoparticles, 2D materials, or polymers may lead to the synthesis of materials that display combined features and novel functions, expanding their range of possible uses.
- The area of study is expected to be significantly influenced by recent advancements in computational modeling and simulation technologies. By combining experimental synthesis with computational screening and design techniques such as quantum calculations (ab initio, density functional theory, etc.), grand canonical Monte-Carlo (GCMC) simulations, and molecular dynamics (MD) simulations, researchers can accelerate the discovery of novel CMPs with specific properties for unique applications.
- CMPs have shown potential across multiple biological applications, including drug delivery, tissue engineering, and biosensing. Furthermore, organic CMPs can be compatible with living organisms, and certain types possess antibacterial capabilities. The presence of microporosity and the specific composition of monomers may impact the fixation of bacteria to the CMP interface, hence promoting the effective exchange of materials between living organisms and organic semiconductors, including charge transfer. Additional research might explore the potential of these chemicals in terms of their ability to interact well with living organisms, modify their functions, and transport materials to specific targets in order to develop healthcare technology.

Authors contributions

The manuscript was written with contributions from all authors. All authors have approved the final version of the manuscript.

Declaration of competing interest

The authors declare that they have no known competing financial interests or personal relationships that could have appeared to influence the work reported in this paper.

Acknowledgment

This work was supported by the King Khalid University, Abha, Saudi Arabia. The authors extend their appreciation to the Deanship of Scientific Research at King Khalid University for funding this work through Large Groups Project under grant number (R.G.P. 2/335/46). The authors also extend their appreciation to the Guangdong Office of Research Projects at the Provincial University (No. 2024KCXTD064).

References

[1] R.M. Barrer, Zeolites and their synthesis, Zeolites 1 (3) (1981) 130–140.
[2] M. Kondo, et al., Three-dimensional structure with channeling cavities for small molecules: $\{[M\text{-}2(4,4'\text{-bpy})_3(NO_3)_4].xH_2O\}_n$ (M = Co, Ni, Zn) 36 (16) (1997) 1725–1727.
[3] J.R. Long, O.M. Yaghi, The pervasive chemistry of metal–organic structures, Chem. Soc. Rev. 38 (2009).
[4] A.U. Rehman, et al., Nanoengineering of $MgSO_4$ nanohybrid on MXene substrate for efficient thermochemical heat storage material, Appl. Energy 332 (2023) 120549.
[5] R. Shah, et al., Amino functionalized metal-organic structure/rGO composite electrode for flexible Li-ion batteries, J. Alloys Compd. 936 (2023) 168183.
[6] A. Hayat, et al., Synergetic effect of bismuth vanadate over copolymerized carbon nitride composites for highly efficient photocatalytic H_2 and O_2 generation, J. Colloid Interface Sci. 627 (2022) 621–629.
[7] J.R. Holst, A. Trewin, A.I. Cooper, Porous organic molecules, Nat. Chem. 2 (11) (2010) 915–920.
[8] Y. Jin, Y. Zhu, W. Zhang, Development of organic porous materials through Schiff-base chemistry, CrystEngComm 15 (8) (2013) 1484–1499.
[9] M.P. Tsyurupa, V.A. Davankov, Porous structure of hypercrosslinked polystyrene: state-of-the-art mini-review, React. Funct. Polym. 66 (7) (2006) 768–779.
[10] J. Germain, J.M.J. Fréchet, F. Svec, Nanoporous, hypercrosslinked polypyrroles: effect of crosslinking moiety on pore size and selective gas adsorption, Chem. Commun. (12) (2009) 1526–1528.
[11] N.B. McKeown, P.M. Budd, Polymers of intrinsic microporosity (PIMs): organic materials for membrane separations, heterogeneous catalysis and hydrogen storage, Chem. Soc. Rev. 35 (8) (2006) 675–683.
[12] A.P. Côté, et al., Porous, crystalline, covalent organic structures, Science 310 (5751) (2005) 1166–1170.
[13] Lithiated porous aromatic structures with exceptional gas storage capacity, Angew. Chem. 51 (27) (2012) 6639–6642.
[14] Conjugated microporous poly(aryleneethynylene) networks, Angew. Chem. Int. Ed. 119 (45) (2007) 8728.
[15] A. Hayat, et al., Recent advances in ground-breaking conjugated microporous polymers-based materials, their synthesis, modification and potential applications, Mater. Today 64 (2023) 180–208.
[16] J.-X. Jiang, et al., Conjugated microporous poly(aryleneethynylene) networks, Angew. Chem. Int. Ed. 46 (45) (2007) 8574–8578.
[17] Z. Zhou, et al., Conjugated microporous polymer membranes for chemical separations, Chin. J. Chem. Eng. 45 (2022) 1–14.
[18] A.I.J.A.M. Cooper, Conjugated microporous polymers, Adv. Mater. 21 (12) (2009) 1291–1295.
[19] A. Hayat, et al., Recent advances in ground-breaking conjugated microporous polymers-based materials, their synthesis, modification and potential applications, Mater. Today 64 (2023) 180–208.
[20] C. Zhang, et al., Bifunctionalized conjugated microporous polymers for carbon dioxide capture, Polymer 61 (2015) 36–41.
[21] Z. Wang, et al., Dibenzothiophene dioxide based conjugated microporous polymers for visible-light-driven hydrogen production, ACS Catal. 8 (9) (2018) 8590–8596.
[22] K.V. Rao, et al., Dynamic, conjugated microporous polymers: visible light harvesting via guest-responsive reversible swelling, Phys. Chem. Chem. Phys. 18 (1) (2016) 156–163.
[23] J.-X. Jiang, et al., Band gap engineering in fluorescent conjugated microporous polymers, Chem. Sci. 2 (9) (2011) 1777–1781.
[24] C. Gu, et al., Porous organic polymer films with tunable work functions and selective hole and electron flows for energy conversions, Angew. Chem. Int. Ed. 55 (9) (2016) 3049–3053.
[25] S. Luo, et al., Recent advances in conjugated microporous polymers for photocatalysis: designs, applications, and prospects, J. Mater. Chem. A 8 (14) (2020) 6434–6470.
[26] C. Gu, et al., π-conjugated microporous polymer films: designed synthesis, conducting properties, and photoenergy conversions, Angew. Chem. 127 (46) (2015) 13798–13802.
[27] C. Zhang, et al., Toward high performance thiophene-containing conjugated microporous polymer anodes for lithium-ion batteries through structure design, Adv. Funct. Mater. 28 (4) (2018) 1705432.
[28] F. Xu, et al., Redox-active conjugated microporous polymers: a new organic platform for highly efficient energy storage, Chem. Commun. 50 (37) (2014) 4788–4790.

[29] A. Suzuki, Carbon–carbon bonding made easy, Chem. Commun. (38) (2005) 4759–4763.
[30] S.H. Chen, et al., Application of the Ibuka-Yamamoto reaction to a problem in stereochemical communication: a strategy for the stereospecific synthesis and stabilization of the triene substructure of rapamycin through sulfone substitution, J. Org. Chem. 56 (20) (1991) 5834–5845.
[31] X. Cui, et al., 1,3-Dicarbonyl compounds as phosphine-free ligands for Pd-catalyzed Heck and Suzuki reactions, Chin. Chem. Lett. 18 (6) (2007) 625–628.
[32] C. Liu, et al., Bond formations between two nucleophiles: transition metal catalyzed oxidative cross-coupling reactions, Chem. Rev. 111 (3) (2011) 1780–1824.
[33] E.H. Cordes, W.P. Jencks, On the mechanism of Schiff base formation and hydrolysis, J. Am. Chem. Soc. 84 (5) (1962) 832–837.
[34] S. Kotha, E. Brahmachary, K. Lahiri, Transition metal catalyzed [2+2+2] cycloaddition and application in organic synthesis, Eur. J. Org Chem. 2005 (22) (2005) 4741–4767.
[35] B. Karami, S. Khodabakhshi, A facile synthesis of phenazine and quinoxaline derivatives using magnesium sulfate heptahydrate as a catalyst, J. Serb. Chem. Soc. 76 (9) (2011) 1191–1198.
[36] J.A. McCubbin, O.V. Krokhin, Organocatalyzed Friedel–Crafts arylation of benzylic alcohols, Tetrahedron Lett. 51 (18) (2010) 2447–2449.
[37] Q. Liu, et al., Design, preparation and application of conjugated microporous polymers, Polym. Int. 63 (3) (2014) 381–392.
[38] S. Luo, et al., Recent advances in conjugated microporous polymers for photocatalysis: designs, applications, and prospects 8 (14) (2020) 6434–6470.
[39] A. Hayat, et al., Molecular engineering optimized carbon nitride photocatalyst for CO_2 reduction to solar fuels, J. Sci.: Adv. Mater. Devices 7 (4) (2022) 100483.
[40] F. Pan, et al., A facile molecular aggregation of isoquinoline based g-C_3N_4 for high photocatalytic performance under visible light illumination, Mater. Res. Bull. 152 (2022) 111865.
[41] A. Hayat, et al., Molecular engineering control defects within carbon nitride for optimized co-catalyst Pt induced photocatalytic CO_2 reduction and NO_2 oxidation reaction, Int. J. Hydrogen Energy 47 (31) (2022) 14280–14293, 3.
[42] H. Zhou, et al., Synthesis of conjugated microporous polymers through cationic cyclization polymerization, Macromolecules 52 (10) (2019) 3935–3941.
[43] Q. Shi, et al., Synthesis of conjugated microporous polymers for gas storage and selective adsorption, J. Mater. Sci. 50 (2015) 6388–6394.
[44] S. Yuan, et al., Microporous polyphenylenes with tunable pore size for hydrogen storage, Chem. Commun. 46 (25) (2010) 4547–4549.
[45] J.-X. Jiang, et al., Conjugated microporous poly(phenylene butadiynylene)s, Chem. Commun. (4) (2008) 486–488.
[46] J.X. Jiang, et al., Band gap engineering in fluorescent conjugated microporous polymers, Chem. Sci. 2 (9) (2011) 1777–1781.
[47] G. Cheng, et al., Soluble conjugated microporous polymers, Angew. Chem. Int. Ed. 51 (51) (2012) 12727–12731.
[48] Q. Chen, et al., Porous organic polymers based on propeller-like hexaphenylbenzene building units, Macromolecules 44 (14) (2011) 5573–5577.
[49] Y. Kou, et al., Supercapacitive energy storage and electric power supply using an aza-fused π-conjugated microporous structure, Angew. Chem. Int. Ed. 37 (2011) 8912–8916.
[50] Y. Xu, et al., Conjugated microporous polymers: design, synthesis and application, Chem. Soc. Rev. 42 (20) (2013) 8012–8031.
[51] A. Chen, et al., Tunable synthesis, characterization, and CMP performance of dendritic mesoporous silica nanospheres as functionalized abrasives, Colloids Surf. A Physicochem. Eng. Asp. 638 (2022) 128322.
[52] L. An, et al., Superhydrophobic conjugated microporous polymers for separation and adsorption, Energy Environ. Sci. 4 (6) (2011) 2062–2065.
[53] J.X. Jiang, et al., Synthetic control of the pore dimension and surface area in conjugated microporous polymer and copolymer networks, J. Am. Chem. Soc. 130 (24) (2008) 7710–7720.
[54] J.X. Jiang, et al., Conjugated microporous poly(aryleneethynylene) networks, Angew Chem. Int. Ed. Engl. 119 (45) (2010) 8728–8732.
[55] Y. Xie, et al., At ambient conditions by a conjugated microporous polymer, Nat. Commun. 4 (1) (2013) 1960.
[56] J.X. Jiang, et al., Conjugated poly(aryleneethynylene) networks, Angew. Chem. 119 (45) (2007) 8728.
[57] J.X. Jiang, et al., Microporous poly(tri(4-ethynylphenyl)amine) networks: synthesis, properties, and atomistic simulation, Macromolecules 42 (7) (2009) 2658–2666.
[58] X. Qian, et al., Capture and reversible storage of volatile iodine by novel conjugated microporous polymers containing thiophene units, ACS Appl. Mater. Interfaces 8 (32) (2016) 21063–21069.
[59] J. Zang, et al., Synthesis of functional conjugated microporous polymers containing pyridine units with high BET surface area for reversible CO_2 storage, React. Funct. Polym. 99 (Feb) (2016) 95–99.
[60] D. Tan, et al., Study on adsorption performance of conjugated microporous polymers for hydrogen and organic solvents: the role of pore volume, Eur. Polym. J. 48 (4) (2012) 705–711.
[61] J.M.H. Thomas, et al., Artificial synthesis of conjugated microporous polymers via sonogashira–hagihara coupling, J. Phys. Chem. B 124 (33) (2020) 7318–7326.
[62] S. Roy, et al., Redox-active and semi-conducting donor–acceptor conjugated microporous polymers as metal-free ORR catalysts, J. Mater. Chem. A 6 (14) (2018) 5587–5591.
[63] N. Miyaura, A. Suzuki, Stereoselective synthesis of arylated (E)-alkenes by the reaction of alk-1-enylboranes with aryl halides in the presence of palladium catalyst, Chemischer Informationsdienst 19 (19) (1979) 135–152.
[64] J.M. Tobin, et al., BODIPY-based conjugated microporous polymers as reusable heterogeneous photosensitisers in a photochemical flow reactor, Polym. Chem. 7 (43) (2016) 6662–6670.
[65] Yunfeng, et al., Rational design of donor-pi-acceptor conjugated microporous polymers for photocatalytic hydrogen production, Appl. Catal. B Environ.: An Int. J. Devot. Catal. Sci. Appl. 228 (2018) 1–9.
[66] Q. Liu, S. Jin, B. Tan, Retraction: transition-metal-free synthesis of conjugated microporous polymers via amine-catalyzed Suzuki–Miyaura coupling reaction, Chem. Sci. 12 (47) (2021), 15775-15775.
[67] C.-A. Wang, et al., The bulky Pd-PEPPSI-embedded conjugated microporous polymer-catalyzed Suzuki–Miyaura cross-coupling of aryl chlorides and arylboronic acids, Polym. Chem. 13 (11) (2022) 1547–1558.
[68] Y.B. Zhou, Z.P. Zhan, Conjugated microporous polymers for heterogeneous catalysis, Chem.–Asian J. 13 (1) (2018) 9–19.
[69] L. Sun, et al., Luminescent microporous organic polymers containing the 1,3,5-tri(4-ethenylphenyl)benzene unit constructed by Heck coupling reaction, Polym. Chem. 4 (6) (2013) 1932–1938.
[70] R.-H. Li, et al., Thiophene-alkyne-based CMPs as highly selective regulators for oxidative Heck reaction, Org. Lett. 19 (17) (2017) 4432–4435.
[71] Y.-B. Zhou, et al., Conjugated microporous polymer as heterogeneous ligand for highly selective oxidative Heck reaction, J. Am. Chem. Soc. 139 (11) (2017) 3966–3969.
[72] S. Mane, et al., Development of adsorbents for selective carbon capture: role of homo- and cross-coupling in conjugated microporous polymers and their carbonized derivatives, ACS Sustain. Chem. Eng. 6 (2018).
[73] J.R. Holst, et al., High surface area networks from tetrahedral monomers: metal-catalyzed coupling, thermal polymerization, and "click" chemistry, Macromolecules 43 (20) (2010) 8531–8538.
[74] J. Schmidt, M. Werner, A. Thomas, Conjugated microporous polymer networks via Yamamoto polymerization, Macromolecules 42 (13) (2009) 4426–4429.
[75] Y. Liao, et al., Targeted control over the porosities and functionalities of conjugated microporous polycarbazole networks for CO_2-selective capture and H_2 storage, Polym. Chem. 8 (46) (2017) 7240–7247.
[76] Y. Xu, et al., Light-emitting conjugated polymers with microporous network architecture: interweaving scaffold promotes electronic Conjugation,Facilitates exciton migration, and improves luminescence, J. Am. Chem. Soc. 133 (44) (2011) 17622–17625.
[77] Y. Liao, et al., Efficient supercapacitor energy storage using conjugated microporous polymer networks synthesized from Buchwald–Hartwig coupling, Adv. Mater. 30 (12) (2018) 1705710.
[78] H.-C. Tu, et al., Buchwald–Hartwig coupled conjugated microporous polymer for efficient removal COVID-19 antiviral drug famciclovir from waters: adsorption behavior and mechanism, Colloids Surf. A Physicochem. Eng. Asp. 656 (2023) 130393.
[79] J. Germain, F. Svec, J. Fre?Chet, Preparation of size-selective nanoporous polymer networks of aromatic rings: potential adsorbents for hydrogen storage, Chem. Mater. 20 (22) (2008) 7069–7076.
[80] H. Zhang, et al., A COF-like N-rich conjugated microporous polytriphenylamine cathode with pseudocapacitive anion storage behavior for high-energy aqueous zinc dual-ion batteries, Adv. Mater. 33 (34) (2021) 2101857.
[81] S. Yang, et al., A conjugated microporous polymer film fabricated by in situ electro-chemical deposition as a hole transporting layer in organic photovoltaics, J. Mater. Chem. C 6 (34) (2018) 9044–9048.
[82] J.J. Lee, et al., Synthesis of conjugated microporous polymer and its embedding in porous nanofibers for visible-light-driven photocatalysis with reusability, Polymer 211 (2020) 123060.
[83] Z. Chen, et al., Strong synthesis of free-standing and thickness controllable conjugated microporous polymer nanofilms, Chem. Commun. 53 (12) (2017) 1989–1992.
[84] P. Lindemann, et al., Layer-by-layer synthesis and transfer of freestanding conjugated microporous polymer nanomembranes, JoVE J. (106) (2015) e53324.
[85] X. He, et al., Controlling the selectivity of conjugated microporous polymer membrane for efficient organic solvent nanofiltration, Adv. Funct. Mater. 29 (32) (2019) 1900134.
[86] Y. Song, et al., Rational design of bifunctional conjugated microporous polymers, Nanoscale Adv. 3 (17) (2021) 4891–4906.
[87] J.-S.M. Lee, A.I. Cooper, Advances in conjugated microporous polymers, Chem. Rev. 120 (4) (2020) 2171–2214.
[88] Y. Peng, et al., Microwave-assisted synthesis of porphyrin conjugated microporous polymers for microextraction of volatile organic acids in tobaccos, J. Chromatogr. A 1594 (2019) 45–53.
[89] W. Liu, et al., A solution-processable and ultra-permeable conjugated microporous thermoset for selective hydrogen separation, Nat. Commun. 11 (1) (2020) 1633.
[90] C.-A. Wang, et al., The bulky Pd-PEPPSI-embedded conjugated microporous polymer-catalyzed Suzuki–Miyaura cross-coupling of aryl chlorides and arylboronic acids 13 (11) (2022) 1547–1558.
[91] A. Srivastava, et al., Optimal exploitation of supported heterogenized Pd nanoparticles for CC cross-coupling reactions, Coord. Chem. Rev. 507 (2024) 215763.
[92] S. Luo, et al., Recent progress in conjugated microporous polymers for clean energy: synthesis, modification, computer simulations, and applications, Prog. Polym. Sci. 115 (2021) 101374.
[93] J. Jiang, X. Liu, R.J.C.L. Luo, Donor–acceptor type conjugated microporous polymer as a metal-free photocatalyst for visible-light-driven aerobic oxidative coupling of amines, Catal. Lett. (2021) 1–9.

[94] M. Ueda, T. Abe, H. Awano, Synthesis of poly(2,5-dialkoxyphenylene), Macromolecules 25 (20) (1992) 5125–5130.
[95] Q. Chen, et al., Nitrogen-containing microporous conjugated polymers via carbazole-based oxidative coupling polymerization: preparation, porosity, and gas uptake, Small 10 (2) (2014) 308–315.
[96] Y. Zhang, et al., Gas uptake, molecular sensing and organocatalytic performances of a multifunctional carbazole-based conjugated microporous polymer, J. Mater. Chem. A 2 (33) (2014) 13422–13430.
[97] Chunyang, et al., Four simple structure carbazole-based conjugated microporous polymers with different soft connected chains, Macromol. Chem. Phys. 217 (6) (2016) 748–756.
[98] Yongfeng, et al., Construction of donor-acceptor type conjugated microporous polymers: a fascinating strategy for the development of efficient heterogeneous photocatalysts in organic synthesis, Appl. Catal. B Environ. 244 (2019) 36–44.
[99] Y. Xu, et al., Facile synthesis of conjugated microporous polymer-based porphyrin units for adsorption of CO_2 and organic vapors, Polym. Chem. 10 (7) (2019).
[100] M.G. Schwab, et al., Preparation of microporous melamine-based polymer networks in an anhydrous high-temperature miniemulsion, Macromol. Rapid Commun. 32 (22) (2011) 1798–1803.
[101] M.G. Schwab, et al., Catalyst-free preparation of melamine-based microporous polymer networks through Schiff base chemistry, J. Am. Chem. Soc. 131 (21) (2009) 7216–7217.
[102] D. Wu, et al., Design and preparation of porous polymers, Chem. Rev. 112 (7) (2012) 3959–4015.
[103] F.S. Xiao, et al., New developments in microporous materials, Adv. Mater. 11 (13) (1999) 1091–1099.
[104] Chai, et al., Synthesis of a novel beta-ketoenamine-linked conjugated microporous polymer with N-H functionalized pore surface for carbon dioxide capture, Appl. Surf. Sci.: A Journal Devoted to the Properties of Interfaces in Relation to the Synthesis & Behaviour of Materials 384 (2016) 539–543.
[105] Singh, et al., Metallophthalocyanine-based redox active metal-organic conjugated microporous polymers for OER catalysis, Chem. Commun. 54 (35) (2018) 4465–4468.
[106] Y. Wang, et al., Ferrocene-based porous organic polymers for high-affinity iodine capture, Chem. Eng. J. 380 (2020) 122420.
[107] X. Zhu, et al., Thiazolothiazole-linked porous organic polymers, Chem. Commun. 50 (95) (2014) 15055–15058.
[108] B.P. Biswal, et al., Exploration of thiazolo[5,4-d]thiazole linkages in conjugated porous organic polymers for chemoselective molecular sieving, Chem. Eur J. 24 (42) (2018) 10868–10875.
[109] V. Briega-Martos, et al., An aza-fused π-conjugated microporous structure catalyzes the production of hydrogen peroxide 7 (2) (2017) 1015–1024.
[110] Y. Kou, et al., Supercapacitive energy storage and electric power supply using an aza-fused π-conjugated microporous structure, Angew. Chem. Int. Ed. 50 (37) (2011) 8753–8757.
[111] Q. Su, et al., Two-stage polymerization towards C–C bonded Conjugated microporous polymer membranes with excellent nanofiltration performance, J. Membr. Sci. 647 (2022) 120314.
[112] Wang, et al., Covalent triazine structures for carbon dioxide capture, J. Mater. Chem. A 7 (40) (2019) 22848–22870.
[113] Pierre, et al., Porous, covalent triazine-based structures prepared by ionothermal synthesis, Angew. Chem. Int. Ed. 47 (18) (2008) 3450–3453.
[114] P. Kuhn, et al., Toward tailorable porous organic polymer networks: a high-temperature dynamic polymerization scheme based on aromatic nitriles, Macromolecules 42 (1) (2009) 319–326.
[115] S. Yuan, et al., Microporous polyphenylenes with tunable pore size for hydrogen storage, Chem. Commun. 46 (25) (2010) 4547–4549.
[116] J. Kim, et al., Conjugated microporous polymers via solvent-free ionothermal cyclotrimerization of methyl ketones, Chem. Mater. 33 (21) (2021) 8334–8342.
[117] S. Itsuno, K. Komura, Highly stereoselective synthesis of chiral aldol polymers using repeated asymmetric Mukaiyama aldol reaction, Tetrahedron 58 (41) (2002) 8237–8246.
[118] X. Jing, et al., Novel method for the synthesis of 1,3,5-triarylbenzenes from ketones, Synth. Commun. 35 (24) (2005) 3167–3171.
[119] C. Krishnaraj, et al., Covalent triazine structures – a sustainable perspective, Green Chem. 22 (2020).
[120] A.A. Thomas, Porous,Covalent triazine-based structures prepared by ionothermal synthesis, Angew. Chem. 47 (18) (2008).
[121] C. Sreenivasulu, et al., A simple Lewis acid induced reaction of phenols with electrophiles: synthesis of functionalized 4H-chromenes and ortho-benzylphenols, Synth. Commun. 50 (1) (2019) 1–11.
[122] D. Saravanan, Review of supercapacitors: materials and devices, J. Energy Storage 21 (2019) 801–825.
[123] S. Wang, et al., Post-synthetic modification of conjugated microporous polymer with imidazolium for highly efficient anionic dyes removal from water, Separate Purification Technol. 284 (2022) 120245.
[124] B. Yao, et al., Catalyst-free thiol–yne click polymerization: a powerful and facile tool for preparation of functional poly(vinylene sulfide)s, Macromolecules 47 (4) (2014) 1325–1333.
[125] A. Qi, et al., Fast and efficient synthesis of microporous polymer nanomembranes via light-induced click reaction, Beilstein J. Org. Chem. 13 (1) (2017) 558–563.
[126] Z. Ajmal, et al., Use of carbon-based advanced materials for energy conversion and storage applications: recent Development and Future Outlook, Fuel 367 (2024) 131295.
[127] Y. Liu, et al., Post-cationic modification of pyrimidine-based conjugated microporous polymer for enhancing removal performance of anionic dyes in aqueous, Chemistry 24 (29) (2018).
[128] B. Kiskan, J. Weber, Versatile postmodification of conjugated microporous polymers using thiol-yne chemistry, ACS Macro Lett. 1 (1) (2012) 37–40.
[129] T. Ratvijitvech, et al., Post-synthetic modification of conjugated microporous polymers, Polymer 55 (1) (2014) 321–325.
[130] C. Di, Y. Chan, Y. Xu, Conjugated microporous polymers with azide groups: a new strategy for postsynthetic fluoride functionalization and effectively enhanced CO_2 adsorption properties, Chem. Commun. 53 (2017).
[131] S.J. Yang, X. Ding, B.H. Han, Conjugated microporous polymers with extended ϵ-Structures for organic vapor adsorption, Macromolecules 51 (3) (2018).
[132] S.-J. Yang, X. Ding, B.-H. Han, Conjugated microporous polymers with extended π-structures for organic vapor adsorption, Macromolecules 51 (3) (2018) 947–953.
[133] Q. Hao, et al., Confined synthesis of two-dimensional covalent organic structure thin films within superspreading water layer, J. Am. Chem. Soc. 140 (38) (2018) 12152–12158.
[134] Q. Su, et al., Ultrafast organic solvent nanofiltration in CC bonded conjugated microporous membrane-based nanochannels by space-confined polymerization, Chem. Eng. J. 457 (2023) 141130.
[135] P. Cheng, et al., Enhancing nanofiltration selectivity of metal–organic structure membranes via a confined interfacial polymerization strategy, Environ. Sci. Technol. 57 (34) (2023) 12879–12889.
[136] T. Wang, et al., Space-confined polymerization: controlled fabrication of nitrogen-doped polymer and carbon microspheres with refined hierarchical architectures, Adv. Mater. 31 (16) (2019) 1807876.
[137] M. Barawi, et al., Advanced nanostructured conjugated microporous polymer application in a tandem photoelectrochemical cell for hydrogen evolution reaction, Small 18 (37) (2022) 2201351.
[138] C.M. Aitchison, et al., Structure–activity relationships in well-defined conjugated oligomer photocatalysts for hydrogen production from water, Chem. Sci. 11 (33) (2020) 8744–8756.
[139] Q. Wei, et al., Nanostructured lateral boryl substitution conjugated donor–acceptor oligomers for visible-light-driven hydrogen production, Small 17 (23) (2021) 2100132.
[140] Y.-X. Zhang, The tris [4-(2-thienyl) phenyl] amine-based conjugated microporous polymers synthesized via direct arylation polymerization for fluorescence-sensing iodine and nitrophenols, J. Solid State Chem. 318 (2023) 123736.
[141] Z. Zhang, et al., Porous organic polymers for light-driven organic transformations, Chem. Soc. Rev. 51 (7) (2022) 2444–2490.
[142] W. Zhang, et al., Enhanced reducibility via altering exciton binding energy of conjugated microporous polymers for photocatalytic reduction, Macromolecules 56 (11) (2023) 4022–4029.
[143] Z. Yang, et al., Tailoring heteroatoms in conjugated microporous polymers for boosting oxygen electrochemical reduction to hydrogen peroxide, ACS Catal. 13 (7) (2023) 4790–4798.
[144] X. Dong, et al., Combining Brønsted base and photocatalysis into conjugated microporous polymers: visible light-induced oxidation of thiols into disulfides with oxygen, J. Colloid Interface Sci. 622 (2022) 1045–1053.
[145] Z. Gao, et al., Interfacial Ti− S bond modulated S-scheme MOF/covalent triazine structure nanosheet heterojunctions for photocatalytic C− H functionalization, Angew. Chem. Int. Ed. 62 (27) (2023) e202304173.
[146] M. Mahl, et al., Multilayer stacks of polycyclic aromatic hydrocarbons, Nat. Chem. 14 (4) (2022) 457–462.
[147] S. Patial, et al., Recent advances in photocatalytic multivariate metal organic structures-based nanostructures toward renewable energy and the removal of environmental pollutants, Mater. Today Energy 19 (2021) 100589.
[148] X. Dong, et al., Pyrene-based conjugated microporous polymers for red light-powered oxidation of amines to imines, Appl. Catal. B Environ. 318 (2022) 121875.
[149] Y. Jing, et al., In situ electrochemical recomposition of decomposed redox-active species in aqueous organic flow batteries, Nat. Chem. 14 (10) (2022) 1103–1109.
[150] X. Ma, et al., Z-scheme g-C_3N_4-AQ-MoO_3 photocatalyst with unique electron transfer channel and large reduction area for enhanced sunlight photocatalytic hydrogen production, Appl. Catal. B Environ. 288 (2021) 120025.
[151] X. Dong, et al., Selective oxidation of sulfides by pyrene-π-anthraquinone conjugated microporous polymer photocatalysis, Mater. Today Energy 38 (2023) 101443.
[152] W. Zhang, et al., Visible light-driven C-3 functionalization of indoles over conjugated microporous polymers, ACS Catal. 8 (9) (2018) 8084–8091.
[153] W. Liu, et al., Difluoroborate-based conjugated organic polymer: a high-performance heterogeneous photocatalyst for oxidative coupling reactions, J. Mater. Sci. 54 (2) (2019) 1205–1212.
[154] J. Byun, K.A. Zhang, Designing conjugated porous polymers for visible light-driven photocatalytic chemical transformations, Mater. Horiz. 7 (1) (2020) 15–31.
[155] Y. Yuan, G. Zhu, Porous aromatic structures as a platform for multifunctional applications, ACS Cent. Sci. 5 (3) (2019) 409–418.
[156] A. Atilgan, et al., Post-synthetically elaborated BODIPY-based porous organic polymers (POPs) for the photochemical detoxification of a sulfur mustard simulant, J. Am. Chem. Soc. 142 (43) (2020) 18554–18564.
[157] W. Gong, et al., A boranil-based conjugated microporous polymer for efficient visible-light-driven heterogeneous photocatalysis, Polym. Chem. 12 (21) (2021) 3153–3159.
[158] K. Ishii, Functional singlet oxygen generators based on phthalocyanines, Coord. Chem. Rev. 256 (15–16) (2012) 1556–1568.

[159] X. Ding, B.H. Han, Metallophthalocyanine-based conjugated microporous polymers as highly efficient photosensitizers for singlet oxygen generation, Angew. Chem. Int. Ed. 54 (22) (2015) 6536–6539.
[160] X. Liu, et al., Porous organic polymers as promising electrode materials for energy storage devices, Adv. Mater. Technol. 5 (9) (2020) 2000154.
[161] C. Yan, et al., Hierarchical porous hollow carbon spheres derived from spirofluorene-and aniline-linked conjugated microporous polymer for phase change energy storage, Carbon 176 (2021) 178–187.
[162] Y. Liao, J. Weber, C.F. Faul, Conjugated microporous polytriphenylamine networks, Chem. Commun. 50 (59) (2014) 8002–8005.
[163] Y. Liao, et al., Efficient supercapacitor energy storage using conjugated microporous polymer networks synthesized from Buchwald–Hartwig coupling, Adv. Mater. 30 (12) (2018) 1705710.
[164] W. Lyu, et al., Spirobifluorene-based conjugated microporous polymer-grafted carbon nanotubes for efficient supercapacitive energy storage, ACS Appl. Energy Mater. 5 (3) (2022) 3706–3714.
[165] S. You, et al., Confined synthesis of conjugated microporous polymers for selective photocatalytic oxidation of amines, J. Colloid Interface Sci. 664 (2024) 63–73.
[166] A.F. El-Mahdy, et al., Secondary structures of polypeptide-based diblock copolymers influence the microphase separation of templates for the fabrication of microporous carbons, Macromolecules 54 (2) (2020) 1030–1042.
[167] D. Chen, et al., Recent advances in fiber supercapacitors: materials, device configurations, and applications, Adv. Mater. 32 (5) (2020) 1901806.
[168] M.M. Samy, M.G. Mohamed, S.-W. Kuo, Pyrene-functionalized tetraphenylethylene polybenzoxazine for dispersing single-walled carbon nanotubes and energy storage, Compos. Sci. Technol. 199 (2020) 108360.
[169] L. Mei, et al., Metal phthalocyanine-linked conjugated microporous polymer hybridized with carbon nanotubes as a high-performance flexible electrode for supercapacitors, Int. J. Hydrogen Energy 45 (43) (2020) 22950–22958.
[170] Y. Han, et al., Core-shell nanostructure of single-wall carbon nanotubes and covalent organic structures for supercapacitors, Chin. Chem. Lett. 28 (12) (2017) 2269–2273.
[171] M.M. Samy, et al., High-performance supercapacitor electrodes prepared from dispersions of tetrabenzonaphthalene-based conjugated microporous polymers and carbon nanotubes, ACS Appl. Mater. Interfaces 13 (44) (2021) 51906–51916.
[172] C.N. Gannett, et al., Performance optimization and fast rate capabilities of novel polymer cathode materials through balanced electronic and ionic transport, J. Mater. Chem. A 9 (9) (2021) 5657–5663.
[173] M. Lee, et al., Multi-electron redox phenazine for ready-to-charge organic batteries, Green Chem. 19 (13) (2017) 2980–2985.
[174] G. Dai, et al., A dual-ion organic symmetric battery constructed from phenazine-based artificial bipolar molecules, Angew. Chem. Int. Ed. 58 (29) (2019) 9902–9906.
[175] G. Dai, et al., The design of quaternary nitrogen redox center for high-performance organic battery materials, Matter 1 (4) (2019) 945–958.
[176] C.N. Gannett, et al., Cross-linking effects on performance metrics of phenazine-based polymer cathodes, ChemSusChem 13 (9) (2020) 2428–2435.
[177] L. Huang, et al., π-Extended dihydrophenazine-based polymeric cathode material for high-performance organic batteries, ACS Sustain. Chem. Eng. 8 (48) (2020) 17868–17875.
[178] W. Ma, et al., Toward high-performance dihydrophenazine-based conjugated microporous polymer cathodes for dual-ion batteries through donor–acceptor structural design, Adv. Funct. Mater. 31 (45) (2021) 2105027.
[179] Z. Zhou, et al., Electropolymerization of strong conjugated microporous polymer membranes for rapid solvent transport and narrow molecular sieving, Nat. Commun. 11 (1) (2020) 5323.
[180] Y. Xu, et al., Facile synthesis of conjugated microporous polymer-based porphyrin units for adsorption of CO_2 and organic vapors, Polym. Chem. 10 (7) (2019) 819–822.
[181] O. Ucarli, et al., Investigation of competitive and noncompetitive adsorption of some heavy metals ions on Leucodon sciuroides (Hedw.) Schwagr, Langmuir 36 (28) (2020) 8265–8271.
[182] K. Vaid, et al., Experimental and computational study on the selective interaction of functionalized gold nanoparticles with metal ions: sensing prospects, Langmuir 36 (41) (2020) 12319–12326.
[183] Q.-M. Hasi, et al., Porphyrin-based conjugated microporous polymers for highly efficient adsorption of metal ions, Langmuir 38 (31) (2022) 9507–9517.
[184] X. Dong, et al., Pyrene-based porous organic materials for visible light photocatalysis, Coord. Chem. Rev. 513 (2024) 215902.
[185] J.-X.T.A. Jiang, DJ.Cooper AI. Adams, Chem. Sci. 2 (2011) 1777–1781.
[186] M. Yu, et al., Conjugated microporous copolymer networks with enhanced gas adsorption, Polym. Chem. 6 (17) (2015) 3217–3223.
[187] D. Wang, S. Feng, H. Liu, Fluorescence-tuned polyhedral oligomeric silsesquioxane-based porous polymers, Chem.–Eur. J. 22 (40) (2016) 14319–14327.
[188] R.S. Sprick, et al., Tunable organic photocatalysts for visible-light-driven hydrogen evolution, J. Am. Chem. Soc. 137 (9) (2015) 3265–3270.
[189] G. Das, et al., Morphological diversity in nanoporous covalent organic materials derived from viologen and pyrene, ChemNanoMat 4 (1) (2018) 61–65.
[190] S. Dalapati, et al., An azine-linked covalent organic structure, J. Am. Chem. Soc. 135 (46) (2013) 17310–17313.
[191] G. Cheng, et al., Conjugated polymers of intrinsic microporosity (C-PIMs), Adv. Funct. Mater. 24 (33) (2014) 5219–5224.
[192] T.-M. Geng, et al., Synthesis of 1, 6-disubstituted pyrene-based conjugated microporous polymers for reversible adsorption and fluorescence sensing of iodine, New J. Chem. 44 (6) (2020) 2312–2320.
[193] G. Zhang, et al., Stable, carrier separation tailorable conjugated microporous polymers as a platform for highly efficient photocatalytic H_2 evolution 245 (2019) 114–121.
[194] Z. Cheng, et al., Rapid metal-free synthesis of pyridyl-functionalized conjugated microporous polymers for visible-light-driven water splitting, Polym. Chem. 11 (20) (2020) 3393–3397.
[195] M.S. Najare, et al., Synthesis, characterization and photophysical properties of a new class of pyrene substituted 1, 3, 4-oxadiazole derivatives, Opt. Mater. 88 (2019) 256–265.
[196] T. Geng, et al., Fluorescent conjugated microporous polymers containing pyrazine moieties for adsorbing and fluorescent sensing of iodine, Environ. Sci. Pollut. Control Ser. 27 (2020) 20235–20245.
[197] C. Rodriguez-Seco, et al., Benzothiadiazole aryl-amine based materials as efficient hole carriers in perovskite solar cells, ACS Appl. Mater. Interfaces 12 (29) (2020) 32712–32718.
[198] P.-I. Wang, et al., Novel poly (triphenylamine-alt-fluorene) with asymmetric hexaphenylbenzene and pyrene moieties: synthesis, fluorescence, flexible near-infrared electrochromic devices and theoretical investigation, Polym. Chem. 7 (7) (2016) 1505–1516.
[199] M.G. Kotp, et al., Tunable pyridyl-based conjugated microporous polymers for visible light-driven hydrogen evolution, ACS Appl. Energy Mater. 4 (11) (2021) 13140–13151.
[200] D. Xu, J. Guo, F. Yan, Porous ionic polymers: design, synthesis, and applications, Prog. Polym. Sci. 79 (2018) 121–143.
[201] S. Zhang, K. Dokko, M. Watanabe, Porous ionic liquids: synthesis and application, Chem. Sci. 6 (2015) 3684–3691.
[202] H.P. van Kuringen, et al., Responsive nanoporous smectic liquid crystal polymer networks as efficient and selective adsorbents, Adv. Funct. Mater. 24 (32) (2014) 5045–5051.
[203] X. Huang, et al., Corrigendum: targeted fluorination with the fluoride ion by manganese-catalyzed decarboxylation, Angew. Chem. Int. Ed. 54 (48) (2015), 14215-14215.
[204] S.M. Cohen, Postsynthetic methods for the functionalization of metal–organic structures, Chem. Rev. 112 (2) (2012) 970–1000.
[205] Y. Liu, et al., Post-cationic modification of a pyrimidine-based conjugated microporous polymer for enhancing the removal performance of anionic dyes in water, Chem.–Eur. J. 24 (29) (2018) 7480–7488.
[206] Z. Zhou, et al., Spiro-functionalized diphenylethenes: suppression of a reversible photocyclization contributes to the aggregation-induced emission effect, J. Am. Chem. Soc. 141 (25) (2019) 9803–9807.
[207] S. AnjumáShahzad, Specific detection of cancer cells through aggregation-induced emission of a light-up bioprobe, Chem. Commun. 53 (15) (2017) 2398–2401.
[208] T. Sanji, et al., Fluorescence "turn-on" detection of melamine with aggregation-induced-emission-active tetraphenylethene, Chem.–Eur. J. 48 (18) (2012) 15254–15257.
[209] P. Lu, et al., Aggregation-induced emission in a hyperbranched poly (silylenevinylene) and superamplification in its emission quenching by explosives, Macromol. Rapid Commun. 31 (9-10) (2010) 834–839.
[210] W. Wu, et al., A photostable far-red/near-infrared conjugated polymer photosensitizer with aggregation-induced emission for image-guided cancer cell ablation, Macromolecules 49 (14) (2016) 5017–5025.
[211] J. Mei, et al., Aggregation-induced emission: together we shine, united we soar, Chem. Rev. 115 (21) (2015) 11718–11940.
[212] Q. Chen, et al., Tetraphenylethylene-based fluorescent porous organic polymers: preparation, gas sorption properties and photoluminescence properties, J. Mater. Chem. 21 (35) (2011) 13554–13560.
[213] N.B. Shustova, B.D. McCarthy, M. Dinca, Turn-on fluorescence in tetraphenylethylene-based metal–organic structures: an alternative to aggregation-induced emission, J. Am. Chem. Soc. 133 (50) (2011) 20126–20129.
[214] S. Dalapati, C. Gu, D. Jiang, Luminescent porous polymers based on aggregation-induced mechanism: design, synthesis and functions, Small 12 (47) (2016) 6513–6527.
[215] J. Lee, et al., Energy band-gap engineering of conjugated microporous polymers via acidity-dependent in situ cyclization, J. Am. Chem. Soc. 140 (35) (2018) 10937–10940.
[216] Z. Wang, et al., Donor–acceptor conjugated polymer dots for tunable electrochemiluminescence activated by aggregation-induced emission-active moieties, J. Phys. Chem. Lett. 9 (18) (2018) 5296–5302.
[217] L. Cui, et al., Tetraphenylenthene-based conjugated microporous polymer for aggregation-induced electrochemiluminescence, ACS Appl. Mater. Interfaces 12 (7) (2020) 7966–7973.
[218] U. Mehmood, A. Al-Ahmed, I.A. Hussein, Review on recent advances in polythiophene based photovoltaic devices, Renew. Sustain. Energy Rev. 57 (2016) 550–561.
[219] M. Jaymand, M. Hatamzadeh, Y. Omidi, Modification of polythiophene by the incorporation of processable polymeric chains: recent progress in synthesis and applications, Prog. Polym. Sci. 47 (2015) 26–69.
[220] T.-L. Lee, et al., Carbazole-and thiophene-containing conjugated microporous polymers with different planarity for enhanced photocatalytic hydrogen evolution, Chem. Commun. 57 (90) (2021) 11968–11971.
[221] M.G. Kotp, et al., Tunable thiophene-based conjugated microporous polymers for the disposal of toxic hexavalent chromium, J. Mater. Chem. A 11 (27) (2023) 15022–15032.
[222] S. Han, et al., Bandgap engineering in benzotrithiophene-based conjugated microporous polymers: a strategy for screening metal-free heterogeneous photocatalysts, J. Mater. Chem. A 9 (6) (2021) 3333–3340.

[223] C. Gu, et al., Synthesis of covalent triazine-based structures with high CO_2 adsorption and selectivity, Polym. Chem. 6 (42) (2015) 7410–7417.
[224] M. Saleh, et al., Triazine-based microporous polymers for selective adsorption of CO_2, J. Phys. Chem. C 119 (10) (2015) 5395–5402.
[225] S. Ren, et al., Functional conjugated microporous polymers: from 1, 3, 5-benzene to 1, 3, 5-triazine, Polym. Chem. 3 (4) (2012) 928–934.
[226] T. Geng, et al., A nitrogen-rich fluorescent conjugated microporous polymer with triazine and triphenylamine units for high iodine capture and nitro aromatic compound detection, J. Mater. Chem. A 5 (16) (2017) 7612–7617.
[227] K. Iwase, et al., Copper-modified covalent triazine structures as non-noble-metal electrocatalysts for oxygen reduction, Angew. Chem. Int. Ed. 54 (38) (2015) 11068–11072.
[228] Q. Chen, et al., Microporous polycarbazole with high specific surface area for gas storage and separation, J. Am. Chem. Soc. 134 (14) (2012) 6084–6087.
[229] J.Y. Weng, et al., Tuning the adsorption and fluorescence properties of aminal-linked porous organic polymers through N-heterocyclic group decoration, J. Polym. Sci. Polym. Chem. 54 (12) (2016) 1724–1730.
[230] W. Hao, et al., Triazine-based conjugated microporous polymers for efficient hydrogen production, ACS Omega 6 (37) (2021) 23782–23787.
[231] T. Geng, et al., Triazine-based conjugated microporous polymers with N, N, N′, N′-tetraphenyl-1, 4-phenylenediamine, 1, 3, 5-tris (diphenylamino) benzene and 1, 3, 5-tris [(3-methylphenyl)-phenylamino] benzene as the core for high iodine capture and fluorescence sensing of o-nitrophenol, J. Mater. Chem. A 6 (6) (2018) 2808–2816.
[232] X. Han, et al., Effect of the cross-linker length of thiophene units on photocatalytic hydrogen production of triazine-based conjugated microporous polymers, RSC Adv. 12 (2) (2022) 708–718.
[233] A.G. Slater, A.I. Cooper, Porous materials. Function-led design of new porous materials, Science (New York, NY) 348 (6238) (2015) aaa8075-aaa8075.
[234] X. Zhuang, et al., Graphene coupled Schiff-base porous polymers: towards nitrogen-enriched porous carbon nanosheets with ultrahigh electrochemical capacity, Adv. Mater. 26 (19) (2014) 3081–3086.
[235] K. Yuan, et al., Two-dimensional core-shelled porous hybrids as highly efficient catalysts for the oxygen reduction reaction, Angew. Chem. 128 (24) (2016) 6972–6977.
[236] X. Feng, et al., Synthesis of microporous carbon nanofibers and nanotubes from conjugated polymer network and evaluation in electrochemical capacitor, Adv. Funct. Mater. 19 (13) (2009) 2125–2129.
[237] M. Shao, et al., Recent advances in electrocatalysts for oxygen reduction reaction, Chem. Rev. 116 (6) (2016) 3594–3657.
[238] H.-W. Liang, et al., Hierarchically porous carbons with optimized nitrogen doping as highly active electrocatalysts for oxygen reduction, Nat. Commun. 5 (1) (2014) 4973.
[239] A. Chen, C. Ostrom, Palladium-based nanomaterials: synthesis and electrochemical applications, Chem. Rev. 115 (21) (2015) 11999–12044.
[240] D. Guo, et al., Active sites of nitrogen-doped carbon materials for oxygen reduction reaction clarified using model catalysts, Science 351 (6271) (2016) 361–365.
[241] L. Dai, et al., Metal-free catalysts for oxygen reduction reaction, Chem. Rev. 115 (11) (2015) 4823–4892.
[242] J. Wei, et al., Nitrogen-doped nanoporous carbon/graphene nano-sandwiches: synthesis and application for efficient oxygen reduction, Adv. Funct. Mater. 25 (36) (2015) 5768–5777.
[243] Y. He, et al., Highly efficient electrocatalysts for oxygen reduction reaction based on 1D ternary doped porous carbons derived from carbon nanotube directed conjugated microporous polymers, Adv. Funct. Mater. 26 (45) (2016) 8255–8265.
[244] S.-H. Hwang, et al., Synchronous preparation of length-controllable 1D nanoparticles via crystallization-driven in situ nanoparticlization of conjugated polymers, J. Am. Chem. Soc. 144 (13) (2022) 5921–5929.
[245] L. Tan, B. Tan, Hypercrosslinked porous polymer materials: design, synthesis, and applications, Chem. Soc. Rev. 46 (11) (2017) 3322–3356.
[246] A.P. Cote, et al., Porous, crystalline, covalent organic structures, Science 310 (5751) (2005) 1166–1170.
[247] S. Chong, et al., Applications of machine learning in metal-organic structures, Coord. Chem. Rev. 423 (2020) 213487.
[248] D. Chen, et al., Fluorescent porous organic polymers, Polym. Chem. 10 (10) (2019) 1168–1181.
[249] N.B. McKeown, Polymers of intrinsic microporosity (PIMs), Polymer 202 (2020) 122736.
[250] Z. Ajmal, et al., Current progresses in two-dimensional MXene-based structure: prospects from superficial synthesis to energy conversion and storage applications, Mater. Today Chem. 27 (2023) 101238.
[251] X. Zhang, et al., A historical overview of the activation and porosity of metal–organic structures, Chem. Soc. Rev. 49 (20) (2020) 7406–7427.
[252] M.S. Lohse, T. Bein, Covalent organic structures: covalent organic structures: structures, synthesis, and applications, Adv. Funct. Mater. 28 (33) (2018) 1870229.
[253] P. Liu, et al., Autoperforation of 2D materials for generating two-terminal memristive Janus particles, Nat. Mater. 17 (11) (2018) 1005–1012.
[254] L. Wang, et al., Conjugated microporous polymer nanosheets for overall water splitting using visible light, Adv. Mater. 29 (38) (2017) 1702428.
[255] J. Tan, W.-J. Chen, J. Guo, Conjugated microporous polymers with distinctive π-electronic properties exhibiting enhanced optical applications, Chin. Chem. Lett. 27 (8) (2016) 1405–1411.
[256] R. Hardian, et al., 2D conjugated microporous polymer membranes for organic solvent nanofiltration, Chem. Eng. J. 452 (2023) 139457.
[257] B. Liang, et al., Microporous membranes comprising conjugated polymers with rigid backbones enable ultrafast organic-solvent nanofiltration, Nat. Chem. 10 (9) (2018) 961–967.
[258] Z. Liu, et al., Two-dimensional conjugated microporous polymer with structural stability and electrical bistability for rectifying memory array, Adv. Intel. Syst. 1 (4) (2019) 1900052.
[259] Z. Liu, et al., Wafer-scale ultrathin two-dimensional conjugated microporous polymers: preparation and application in heterostructure devices, ACS Appl. Mater. Interfaces 10 (4) (2018) 4010–4017.
[260] X.-C. Li, et al., Redox-active triazatruxene-based conjugated microporous polymers for high-performance supercapacitors, Chem. Sci. 8 (4) (2017) 2959–2965.
[261] S. Najib, E. Erdem, Current progress achieved in novel materials for supercapacitor electrodes: mini review, Nanoscale Adv. 1 (8) (2019) 2817–2827.
[262] Q. Wang, et al., High-performance microsized Si anodes for lithium-ion batteries: insights into the polymer configuration conversion mechanism, Adv. Mater. 34 (16) (2022) 2109658.
[263] K. Amin, et al., Conjugated microporous polymers for energy storage: recent progress and challenges, Nano Energy 85 (2021) 105958.
[264] X. Jiang, et al., Conjugated microporous polymer with C≡ C and C–F bonds: achieving remarkable stability and super anhydrous proton conductivity, ACS Appl. Mater. Interfaces 13 (13) (2021) 15536–15541.
[265] M.G. Mohamed, et al., Ultrastable covalent triazine organic structure based on anthracene moiety as platform for high-performance carbon dioxide adsorption and supercapacitors, Int. J. Mol. Sci. 23 (6) (2022) 3174.
[266] M.M. Samy, et al., Conjugated microporous polymers containing ferrocene units for high carbon dioxide uptake and energy storage, Mater. Chem. Phys. 287 (2022) 126177.
[267] M.G. Mohamed, T.-C. Chen, S.-W. Kuo, Solid-state chemical transformations to enhance gas capture in benzoxazine-linked conjugated microporous polymers, Macromolecules 54 (12) (2021) 5866–5877.
[268] A. Hassan, et al., Hydroxy functionalized triptycene based covalent organic polymers for ultra-high radioactive iodine uptake, Chem. Eng. J. 427 (2022) 130950.
[269] T.-H. Weng, et al., Ultrastable three-dimensional triptycene-and tetraphenylethene-conjugated microporous polymers for energy storage, ACS Appl. Energy Mater. 5 (11) (2022) 14239–14249.
[270] J.-X. Qi, et al., 3D ionic olefin-linked conjugated microporous polymers for selective detection and removal of TcO_4–/ReO_4–from wastewater 94 (30) (2022 2) 10850–10856.
[271] T.-H. Weng, et al., Rationally engineered ultrastable three-dimensional (3D) conjugated microporous polymers containing triptycene, tetraphenylethene, and benzothiadiazole units as exceptional high-performance organic electrodes for supercapacitors, ACS Appl. Energy Mater. 6 (17) (2023) 9012–9024.
[272] L. Yang, et al., Mechanically strong conjugated microporous polymer membranes prepared using polyvinylpyrrolidone (PVP) electrospun nanofibers as a template for efficient PM capture, J. Colloid Interface Sci. 637 (2023) 305–316.
[273] S. Lou, et al., Morphological optimization by a controlled external electric field applied during thermal annealing of organic Solar Cells 14 (35) (2022) 39701–39726.
[274] L. Liu, et al., User-friendly synthesis of nitrogen-containing polymer and microporous carbon spheres for efficient CO_2 capture, J. Mater. Chem. 22 (31) (2012) 15540–15548, 8.
[275] K. Tabata, et al., Self-assembled conjugated polymer spheres as fluorescent microresonators, Sci. Rep. 4 (1) (2014) 5902.
[276] J.S. Chen, L.A. Archer, X.W.D. Lou, SnO_2 hollow structures and TiO_2 nanosheets for lithium-ion batteries, J. Mater. Chem. 21 (27) (2011) 9912–9924.
[277] G. Li, et al., Architecture of graphdiyne nanoscale films, Chem. Commun. 46 (19) (2010) 3256–3258.
[278] A.O. Mousa, et al., Designing strategically functionalized conjugated microporous polymers with pyrene and perylenetetracarboxylic dianhydride moieties with single-walled carbon nanotubes to enhance supercapacitive energy storage efficiency, J. Power Sources 608 (2024) 234624.
[279] M. Ejaz, et al., Pyrene-based covalent organic polymers with nano carbonaceous composites for efficient supercapacitive energy storage, J. Mater. Chem. A 11 (42) (2023) 22868–22883.
[280] Y. He, et al., Highly efficient electrocatalysts for oxygen reduction reaction based on 1D ternary doped porous carbons derived from carbon nanotube directed conjugated microporous polymers, Adv. Funct. Mater. 26 (45) (2016).
[281] V. Senkovskyy, I. Senkovska, A. Kiriy, Surface-initiated synthesis of conjugated microporous polymers: chain-growth kumada catalyst-transfer polycondensation at work, ACS Macro Lett. 1 (4) (2012) 494–498.
[282] N. Kang, et al., Microporous organic network hollow spheres: useful templates for nanoparticulate Co_3O_4 hollow oxidation catalysts, J. Am. Chem. Soc. 135 (51) (2013) 19115–19118.
[283] Guipeng, et al., Synthesis of metalloporphyrin-based conjugated microporous polymer spheres directed by bipyridine-type ligands, Chem. Commun. 51 (34) (2015) 7352–7355.
[284] D. Tan, et al., Study on the morphologies of covalent organic microporous polymers: the role of reaction solvents, Macromol. Chem. Phys. 213 (14) (2012) 1435–1440.
[285] X. Li, et al., Shape-Controlled synthesis of conjugated microporous polymer nanotubes and their implementation in continuous flow polymerization, Chem. Eng. J. 465 (2023) 142861.
[286] M.G. Mohamed, et al., Dispersions of 1, 3, 4-oxadiazole-linked conjugated microporous polymers with carbon nanotubes as a high-performance electrode for supercapacitors, ACS Appl. Energy Mater. 5 (3) (2022) 3677–3688.

[287] C. Ma, M. Su, Z. Zhu, Composite flame retardants based on conjugated microporous polymer hollow nanospheres with excellent flame retardancy, ACS Omega 9 (9) (2024) 10478–10487.
[288] M. Barawi, et al., Conjugated porous polymers: ground-breaking materials for solar energy conversion, Adv. Energy Mater. 11 (43) (2021) 2101530.
[289] G. Li, et al., Metalorganic quantum dots and their graphene-like derivative porous graphitic carbon for advanced lithium-ion hybrid supercapacitor, Adv. Energy Mater. 9 (2) (2019) 1802878.
[290] Y. Gao, et al., Insights into the heteroatom-incorporated storage mechanism of hierarchically interconnected porous conjugated polymer networks for extremely stable potassium-ion storage, Chem. Eng. J. 483 (2024) 149200.
[291] M. Zhang, et al., Bottom-up construction of conjugated microporous polyporphyrin-coated graphene hydrogel composites with hierarchical pores for high-performance capacitors, Chemelectrochem 6 (24) (2019) 5946–5950.
[292] D. Taylor, et al., Conjugated porous polymers: incredibly versatile materials with far-reaching applications, Chem. Soc. Rev. 49 (12) (2020) 3981–4042.
[293] Cheng, et al., π-Conjugated microporous polymer films: designed synthesis, conducting properties, and photoenergy conversions, Angew. Chem. 127 (46) (2015) 13798–13802.
[294] P.K. Zhou, et al., Photoelectric multilevel memory device based on covalent organic polymer film with keto–enol tautomerism for harsh environments applications, Adv. Funct. Mater. 34 (1) (2024) 2306593.
[295] P. Zhou, et al., Electron push-pull effects induced performance promotion in covalent organic polymer thin films-based memristor for neuromorphic application, Chin. Chem. Lett. 35 (5) (2024) 109279.
[296] O. Buyukcakir, et al., Synthesis of porous covalent quinazoline networks (CQNs) and their gas sorption properties, Angew. Chem. Int. Ed. 58 (3) (2019) 872–876.
[297] K. Mi, et al., Molecular layer deposition of conjugated microporous polymers (CMPs) thin films for fast molecular sieving, Separ. Purif. Technol. 332 (2024) 125783.
[298] P. Lindemann, et al., Surface functionalization of conjugated microporous polymer thin films and nanomembranes using orthogonal chemistries, J. Mater. Chem. A 4 (2016).
[299] J. Zhu, et al., Two-dimensional porous polymers: from sandwich-like structure to layered skeleton, Accounts Chem. Res. 51 (2018).
[300] S. Wang, et al., Exfoliation of covalent organic structures into few-layer redox-active nanosheets as cathode materials for lithium-ion batteries, J. Am. Chem. Soc. 139 (12) (2017) 4258–4261.
[301] W. Liu, et al., Exfoliation of amorphous phthalocyanine conjugated polymers into ultrathin nanosheets for highly efficient oxygen reduction, J. Mater. Chem. A 7 (7) (2019) 3112–3119.
[302] B. Xie, et al., Mechanics of carbon nanotube networks: microstructural evolution and optimal design, Soft Matter 7 (21) (2011) 10039–10047.
[303] C.T. Lim, Nanofiber technology: current status and emerging developments, Prog. Polym. Sci. 70 (2017) 1–17.
[304] A. Hayat, et al., Nickel oxide nano-particles on 3D nickel foam substrate as a non-enzymatic glucose sensor, J. Electrochem. Soc. 166 (15) (2019) B1602.
[305] G. Chen, et al., Smart textiles for electricity generation, Chem. Rev. 120 (8) (2020) 3668–3720.
[306] J.M. Ziegler, et al., Sensors based upon nanowires, nanotubes, and nanoribbons: 2016–2020, Anal. Chem. 93 (1) (2020) 124–166.
[307] K. Lin, et al., Single small molecule-assembled mitochondria targeting nanofibers for enhanced photodynamic cancer therapy in vivo, Adv. Funct. Mater. 31 (10) (2021) 2008460.
[308] M. Zhang, et al., Using fluorescence on/off to trace tandem nanofiber assembly/disassembly in living cells, Anal. Chem. 93 (14) (2021) 5665–5669.
[309] P. Mu, et al., Superwetting monolithic hollow-carbon-nanotubes aerogels with hierarchically nanoporous structure for efficient solar steam generation, Adv. Energy Mater. 9 (1) (2019) 1802158.
[310] D. Kim, H. Kim, J.Y. Chang, Designing internal hierarchical porous networks in polymer monoliths that exhibit rapid removal and photocatalytic degradation of aromatic pollutants, Small 16 (22) (2020) 1907555.
[311] L. Zhao, et al., Low-resistance and high-tolerance monolithic spiro-bifluorene-based conjugated microporous polymer for co-capture of PM and CO_2 in waste gas, Separ. Purif. Technol. (2024) 126825.
[312] S. Jeong, et al., Hierarchical design of functional, fibrous, and microporous polymer monoliths for the molecular recognition of diethylstilbestrol, Anal. Chem. 93 (40) (2021) 13513–13519.
[313] H. Wei, et al., Superhydrophobic fluorine-rich conjugated microporous polymers monolithic nanofoam with excellent heat insulation property, Chem. Eng. J. 351 (2018) 856–866.
[314] L. Chen, et al., Selective adsorption and efficient degradation of petroleum hydrocarbons by a hydrophobic/lipophilic biomass porous foam loaded with microbials, ACS Appl. Mater. Interfaces 13 (45) (2021) 53586–53598.
[315] Y. Dai, et al., The adsorption, regeneration and engineering applications of biochar for removal organic pollutants: a review, Chemosphere 223 (2019) 12–27.
[316] F. Raziq, et al., Photocatalytic solar fuel production and environmental remediation through experimental and DFT based research on CdSe-QDs-coupled P-doped-g-C_3N_4 composites, Appl. Catal. B Environ. 270 (2020) 118867.
[317] L. Bai, et al., Construction of a carbon/lignosulfonate adsorbent to remove Pb^{2+} and Cu^{2+}, ACS Omega 7 (1) (2021) 351–361.
[318] F. Raziq, et al., Promoting visible-light photocatalytic activities for carbon nitride based 0D/2D/2D hybrid system: beyond the conventional 4-electron mechanism, Appl. Catal. B Environ. 270 (2020) 118870.
[319] S.I. Mohammadabadi, V. Javanbakht, Fabrication of dual cross-linked spherical treated waste biomass/alginate adsorbent and its potential for efficient removal of lead ions from aqueous solutions. Industrial Crops and Products, Ind. Crop. Prod. 168 (2021) 113575.
[320] T. Zhang, et al., Polydopamine functionalized cellulose-MXene composite aerogel with superior adsorption of methylene blue, Cellulose 28 (2021) 4281–4293.
[321] Y. Zhou, et al., Recent advances for dyes removal using novel adsorbents: a review, Environ. Pollut. 252 (2019) 352–365.
[322] H. Raza, et al., Synthesis of a 2D copper (II)-carboxylate structure having ultrafast adsorption of organic dyes, J. Colloid Interface Sci. 602 (2021) 43–54.
[323] Y. Zhang, et al., In situ assembly of a covalent organic structure composite membrane for dye separation, J. Membr. Sci. 628 (2021) 119216.
[324] H. Zhao, Y. Li, Removal of heavy metal ion by floatable hydrogel and reusability of its waste material in photocatalytic degradation of organic dyes, J. Environ. Chem. Eng. 9 (4) (2021) 105316.
[325] S.K. Panda, et al., Magnetite nanoparticles as sorbents for dye removal: a review, Environ. Chem. Lett. 19 (2021) 2487–2525.
[326] R. Gurav, et al., Adsorptive removal of synthetic plastic components bisphenol-A and solvent black-3 dye from single and binary solutions using pristine pinecone biochar, Chemosphere 296 (2022) 134034.
[327] T. Saeed, et al., Synthesis of chitosan composite of metal-organic structure for the adsorption of dyes; kinetic and thermodynamic approach, J. Hazard Mater. 427 (2022) 127902.
[328] Z. Xiao, et al., Highly efficient oil/water separation and trace organic contaminants removal based on superhydrophobic conjugated microporous polymer coated devices, Chem. Eng. J. 326 (2017) 640–646.
[329] G. Yang, et al., Preparation and dye adsorption properties of an oxygen-rich porous organic polymer, RSC Adv. 11 (26) (2021) 15921–15926.
[330] F. Yu, et al., Sulfonated perylene-based conjugated microporous polymer as a high-performance adsorbent for photo-enhanced uranium extraction from seawater, Polym. Chem. 12 (6) (2021) 867–875.
[331] M. Shi, et al., Sulfonated tetraphenylethylene polymers with negative charges for high-capacity removal of organic dyes from waste water, Colloids Surf. A Physicochem. Eng. Asp. 647 (2022) 128948.
[332] N. Park, et al., Hollow and sulfonated microporous organic polymers: versatile platforms for non-covalent fixation of molecular photocatalysts, RSC Adv. 5 (58) (2015) 47270–47274.
[333] X. Sheng, et al., Rationally designed conjugated microporous polymers for contaminants adsorption, Sci. Total Environ. 750 (2021) 141683.
[334] Y. Guo, et al., Carboxymethyl cellulose/sulfonated conjugated microporous polymer composite aerogel for efficient pollution removal and water evaporation, Separ. Purif. Technol. 324 (2023) 124518.
[335] J. Zhou, et al., Hollow glass microspheres incoporated conjugated microporous polymers composite aerogels for sustainable evaporation, Chem. Eng. J. 488 (2024) 150892.
[336] X. Ye, et al., Polypyrrole-coated conjugated microporous polymers/expanded graphene carbon aerogels based phase change materials composites for efficient energy conversion and storage, Sol. Energy Mater. Sol. Cell. 245 (2022) 111873.
[337] M. Elimelech, W.A. Phillip, The future of seawater desalination: energy, technology, and the environment, Science 333 (6043) (2011) 712–717.
[338] G. Doornbusch, et al., Multistage electrodialysis for desalination of natural seawater, Desalination 505 (2021) 114973.
[339] P. Zhao, et al., The feasibility survey of an autonomous renewable seawater reverse osmosis system with underwater compressed air energy storage, Desalination 505 (2021) 114981.
[340] H. Yu, et al., The intercalation of nanoscale lattices into micro-sized graphene oxide sheets for enhancing pressure-driven desalination performances, Desalination 500 (2021) 114868.
[341] Z. Zhu, et al., Highly efficient solar steam generation of bilayered ultralight aerogels based on N-rich conjugated microporous polymers nanotubes, Eur. Polym. J. 126 (2020) 109560.
[342] A. Hayat, T. Li, A facile supramolecular aggregation of trithiocyanuric acid with PCN for high photocatalytic hydrogen evolution from water splitting, Int. J. Energy Res. 43 (10) (2019) 5479–5492.
[343] C. Chen, Y. Kuang, L. Hu, Challenges and opportunities for solar evaporation, Joule 3 (3) (2019) 683–718.
[344] F. Liu, et al., Highly efficient solar seawater desalination with environmentally friendly hierarchical porous carbons derived from halogen-containing polymers, RSC Adv. 9 (50) (2019) 29414–29423.
[345] H. Jin, et al., Nanoparticle-based solar vapor generation: an experimental and numerical study, Energy 178 (2019) 447–459.
[346] A. Politano, et al., Overcoming temperature polarization in membrane distillation by thermoplasmonic effects activated by Ag nanofillers in polymeric membranes, Desalination 451 (2019) 192–199.
[347] Y. Liu, et al., IR-Driven strong plasmonic-coupling on Ag nanorices/$W_{18}O_{49}$ nanowires heterostructures for photo/thermal synergistic enhancement of H_2 evolution from ammonia borane, Appl. Catal. B Environ. 252 (2019) 164–173.
[348] A. Hayat, et al., Molecular engineering of polymeric carbon nitride based Donor-Acceptor conjugated copolymers for enhanced photocatalytic full water splitting, J. Colloid Interface Sci. 560 (2020) 743–754.
[349] A. Hayat, et al., Graphitic carbon nitride (g–C_3N_4)–based semiconductor as a beneficial candidate in photocatalysis diversity, Int. J. Hydrogen Energy 47 (8) (2022) 5142–5191, 1.
[350] A. Hayat, et al., Fusion of conjugated bicyclic co-polymer within polymeric carbon nitride for high photocatalytic performance, J. Colloid Interface Sci. 554 (2019) 627–639.
[351] V.D. Dao, H.S. Choi, Carbon-based sunlight absorbers in solar-driven steam generation devices, Global Challenges 2 (2) (2018) 1700094.

[352] A. Hayat, et al., State of the art advancement in rational design of g-C_3N_4 photocatalyst for efficient solar fuel transformation, environmental decontamination and future perspectives, Int. J. Hydrogen Energy 47 (20) (2022) 10837–10867.

[353] A. Hayat, et al., A targeted review of current progress, challenges and future perspective of g-C_3N_4 based hybrid photocatalyst toward multidimensional applications, Chem. Rec. 23 (1) (2023) e202200143.

[354] Y. Wang, et al., Photothermal-responsive conjugated polymer nanoparticles for remote control of gene expression in living cells, Adv. Mater. 30 (8) (2018) 1705418.

[355] A.I. Cooper, Conjugated microporous polymers, Adv. Mater. 21 (12) (2009) 1291–1295.

[356] H.-X. Wang, et al., Photoactive graphene sheets prepared by "click" chemistry, Chem. Commun. 47 (20) (2011) 5747–5749.

[357] J. Yang, et al., Convertible organic nanoparticles for near-infrared photothermal ablation of cancer cells, Angew. Chem. Int. Ed. 50 (2) (2011) 441–444.

[358] F. Wang, et al., Salt-rejection solar absorbers based on porous ionic polymers nanowires for desalination, Macromol. Rapid Commun. 42 (4) (2021) 2000536.

[359] C. Xiao, et al., Sugarcane-based photothermal materials for efficient solar steam generation, ChemistrySelect 4 (27) (2019) 7891–7895.

[360] Q. Fang, et al., Full biomass-derived solar stills for strong and stable evaporation to collect clean water from various water-bearing media, ACS Appl. Mater. Interfaces 11 (11) (2019) 10672–10679.

[361] C. Liu, et al., An 'antifouling'porous loofah sponge with internal microchannels as solar absorbers and water pumpers for thermal desalination, J. Mater. Chem. A 8 (25) (2020) 12323–12333.

[362] Y. Ma, D. Song, J. Cao, Preparation of activated carbon monolith from waste corrugated cardboard box via catalytic pyrolysis and gasification under CO_2 atmosphere for adsorption and solar steam generation, J. Porous Mater. 27 (6) (2020) 1711–1726.

[363] S. Wang, et al., Potentially scalable fabrication of salt-rejection evaporator based on electrogenerated polypyrrole-coated nickel foam for efficient solar steam generation, Desalination 505 (2021) 114982.

[364] J. He, et al., High-performance salt-rejecting and cost-effective superhydrophilic porous monolithic polymer foam for solar steam generation, ACS Appl. Mater. Interfaces 12 (14) (2020) 16308–16318.

[365] Y. Shi, et al., Scalable fabrication of conjugated microporous polymer sponges for efficient solar steam generation, ACS Appl. Mater. Interfaces 14 (3) (2022) 4522–4531.

[366] Q.M. Hasi, et al., Conjugated microporous polymer-coated sponges for effectively removal of oils and trace aromatic pollution in water, J. Appl. Polym. Sci. 139 (31) (2022) e52731.

[367] J.G. Kim, et al., Preparation of a sulfur-functionalized microporous polymer sponge and in situ growth of silver nanoparticles: a compressible monolithic catalyst, ACS Appl. Mater. Interfaces 9 (43) (2017) 38081–38088.

[368] A. Hayat, et al., Recent advances and future perspectives of metal-based electrocatalysts for overall electrochemical water splitting, Chem. Rec. 23 (2) (2023) e202200149.

[369] A. Hayat, et al., Different dimensionalities, morphological advancements and engineering of g-C_3N_4-based nanomaterials for energy conversion and storage, Chem. Rec. 23 (5) (2023) e202200171.

[370] A. Hayat, et al., Visible-light enhanced photocatalytic performance of polypyrrole/g-C_3N4 composites for water splitting to evolve H_2 and pollutants degradation, J. Photochem. Photobiol. Chem. 379 (2019) 88–98.

[371] Z. Ajmal, et al., Use of conductive polymer-supported oxide-based photocatalysts for efficient VOCs & SVOCs removal in gas/liquid phase, J. Environ. Chem. Eng. 11 (1) (2023) 108935.

[372] Y. Liu, B. Li, Z. Xiang, Pathways towards boosting solar-driven hydrogen evolution of conjugated polymers, Small 17 (34) (2021) 2007576.

[373] W. Zhang, et al., Visible-light responsive TiO_2-based materials for efficient solar energy utilization, Adv. Energy Mater. 11 (15) (2021) 2003303.

[374] Y. Wang, et al., Design of well-defined shell–core covalent organic structures/metal sulfide as an efficient Z-scheme heterojunction for photocatalytic water splitting, Chem. Sci. 12 (48) (2021) 16065–16073.

[375] L. Li, et al., Photocatalysts based on cobalt-chelating conjugated polymers for hydrogen evolution from water, Chem. Mater. 28 (15) (2016) 5394–5399.

[376] A. Hayat, et al., Recent advances, properties, fabrication and opportunities in two-dimensional materials for their potential sustainable applications, Energy Storage Mater. 59 (2023) 102780.

[377] O. Iqbal, et al., *A review on the synthesis, properties, and characterizations of graphitic carbon nitride (g-C_3N_4) for energy conversion and storage applications*, Materials Today Physics 34 (2023) 101080.

[378] Z.-A. Lan, et al., Conjugated donor-acceptor polymer photocatalysts with electron-output "tentacles" for efficient hydrogen evolution, Appl. Catal. B Environ. 245 (2019) 596–603.

[379] S. Wang, et al., Efficient photocatalytic production of hydrogen peroxide using dispersible and photoactive porous polymers, Nat. Commun. 14 (1) (2023) 6891.

[380] Li, C., et al., Π-bridge modulations in D–π–A conjugated microporous polymers to facilitate charge separation and transfer kinetics for efficient photocatalysis. Adv. Funct. Mater.: p. 2405539..

[381] C. Qin, et al., Dual donor-acceptor covalent organic structures for hydrogen peroxide photosynthesis, Nat. Commun. 14 (1) (2023) 5238.

[382] Z. Ajmal, et al., Current progresses in two-dimensional MXene-based structure: prospects from superficial synthesis to energy conversion and storage applications, Mater. Today Chem. 27 (2023) 101238.

[383] M. Khan, et al., Functionalized nano diamond composites for photocatalytic hydrogen evolution and effective pollutant degradation, Int. J. Hydrogen Energy 45 (53) (2020) 29070–29081.

[384] W. Li, et al., Recent progress in g–C_3N_4–Based materials for remarkable photocatalytic sustainable energy, Int. J. Hydrogen Energy 47 (49) (2022) 21067–21118.

[385] R.S. Sprick, et al., Visible-light-driven hydrogen evolution using planarized conjugated polymer photocatalysts, Angew. Chem. Int. Ed. 55 (5) (2016) 1792–1796.

[386] P.B. Pati, et al., An experimental and theoretical study of an efficient polymer nano-photocatalyst for hydrogen evolution, Energy Environ. Sci. 10 (6) (2017) 1372–1376.

[387] A. Hayat, et al., Developing new-generation covalent organic structures as sustainable catalysts: synthesis, properties, types and solar energy production, Mater. Sci. Eng. R Rep. 157 (2024) 100771.

[388] X. Wang, et al., A metal-free polymeric photocatalyst for hydrogen production from water under visible light, Nat. Mater. 8 (1) (2009) 76–80.

[389] X. Wang, et al., Polymer semiconductors for artificial photosynthesis: hydrogen evolution by mesoporous graphitic carbon nitride with visible light, J. Am. Chem. Soc. 131 (5) (2009) 1680–1681.

[390] J. Zhang, et al., Sulfur-mediated synthesis of carbon nitride: band-gap engineering and improved functions for photocatalysis, Energy Environ. Sci. 4 (3) (2011) 675–678.

[391] A. Hayat, et al., Different dimensionalities, morphological advancements and engineering of g-C_3N_4-based nanomaterials for energy conversion and storage, Chem. Rec. 23 (5) (2023) e202200171.

[392] A. Hayat, et al., Recent advances, properties, fabrication and opportunities in two-dimensional materials for their potential sustainable applications, Energy Storage Mater. 59 (2023) 102780.

[393] O. Iqbal, et al., A review on the synthesis, properties, and characterizations of graphitic carbon nitride (g-C3N4) for energy conversion and storage applications, Materials Today Physics 34 (2023) 101080.

[394] A. Hayat, et al., Rational ionothermal copolymerization of TCNQ with PCN semiconductor for enhanced photocatalytic full water splitting, ACS Appl. Mater. Interfaces 11 (50) (2019) 46756–46766.

[395] A. Hayat, et al., Conjugated electron donor–acceptor hybrid polymeric carbon nitride as a photocatalyst for CO_2 reduction, Molecules 24 (9) (2019) 1779.

[396] A. Hayat, et al., Recent advancement of the current aspects of g-C_3N_4 for its photocatalytic applications in sustainable energy system, Chem. Rec. 22 (7) (2022) e202100310.

[397] Y. Xu, et al., Homogeneous carbon/potassium-incorporation strategy for synthesizing red polymeric carbon nitride capable of near-infrared photocatalytic H_2 production, Adv. Mater. 33 (39) (2021) 2101455.

[398] Z.A. Lan, et al., Molecular design of covalent triazine structures with anisotropic charge migration for photocatalytic hydrogen production, Small 18 (16) (2022) 2200129.

[399] M. Sohail, et al., Nanostructured materials based on g-C_3N_4 for enhanced photocatalytic activity and potentials application: a review, Arab. J. Chem. 15 (9) (2022) 104070.

[400] T. Uemura, et al., Effect of organic polymer additive on crystallization of porous coordination polymer, Chem. Mater. 18 (4) (2006) 992–995.

[401] M.M. Samy, et al., Conjugated microporous polymers incorporating Thiazolo [5, 4-d] thiazole moieties for Sunlight-Driven hydrogen production from water, Chem. Eng. J. 446 (2022) 137158.

[402] Z. Xie, et al., A heptazine-based polymer photocatalyst with donor-acceptor configuration to promote exciton dissociation and charge separation, Appl. Catal. B Environ. 325 (2023) 122312.

[403] Z. Luo, et al., Side-chain molecular engineering of triazole-based donor-acceptor polymeric photocatalysts with strong electron push-pull interactions, Angew. Chem. 135 (30) (2023) e202304875.

[404] P. Xie, et al., Toward high-performance dibenzo [g, p] chrysene-based conjugated polymer photocatalysts for photocatalytic hydrogen production through donor-acceptor-acceptor structure design, Chem. Eng. J. 459 (2023) 141553.

[405] C. Han, et al., Rational design of conjugated microporous polymer photocatalysts with definite D− π–A structures for ultrahigh photocatalytic hydrogen evolution activity under natural sunlight, ACS Catal. 13 (1) (2022) 204–212.

[406] K. Kailasam, et al., Donor–acceptor-type heptazine-based polymer networks for photocatalytic hydrogen evolution, Energy Technol. 4 (6) (2016) 744–750.

[407] L. Li, et al., Rational design of porous conjugated polymers and roles of residual palladium for photocatalytic hydrogen production, J. Am. Chem. Soc. 138 (24) (2016) 7681–7686.

[408] C. Yang, et al., Molecular engineering of conjugated polybenzothiadiazoles for enhanced hydrogen production by photosynthesis, Angew. Chem. Int. Ed. 55 (32) (2016) 9202–9206.

[409] V.S. Mothika, et al., Regulating charge-transfer in conjugated microporous polymers for photocatalytic hydrogen evolution, Chem.–Eur. J. 25 (15) (2019) 3867–3874.

[410] C. Han, et al., An efficient electron donor for conjugated microporous polymer photocatalysts with high photocatalytic hydrogen evolution activity, Small 18 (28) (2022) 2202072.

[411] C. Han, et al., Molecular engineering in D-π-AA-type conjugated microporous polymers for boosting photocatalytic hydrogen evolution, ACS Appl. Mater. Interfaces 15 (30) (2023) 36404–36411.

[412] S. Chen, T. Takata, K. Domen, Particulate photocatalysts for overall water splitting, Nat. Rev. Mater. 2 (10) (2017) 17050.

[413] S. Raza, et al., Engineering approaches for CO_2 converting to biomass coupled with nanobiomaterials as biomediated towards circular bioeconomy, J. CO2 Util. 67 (2023) 102295.
[414] A. Hayat, et al., Graphitic carbon nitride (g–C_3N_4)–based semiconductor as a beneficial candidate in photocatalysis diversity, Int. J. Hydrogen Energy 47 (8) (2021) 5142–5191.
[415] M. Sohail, et al., Nanostructure engineering via intramolecular construction of carbon nitride as efficient photocatalyst for CO_2 reduction, Nanomaterials 11 (12) (2021) 3245.
[416] A. Hayat, et al., Molecular grafting based polymeric carbon nitride for wondrous artificial photosynthesis, Int. J. Energy Res. 46 (2) (2022) 1882–1893.
[417] A.M. Alenad, et al., Selectivity, stability and reproducibility effect of Uric acid integrated carbon nitride for photocatalytic application, J. Photochem. Photobiol. Chem. 423 (2022) 113591.
[418] A. Hayat, et al., Organic conjugation of polymeric carbon nitride for improved photocatalytic CO_2 conversion and H_2 fixation, Energy Technol. 9 (10) (2021) 2100091.
[419] A. Hayat, et al., A molecular amalgamation of carbon nitride polymer as emphasized photocatalytic performance, Int. J. Energy Res. 45 (14) (2021) 19921–19928.
[420] L. Weng, et al., The preferred adsorption sites and catalytic mechanism of FCC_CoFeGaNiZn multi-principal element alloy for oxygen evolution reaction catalysis based on site preference of constituent atom on sublattice, Intermetallics 165 (2024) 108132.
[421] R. Chen, et al., A general approach to simulate the atom distribution, lattice distortion, and mechanical properties of multi-principal element alloys based on site preference: using FCC_CoNiV and CoCrNi to demonstrate and compare, J. Alloys Compd. 935 (2023) 168016.
[422] A. Hayat, et al., Recent advances and future perspectives of metal-based electrocatalysts for overall electrochemical water splitting, Chem. Rec. 23 (2) (2023) e202200149.
[423] H. Ali, et al., The ordering behavior of Co_3Al-based γ′ phase with $L1_2$ structure predicted by the thermodynamic model with support of first-principles calculations, Mater. Today Commun. 33 (2022) 104447.
[424] G. Zhang, et al., Overall water splitting by Pt/g-C_3N_4 photocatalysts without using sacrificial agents, Chem. Sci. 7 (5) (2016) 3062–3066.
[425] M. Sohail, et al., Nanostructured materials based on g-C_3N_4 for enhanced photocatalytic activity and potentials application: a review, Arab. J. Chem. 15 (9) (2022) 104070.
[426] A. Hayat, et al., Enhanced photocatalytic overall water splitting from an assembly of donor-π-acceptor conjugated polymeric carbon nitride, J. Colloid Interface Sci. 624 (2022) 411–422.
[427] A. Hayat, et al., Organic conjugation of polymeric carbon nitride for improved photocatalytic CO_2 conversion and H_2 fixation 9 (10) (2021) 2100091.
[428] S. Cao, et al., Photocatalytic pure water splitting with high efficiency and value by Pt/porous brookite TiO_2 nanoflutes, Nano Energy 67 (2020) 104287.
[429] L. Wang, et al., Conjugated microporous polymer nanosheets for overall water splitting using visible light, Adv. Mater. 29 (38) (2017) 1702428.
[430] A.F. Saber, et al., Donor-acceptor carbazole-based conjugated microporous polymers as photocatalysts for visible-light-driven H_2 and O_2 evolution from water splitting, Appl. Catal. B Environ. 316 (2022) 121624.
[431] F. Yi, et al., A 1, 3, 5-triazine and benzodithiophene based donor-acceptor type semiconducting conjugated polymer for photocatalytic overall water splitting, J. Solid State Chem. 318 (2023) 123769.
[432] C. Wang, et al., Tunable covalent benzo-heterocyclic rings constructed using two-dimensional conjugated polymers for visible-light-driven water splitting, Nanoscale 15 (46) (2023) 18883–18890.
[433] P. Kongto, et al., Intensive exploration of the fuel properties of biomass and biochar from oil palm trunk and oil palm fronds for supporting increasing demand of solid biofuels in Thailand, Energy Rep. 8 (2022) 5640–5652.
[434] A. Hayat, et al., A targeted review of current progress, challenges and future perspective of g-C_3N4 based hybrid photocatalyst toward multidimensional applications, Chem. Rec. (2022) e202200143.
[435] Z. Ajmal, et al., Embedding aromatic conjugated monomer within carbon nitride for efficient photocatalytic reduction reactions, J. Mol. Liq. 368 (2022) 120617.
[436] Z. Ajma, et al., Recent advancement in conjugated polymers based photocatalytic technology for air pollutants abatement: cases of CO_2, NO_x, and VOCs, Chemosphere (2022) 136358.
[437] H. Ali, et al., Adsorption/desorption properties of novel Fe_3O_4 impregnated N-doped biochar (Fe_3O_4@ N/BC) for arsenic (III and V) removal from aqueous solution: insight into mechanistic understanding and reusability potential, Arab. J. Chem. (2022) 104209.
[438] A. Hayat, et al., Molecular engineering optimized carbon nitride photocatalyst for CO_2 reduction to solar fuels, J. Sci.: Adv. Mater. Devices 7 (4) (2022) 100483.
[439] A. Dhakshinamoorthy, et al., Photocatalytic CO_2 reduction by TiO_2 and related titanium containing solids, Energy Environ. Sci. 5 (11) (2012) 9217–9233.
[440] A. Hayat, et al., Molecular engineering of polymeric carbon nitride based Donor-Acceptor conjugated copolymers for enhanced photocatalytic full water splitting, J. Colloid Interface Sci. 560 (2020) 743–754.
[441] A. Hayat, et al., Fabrication, properties, and applications of boron nitride and their composite nanomaterials, Surf. Interfaces 29 (2022) 101725.
[442] Z. Ajmal, et al., Embedding aromatic conjugated monomer within carbon nitride for efficient photocatalytic reduction reactions, J. Mol. Liq. 368 (2022) 120617.
[443] A. Hayat, et al., A simplistic molecular agglomeration of carbon nitride for optimized photocatalytic performance, Surf. Interfaces 25 (2021) 101166.
[444] N.R. Kumar, et al., Thienyltriazine based conjugated porous organic polymers: tuning of the porosity and band gap, and CO_2 capture, Mater. Adv. 2 (22) (2021) 7473–7481.
[445] A. Hayat, et al., π-deficient pyridine ring-incorporated carbon nitride polymers for photocatalytic H_2 evolution and CO_2 fixation, Res. Chem. Intermed. 47 (1) (2021) 15–27.
[446] R.S. Sprick, et al., Water oxidation with cobalt-loaded linear conjugated polymer photocatalysts, Angew. Chem. Int. Ed. 59 (42) (2020) 18695–18700.
[447] L. Wang, et al., 2D polymers as emerging materials for photocatalytic overall water splitting 30 (48) (2018) e1801955.
[448] A. Hayat, et al., A butterfly shaped organic heterojunction photocatalyst for effective photocatalytic CO_2 reduction, CrystEngComm 23 (28) (2021) 4963–4974.
[449] S. Barman, et al., Metal-free catalysis: a redox-active donor–acceptor conjugated microporous polymer for selective visible-light-driven CO_2 reduction to CH_4, J. Am. Chem. Soc. 143 (39) (2021) 16284–16292.
[450] F. Meng, et al., Extending the π-conjugated system in conjugated microporous polymers to modulate excitonic effects for metal-free selective CO_2 photoreduction to CH_4, ACS Catal. 13 (18) (2023) 12142–12152.
[451] F.A. Rahimi, et al., Photocatalytic CO_2 reduction based on a Re (I)-integrated conjugated microporous polymer: role of a sacrificial electron donor in product selectivity and efficiency, ACS Catal. 13 (9) (2023) 5969–5978.
[452] K. Rogers, T.P. Seager, Environmental Decision-Making Using Life Cycle Impact Assessment and Stochastic Multiattribute Decision Analysis: a Case Study on Alternative Transportation Fuels, ACS Publications, 2009, pp. 1718–1723.
[453] N. Arif, et al., Homogeneous iron-doped carbon-nitride-based organo-catalysts for sensational photocatalytic performance driven by visible light, Polym. Int. 70 (9) (2021) 1273–1281.
[454] A. Hayat, et al., Molecular grafting based polymeric carbon nitride for wondrous artificial photosynthesis, Int. J. Energy Res. 46 (2) (2022) 1882–1893.
[455] M.T.B. Martinelli, O pacto ecológico europeu e seus efeitos sobre a comunidade internacional, 2021.
[456] J. Tang, et al., Emerging energy harvesting technology for electro/photo-catalytic water splitting application, Catalysts 11 (1) (2021) 142.
[457] S. Wang, et al., Metal-organic structure derived ellipse-like NiS_2 nanocatalyst for stable electrochemical hydrogen generation in alkaline electrolyte, Int. J. Hydrogen Energy 47 (97) (2022) 40932–40942.
[458] Z. Wan, et al., Sulfur engineering on NiFe layered double hydroxide at ambient temperature for high current density oxygen evolution reaction, ACS Appl. Energy Mater. 5 (4) (2022) 4603–4612.
[459] T. Audichon, et al., Elaboration and characterization of ruthenium nano-oxides for the oxygen evolution reaction in a Proton Exchange Membrane Water Electrolyzer supplied by a solar profile, Electrochim. Acta 132 (2014) 284–291.
[460] F. Cheng, et al., Metal oxide supported Ni-impregnated bifunctional catalysts for controlling char formation and maximizing energy recovery during catalytic hydrothermal liquefaction of food waste, Sustain. Energy Fuels 5 (4) (2021) 941–955.
[461] A. Hayat, et al., Organic heterostructure modified carbon nitride as apprehension for Quercetin Biosensor, Synth. Met. 278 (2021) 116813.
[462] B. Wurster, et al., Driving the oxygen evolution reaction by nonlinear cooperativity in bimetallic coordination catalysts, J. Am. Chem. Soc. 138 (11) (2016) 3623–3626.
[463] S. Bhunia, et al., Efficacious electrochemical oxygen evolution from a novel Co (II) porphyrin/pyrene-based conjugated microporous polymer, ACS Appl. Mater. Interfaces 11 (1) (2018) 1520–1528.
[464] H. Jia, et al., Pyrolyzed cobalt porphyrin-based conjugated mesoporous polymers as bifunctional catalysts for hydrogen production and oxygen evolution in water, Chem. Commun. 52 (92) (2016) 13483–13486.
[465] J.-S. Lee, et al., Ketjenblack carbon supported amorphous manganese oxides nanowires as highly efficient electrocatalyst for oxygen reduction reaction in alkaline solutions, Nano Lett. 11 (12) (2011) 5362–5366.
[466] S.S. Narwade, et al., Graphene oxide decorated with Rh nanospheres for electrocatalytic water splitting, ACS Appl. Nano Mater. 3 (12) (2020) 12288–12296.
[467] A.M. Ahmed, et al., Enhanced photoelectrochemical water splitting activity of carbon nanotubes@ TiO_2 nanoribbons in different electrolytes, Chemosphere 238 (2020) 124554.
[468] Y.B. Zhou, Z.P. Zhan, Conjugated microporous polymers for heterogeneous catalysis, Chem.–Asian J. 13 (1) (2018) 9–19.
[469] Y. Xu, et al., Light-emitting conjugated polymers with microporous network architecture: interweaving scaffold promotes electronic conjugation, facilitates exciton migration, and improves luminescence, J. Am. Chem. Soc. 133 (44) (2011) 17622–17625.
[470] P. Ju, et al., Salen–porphyrin-based conjugated microporous polymer supported Pd nanoparticles: highly efficient heterogeneous catalysts for aqueous C–C coupling reactions, J. Mater. Chem. A 7 (6) (2019) 2660–2666.
[471] Y. Li, et al., Nitrogen-rich conjugated microporous polymers with improved cobalt (II) density for highly efficient electrocatalytic oxygen evolution, ACS Appl. Mater. Interfaces 16 (7) (2024) 8903–8912.
[472] H. Wang, et al., Cobalt nanocrystals encapsulated in heteroatom-rich porous carbons derived from conjugated microporous polymers for efficient electrocatalytic hydrogen evolution, Small 14 (42) (2018) 1803232.
[473] S.K. Das, et al., Ni (II) and Cu (II) grafted porphyrin-pyrene based conjugated microporous polymers as bifunctional electrocatalysts for overall water splitting, Electrochim. Acta 459 (2023) 142553.

[474] O.S. Bushuyev, et al., What should we make with CO_2 and how can we make it? Joule 2 (5) (2018) 825–832.
[475] B. Wu, et al., A reasonable approach to describe the atom distributions and configurational entropy in high entropy alloys based on site preference, Intermetallics 144 (2022) 107489.
[476] H. Ali, et al., The site preference and doping effect on mechanical properties of Ni_3Al-based γ′ phase in superalloys by combing first-principles calculations and thermodynamic model, Arab. J. Chem. 15 (11) (2022) 104278.
[477] S. Liu, et al., Shape-dependent electrocatalytic reduction of CO_2 to CO on triangular silver nanoplates, J. Am. Chem. Soc. 139 (6) (2017) 2160–2163.
[478] S. Gao, et al., Partially oxidized atomic cobalt layers for carbon dioxide electroreduction to liquid fuel, Nature 529 (7584) (2016) 68–71.
[479] Y.-S. Wei, et al., Metal–organic structure-based catalysts with single metal sites, Chem. Rev. 120 (21) (2020) 12089–12174.
[480] H. Fei, et al., Single atom electrocatalysts supported on graphene or graphene-like carbons, Chem. Soc. Rev. 48 (20) (2019) 5207–5241.
[481] S. Lin, et al., Covalent organic structures comprising cobalt porphyrins for catalytic CO_2 reduction in water, Science 349 (6253) (2015) 1208–1213.
[482] X. Zhang, et al., Delocalized electron effect on single metal sites in ultrathin conjugated microporous polymer nanosheets for boosting CO_2 cycloaddition, Sci. Adv. 6 (17) (2020) eaaz4824.
[483] X. Zhuang, et al., Two-dimensional sandwich-type, graphene-based conjugated microporous polymers, Angew. Chem. Int. Ed. 52 (37) (2013).
[484] A. Hayat, et al., State, synthesis, perspective applications, and challenges of Graphdiyne and its analogues: a review of recent research, Adv. Colloid Interface Sci. 319 (2023) 102969.
[485] A. Hayat, et al., Novel 2D MBenes-synthesis, structure, properties with excellent performance in energy conversion and storage: a review, Mater. Sci. Eng. R Rep. 159 (2024) 100796.
[486] G.F. Manbeck, E. Fujita, A review of iron and cobalt porphyrins, phthalocyanines and related complexes for electrochemical and photochemical reduction of carbon dioxide, J. Porphyr. Phthalocyanines 19 (01n03) (2015) 45–64.
[487] X. Zhang, et al., Highly selective and active CO_2 reduction electrocatalysts based on cobalt phthalocyanine/carbon nanotube hybrid structures, Nat. Commun. 8 (1) (2017) 14675.
[488] N. Han, et al., Supported cobalt polyphthalocyanine for high-performance electrocatalytic CO_2 reduction, Chem 3 (4) (2017) 652–664.
[489] C.L. Smith, et al., Metal–organic conjugated microporous polymer containing a carbon dioxide reduction electrocatalyst, Sustain. Energy Fuels 3 (11) (2019) 2990–2994.
[490] A.B. Soliman, et al., The potential of a graphene-supported porous-organic polymer (POP) for CO_2 electrocatalytic reduction, Chem. Commun. 52 (81) (2016) 12032–12035.
[491] Z. Zhu, et al., Achieving efficient electroreduction of CO_2 to CO in a wide potential window by encapsulating Ni nanoparticles in N-doped carbon nanotubes, Carbon 185 (2021) 9–16.
[492] R. Wang, et al., Proton/electron donors enhancing electrocatalytic activity of supported conjugated microporous polymers for CO_2 reduction, Angew. Chem. Int. Ed. 61 (5) (2022) e202115503.
[493] M. Ahmed, et al., Ultrastable carbazole-tethered conjugated microporous polymers for high-performance energy storage, Microporous Mesoporous Mater. 333 (2022) 111766.
[494] Z. Chen, et al., Conjugated microporous polymer based on star-shaped triphenylamine-benzene structure with improved electrochemical performances as the organic cathode material of Li-ion battery, Electrochim. Acta 286 (2018) 187–194.
[495] Y. Dong, et al., Multi-color electrochromism containing green color based on electrochemically polymerized star-shaped phenyl bithiophene, Phys. Chem. Chem. Phys. 20 (18) (2018) 12923–12928.
[496] L.-W. Luo, et al., A redox-active conjugated microporous polymer cathode for high-performance lithium/potassium-organic batteries, Sci. China Chem. 64 (2021) 72–81.
[497] L. Chen, et al., Conjugated microporous polyimide cathodes for sodium/lithium-ion batteries with ultra-long cycling performance, Chem. Eng. J. 464 (2023) 142658.
[498] S.B. Ren, et al., Exploiting polythiophenyl-triazine-based conjugated microporous polymer with superior lithium-storage performance, ChemSusChem 13 (9) (2020) 2295–2302.
[499] L. Shu, et al., Porphyrin-based conjugated microporous polymers with dual active sites as anode materials for lithium-organic batteries, Int. J. Hydrogen Energy 47 (20) (2022) 10902–10910.
[500] T. Yang, et al., Thiophene-rich conjugated microporous polymers as anode materials for high performance lithium-and sodium-ion batteries, Solid State Ionics 347 (2020) 115247.
[501] Y. Li, et al., High-performance Na-ion storage of S-doped porous carbon derived from conjugated microporous polymers, Nano-Micro Lett. 11 (2019) 1–13.
[502] M.G. Mohamed, et al., Direct synthesis of microporous bicarbazole-based covalent triazine structures for high-performance energy storage and carbon dioxide uptake, Chem. Plus Chem. 84 (11) (2019) 1767–1774.
[503] J. Liu, et al., GeP_3/NbX_2 (X= S, Se) nano-heterostructures: promising isotropic flexible anodes for lithium-ion batteries with high lithium storage capacity, ACS Omega 6 (4) (2021) 2956–2965.
[504] M.G. Mohamed, et al., Multifunctional hypercrosslinked porous organic polymers based on tetraphenylethene and triphenylamine derivatives for high-performance dye adsorption and supercapacitor, Polymers 12 (10) (2020) 2426.
[505] J. Kim, J.H. Kim, K. Ariga, Redox-active polymers for energy storage nanoarchitectonics, Joule 1 (4) (2017) 739–768.
[506] N.L.W. Septiani, et al., Self-assembly of nickel phosphate-based nanotubes into two-dimensional crumpled sheet-like architectures for high-performance asymmetric supercapacitors, Nano Energy 67 (2020) 104270.
[507] D. Kim, et al., Ambient temperature synthesis of iron-doped porous nickel pyrophosphate nanoparticles with long-term chemical stability for high-performance oxygen evolution reaction catalysis and supercapacitors, ACS Sustain. Chem. Eng. 8 (7) (2020) 2843–2853.
[508] H. Wang, et al., Conjugated microporous polycarbazole networks as precursors for nitrogen-enriched microporous carbons for CO_2 storage and electrochemical capacitors, Chem. Mater. 29 (11) (2017) 4885–4893.
[509] J.-X. Jiang, et al., Synthetic control of the pore dimension and surface area in conjugated microporous polymer and copolymer networks, J. Am. Chem. Soc. 130 (24) (2008) 7710–7720.
[510] A.F. El-Mahdy, et al., Hollow microspherical and microtubular [3+ 3] carbazole-based covalent organic structures and their gas and energy storage applications, ACS Appl. Mater. Interfaces 11 (9) (2019) 9343–9354.
[511] T. Zhang, et al., Porous organic polymers: a promising platform for efficient photocatalysis, Mater. Chem. Front. 4 (2) (2020) 332–353.
[512] A.F. El-Mahdy, et al., Dual-function fluorescent covalent organic structures: HCl sensing and photocatalytic H_2 evolution from water, Adv. Opt. Mater. 8 (18) (2020) 2000641.
[513] J. Zhang, et al., In situ encapsulation of iron complex nanoparticles into biomass-derived heteroatom-enriched carbon nanotubes for high-performance supercapacitors, Adv. Energy Mater. 9 (4) (2019) 1803221.
[514] H. Ma, et al., Graphene oxide induced hydrothermal carbonization of egg proteins for high-performance supercapacitors, J. Mater. Chem. A 5 (32) (2017) 17040–17047.
[515] M.G. Mohamed, et al., Hypercrosslinked porous organic polymers based on tetraphenylanthraquinone for CO_2 uptake and high-performance supercapacitor, Polymer 205 (2020) 122857.
[516] A.M. Khattak, et al., A redox-active 2D covalent organic structure with pyridine moieties capable of faradaic energy storage, J. Mater. Chem. A 4 (42) (2016) 16312–16317.
[517] A.F. El-Mahdy, et al., Strategic design of triphenylamine-and triphenyltriazine-based two-dimensional covalent organic structures for CO_2 uptake and energy storage, J. Mater. Chem. A 6 (40) (2018) 19532–19541.
[518] J. Zhan, A.F. El-Mahdy, Redox-Active Benzodithiophene-4, 8-dione-Based conjugated microporous polymers for High-Performance faradaic supercapacitor energy storage, Chem. Eng. J. 473 (2023) 145124.
[519] W. Yang, et al., Covalently sandwiching MXene by conjugated microporous polymers with excellent stability for supercapacitors, Small Methods 4 (10) (2020) 2000434.
[520] M. Gratzel, Photoelectrochemical cells. Nature 414, 338, Nature 414 (6861) (2001) 338–344.
[521] Z. Li, et al., Photoelectrochemical cells for solar hydrogen production: current state of promising photoelectrodes, methods to improve their properties, and outlook, Energy Environ. Sci. 6 (2) (2013) 347–370.
[522] I. Uddin, et al., Efficient pyrolysis process of lignin over dual catalyst bed for the production of Phenols and Aromatics, South Afr. J. Bot. 149 (2022) 109–116.
[523] C.A. Martínez-Huitle, et al., Single and coupled electrochemical processes and reactors for the abatement of organic water pollutants: a critical review, Chem. Rev. 115 (24) (2015) 13362–13407.
[524] T. Zhang, et al., Solvent-mediated engineering of copper-metalated acetylenic polymer scaffolds with enhanced photoelectrochemical performance, J. Mater. Chem. A 9 (15) (2021) 9729–9734.
[525] S. Hanjum, et al., Poly(1,4-Diethynylbenzene) gradient homojunction with enhanced charge carrier separation for photoelectrochemical water reduction, Adv. Mater. 31 (9) (2019) 1900961.
[526] C. Dai, et al., 2, 4, 6-triphenyl-1, 3, 5-triazine based covalent organic structures for photoelectrochemical H_2 evolution, Adv. Mater. Interfac. 8 (7) (2021) 2002191.
[527] T. Silk, Oriented films of conjugated 2D covalent organic structures as photocathodes for water splitting, J. Am. Chem. Soc. 140 (6) (2018) 2085.
[528] Z. Zhou, et al., Self-powered heterojunction photodetector based on thermal evaporated p-CuI and hydrothermal synthesised n-TiO_2 nanorods, Opt. Mater. Express 12 (2) (2022) 392–402.
[529] T. Zhang, et al., Copper-surface-mediated synthesis of acetylenic carbon-rich nanofibers for active metal-free photocathodes, Nat. Commun. 9 (1) (2018) 1140.
[530] Z. Fu, et al., A stable covalent organic structure for photocatalytic carbon dioxide reduction, Chem. Sci. 11 (2) (2020) 543–550.
[531] H. Zhou, Q.Y. Zhang, X.B. Lu, Synthesis and catalytic application of N-heterocyclic carbene copper complex functionalized conjugated microporous polymer, RSC Adv. 6 (2016).
[532] A. Hayat, et al., Recent advancement in rational design modulation of MXene: a voyage from environmental remediation to energy conversion and storage 22 (12) (2022) e202200097.
[533] R. Banerjee, et al., Control of pore size and functionality in isoreticular zeolitic imidazolate structures and their carbon dioxide selective capture properties, J. Am. Chem. Soc. 131 (11) (2009) 3875.
[534] R. Vaidhyanathan, et al., Direct observation and quantification of CO_2 binding within an amine-functionalized nanoporous solid, Science 330 (6004) (2010) 650–653.
[535] W. Lu, et al., Sulfonate-grafted porous polymer networks for preferential CO_2 adsorption at low pressure, J. Am. Chem. Soc. 113 (45) (2011) 18126–18129.

[536] R. Dawson, D.J. Adams, A.I. Cooper, Chemical tuning of CO_2 sorption in strong nanoporous organic polymers, Chem. Sci. 2 (6) (2011) 1173–1177.
[537] Y. Naciri, et al., Recent advances of bismuth titanate based photocatalysts engineering for enhanced organic contaminates oxidation in water: a review, Chemosphere 300 (2022) 134622.
[538] A. Qadeer, et al., Rebuttal to comment on "alternative plasticizers as emerging global environmental and health threat: another regrettable substitution?" Focus on DINCH as an example, Environ. Sci. Technol. 56 (8) (2022) 5294–5297.
[539] R. Yuan, et al., Strong tri(4-ethynylphenyl)amine-based porous aromatic structures for carbon dioxide capture, Polym. Chem. 5 (7) (2014) 2266.
[540] H. Ma, et al., Post-metalation of porous aromatic structures for highly efficient carbon capture from $CO_2 + N_2$ and $CH_4 + N_2$ mixtures, Polym. Chem. 5 (2013).
[541] A. Yassin, et al., Structure–thermodynamic-property relationships in cyanovinyl-based microporous polymer networks for the future design of advanced carbon capture materials, Adv. Funct. Mater. 27 (26) (2017) 1700233.
[542] A. Qadeer, et al., Alternative plasticizers as emerging global environmental and health threat: another regrettable substitution? Environ. Sci. Technol. 56 (3) (2022) 1482–1488.
[543] M. North, R. Pasquale, C. Young, Synthesis of cyclic carbonates from epoxides and CO_2, Green Chem. 12 (9) (2010) 1514.
[544] A. Qadeer, et al., Historically linked residues profile of OCPs and PCBs in surface sediments of typical urban river networks, Shanghai: Ecotoxicological state and sources, J. Clean. Prod. 231 (2019) 1070–1078.
[545] K. Xie, et al., Self-doped SrTiO3?δ photocatalyst with enhanced activity for artificial photosynthesis under visible light, Energy Environ. Sci. 4 (10) (2011) 4211.
[546] A. Qadeer, et al., Concentrations, pollution indices and health risk assessment of heavy metals in road dust from two urbanized cities of Pakistan: comparing two sampling methods for heavy metals concentration, Sustain. Cities Soc. 53 (2020) 101959.
[547] C. Chen, et al., Design of iron atom modified thiophene-linked metalloporphyrin 2D conjugated microporous polymer as CO_2 reduction photocatalyst, Phys. Chem. Chem. Phys. Pccp 20 (14) (2018) 9536–9542.
[548] R. Mehmood, et al., 2D–2D heterostructure g-C_3N_4-based materials for photocatalytic H_2 evolution: progress and perspectives, Front. Chem. 10 (2022).
[549] Claudio, et al., CO_2 capture and reduction to liquid fuels in a novel electrochemical setup by using metal-doped conjugated microporous polymers, J. Appl. Electrochem. 45 (7) (2015) 701–713.
[550] J. Qiao, et al., A review of catalysts for the electroreduction of carbon dioxide to produce low-carbon fuels, Chem. Soc. Rev. 45 (2) (2014) 631–675.
[551] S. Alfei, A.M. Schito, Positively charged polymers as promising devices against multidrug resistant gram-negative bacteria: a Review, Polymers 12 (5) (2020) 1195.
[552] B. Subhajit, et al., A conjugated microporous polymer based visual sensing platform for aminoglycoside antibiotics in water, Chem. Commun. 54 (2018) 10–1039.C8CC02865F.
[553] A. Rengaraj, et al., Porous covalent triazine polymer as a potential nanocargo for cancer therapy and imaging, ACS Appl. Mater. Interfaces (2016) 8947–8955.
[554] A. Qadeer, et al., Influence of habitats and physicochemical factors on trophic transfer processes of antibiotics in a freshwater ecosystem: application of stable isotopes and human health risks, Sci. Total Environ. 863 (2023) 160765.
[555] JanHynek, et al., Design of porphyrin-based conjugated microporous polymers with enhanced singlet oxygen productivity. RSC Adv.. 6..
[556] B.C. Ma, et al., Enhanced visible light promoted antibacterial efficiency of conjugated microporous polymer nanoparticles via molecular doping, J. Mater. Chem. B 4 (2016).
[557] Self-sacrificial template-induced modulation of conjugated microporous polymer microcapsules and shape-dependent enhanced photothermal efficiency for ablation of cancer cells, Chem. Commun. 51 (2015).
[558] Z. He, et al., Bio-related applications of porous organic structures (POFs), J. Mater. Chem. B 7 (2019).
[559] J. Wu, et al., Nanomaterials with enzyme-like properties (nanozymes): next-generation artificial enzymes (II), Chem. Soc. Rev. 48 (4) (2019) 1004–1076.
[560] H. Zhang, et al., Discriminative detection of glutathione in cell lysates based on oxidase-like activity of magnetic nanoporous graphene, Anal. Chem. 91 (8) (2019) 5004–5010.
[561] V. Kumar, et al., Size-dependent synthesis of gold nanoparticles and their peroxidase-like activity for the colorimetric detection of glutathione from human blood serum, ACS Sustain. Chem. Eng. 6 (6) (2018) 7662–7675.
[562] Y.L. Liu, et al., A nanosized metal–organic structure of Fe-MIL-88NH_2 as a novel peroxidase mimic used for colorimetric detection of glucose, Analyst 138 (16) (2013) 4526–4531.
[563] X. Zhang, et al., Tuning the oxidase mimics activity of manganese oxides via control of their growth conditions for highly sensitive detection of glutathione, Sensor. Actuator. B Chem. 258 (2018) 80–87.
[564] L. Lin, et al., Intrinsic peroxidase-like catalytic activity of nitrogen-doped graphene quantum dots and their application in the colorimetric detection of H_2O_2 and glucose, Anal. Chim. Acta 869 (2015) 89–95.
[565] Y. Lin, J. Ren, X. Qu, Catalytically active nanomaterials: a promising candidate for artificial enzymes, Acc. Chem. Res. 47 (4) (2014) 1097–1105.
[566] A. Ullah, et al., Fabrication of polymer carbon nitride with organic monomer for effective photocatalytic hydrogen evolution, J. Photochem. Photobiol. Chem. 401 (2020) 112764.
[567] Y. Zhang, et al., Nanozyme decorated metal–organic structures for enhanced photodynamic therapy, ACS Nano 12 (1) (2018) 651–661.
[568] L. Jin, et al., PdPt bimetallic nanowires with efficient oxidase mimic activity for the colorimetric detection of acid phosphatase in acidic media, J. Mater. Chem. B 7 (29) (2019) 4561–4567.
[569] F. Chen, et al., Fabricating MnO_2 nanozymes as intracellular catalytic DNA circuit generators for versatile imaging of base-excision repair in living cells, Adv. Funct. Mater. 27 (45) (2017) 1702748.
[570] A. Swaidan, et al., A facile preparation of CuS-BSA nanocomposite as enzyme mimics: application for selective and sensitive sensing of Cr (VI) ions, Sensor. Actuator. B Chem. 294 (2019) 253–262.
[571] S. Wang, et al., Comparison of the peroxidase-like activity of unmodified, amino-modified, and citrate-capped gold nanoparticles, ChemPhysChem 13 (5) (2012) 1199–1204.
[572] M. Wang, et al., Photo-responsive oxidase mimic of conjugated microporous polymer for constructing a pH-sensitive fluorescent sensor for bio-enzyme sensing, Sensor. Actuator. B Chem. 316 (2020) 128157.
[573] S. Wang, et al., Novel D-π-A conjugated microporous polymer as visible light-driven oxidase mimic for efficient colorimetric detection of glutathione, Sensor. Actuator. B Chem. 326 (2021) 128808.
[574] M. Wu, et al., S, N-heteroacene-based conjugated microporous polymers as fluorescent sensors and effective antimicrobial carriers, ACS Appl. Bio Mater. 1 (2) (2018) 473–479.
[575] A. Lendlein, R.S. Trask, Multifunctional materials: concepts, function-structure relationships, knowledge-based design, translational materials research, Multifunct. Mater. 1 (1) (2018) 010201.
[576] M. Sohail, et al., Nanostructure engineering via intramolecular construction of carbon nitride as efficient photocatalyst for CO2 reduction 11 (12) (2021) 3245.
[577] Z. Ajmal, et al., Assembly of a novel Fe_2TiO_5-impregnated donor-π-acceptor conjugated carbon nitride for highly efficient solar water splitting, Sustain. Mater. Technol. 36 (2023) e00594.
[578] A.M. El-Toni, et al., Design, synthesis and applications of core–shell, hollow core, and nanorattle multifunctional nanostructures, Nanoscale 8 (5) (2016) 2510–2531.
[579] A. Hayat, et al., Synergetic effect of bismuth vanadate over copolymerized carbon nitride composites for highly efficient photocatalytic H_2 and O_2 generation, J. Colloid Interface Sci. 627 (2022) 621–629.
[580] A. Hayat, et al., A superficial intramolecular alignment of carbon nitride through conjugated monomer for optimized photocatalytic CO_2 reduction 11 (8) (2021) 935.
[581] Y. Xu, et al., Preparation of multifunctional hollow microporous organic nanospheres via a one-pot hyper-cross-linking mediated self-assembly strategy, Polym. Chem. 9 (29) (2018) 4017–4024.
[582] A. Hayat, et al., Molecular engineering of carbon nitride towards photocatalytic H_2 evolution and dye degradation, J. Colloid Interface Sci. 597 (2021) 39–47.
[583] A. Hayat, et al., Biomass lignin integrated polymeric carbon nitride for boosted photocatalytic hydrogen and oxygen evolution reactions, Mol. Catal. 518 (2022) 112064.
[584] D.H. Kim, et al., Fe_3O_4@ void@ microporous organic polymer-based multifunctional drug delivery systems: targeting, imaging, and magneto-thermal behaviors, ACS Appl. Mater. Interfaces 12 (33) (2020) 37628–37636.
[585] A.O. Mousa, et al., Conjugated microporous polymers as a novel generation of drug carriers: a systemic study toward efficient carriers of tetracycline antibiotic, Eur. Polym. J. 196 (2023) 112254.
[586] K. Rapsch, et al., Identification of antimicrobial peptides and immobilization strategy suitable for a covalent surface coating with biocompatible properties, Bioconjug. Chem. 25 (2) (2014) 308–319.
[587] S. Liu, et al., Lateral dimension-dependent antibacterial activity of graphene oxide sheets, Langmuir 28 (33) (2012) 12364–12372.
[588] P.R. Judzewitsch, et al., Towards sequence-controlled antimicrobial polymers: effect of polymer block order on antimicrobial activity, Angew. Chem. Int. Ed. 57 (17) (2018) 4559–4564.
[589] Z. Zheng, et al., Structure–antibacterial activity relationships of imidazolium-type ionic liquid monomers, poly (ionic liquids) and poly (ionic liquid) membranes: effect of alkyl chain length and cations, ACS Appl. Mater. Interfaces 8 (20) (2016) 12684–12692.
[590] P.-Y. Wang, et al., Synthesis and biological evaluation of pyridinium-functionalized carbazole derivatives as promising antibacterial agents, Bioorg. Med. Chem. Lett 27 (18) (2017) 4294–4297.
[591] Y. Wang, et al., Red fluorescence conjugated polymer with broad spectrum antimicrobial activity for treatment of bacterial infections in vivo, ACS Appl. Mater. Interfaces 10 (41) (2018) 34878–34885.
[592] J. Qin, et al., Synthesis of pyrrolidinium-type poly (ionic liquid) membranes for antibacterial applications, ACS Appl. Mater. Interfaces 9 (12) (2017) 10504–10511.
[593] Y. Xue, et al., Novel quaternary phosphonium-type cationic polyacrylamide and elucidation of dual-functional antibacterial/antiviral activity, RSC Adv. 4 (87) (2014) 46887–46895.
[594] Y. Yang, et al., Antimicrobial cationic polymers: from structural design to functional control, Polym. J. 50 (1) (2018) 33–44.
[595] Q. Xu, et al., Antimicrobial activity of a conjugated polymer with cationic backbone, Dyes Pigments 160 (2019) 519–523.
[596] A.O. Mousa, et al., Construction of cationic conjugated microporous polymers containing pyrene units through post-cationic modification for enhanced antibacterial performance, J. Taiwan Inst. Chem. Eng. 157 (2024) 105448.
[597] B. Liu, et al., From graphite to graphene oxide and graphene oxide quantum dots, Small 13 (18) (2017) 1601001.

[598] W.-C. Hou, et al., Antibacterial property of graphene oxide: the role of phototransformation, Environ. Sci. Nano 4 (3) (2017) 647–657.
[599] T. Liu, et al., Synthesis of graphene oxide-quaternary ammonium nanocomposite with synergistic antibacterial activity to promote infected wound healing, Burns & trauma 6 (2018).
[600] P. Chen, et al., Composite porphyrin-based conjugated microporous polymer/graphene oxide capable of photo-triggered combinational antibacterial therapy and wound healing, Biomater. Adv. 154 (2023) 213662.